KIT Supports Small Intestinal Tuft Cell Hyperplasia

Heber I. Lara

A dissertation

submitted in partial fulfillment of the

requirements for the degree of

Doctor of Philosophy

University of Washington

2025

Reading Committee:

Jakob von Moltke, Ph.D., Chair

Dan Stetson, Ph.D.

Meghan Koch, Ph.D.

Program Authorized to Offer Degree:

Immunology

University of Washington

Abstract

KIT Supports Small Intestinal Tuft Cell Hyperplasia

Heber I. Lara

Chair of the Supervisory Committee:

Dr. Jakob von Moltke

Department of Immunology

A fundamental characteristic of multicellular biology is the continual turnover of specialized cells. These cells are characterized by their unique combination of transcribed RNA, proteins—such as membrane-bound signals and transcription factors—and spatial localization. Together, these properties generate unique cell types with specialized functions that interdependently maintain the multicellular organism. Historically, immunology focused on a diverse group of cells specialized for pathogen elimination. Early studies primarily investigated white blood cells such as T cells or macrophages[1]; however, there is now a broad appreciation that immune function depends on communication not only among these cells but also with non-hematopoietic cells. Central to this dialogue are secreted proteins, such as cytokines, chemokines, and growth factors, which collectively create an environment that supports the generation and activation of cells critical to an immune

response. This coordinated signaling is exemplified in the immune response against a parasitic worm (helminth), where epithelial and lamina propria cells act in concert to initiate and sustain anti-helminth immunity.

Soil-transmitted helminths (STHs) mature and reproduce in the small intestine, where the primary immune response is enacted. Helminths are detected by tuft cells, a rare specialized epithelial cell that produces interleukin (IL)-25 and cysteinyl leukotrienes (cysLTs). These mediators act synergistically to activate group 2 innate lymphoid cells (ILC2s) which in turn drive helminth clearance. Activated ILC2s secrete IL-5 and -13, characteristic cytokines of type 2 immunity. These interleukins coordinate hallmarks of the type 2 immune response such as increased muscle contraction, mucus secretion, and tuft cell hyperplasia. Among these, tuft cell hyperplasia is critical to the worm clearance, not just for the amplification of pathogen detection, but also for increased production of tuft cell-derived effector molecules. This expansion depends on IL-4/13 signaling within the small intestinal epithelium (SIE) and can increase tuft cell frequency up to 10-fold. Yet, despite the magnitude of this response, how IL-4/13 supports the expansion of tuft cells remains unclear.

We show that tuft cells across all tissues express the receptor tyrosine kinase KIT, a growth factor known to support cell division, differentiation and survival in multiple cell types. We find that IL-4/13 is necessary and sufficient to upregulate KIT on small intestinal (SI) tuft cells. While epithelial KIT is dispensable for homeostatic turnover, KIT deletion from tuft cells during helminth infection reduces tuft cell hyperplasia and delays helminth clearance. Mechanistically, KIT signaling supports the generation of new tuft cells in SIE crypts. These findings identify a novel tuft cell-specific function for KIT in type 2 immune responses and highlight the coordinated efforts of cytokines and growth factors in establishing and maintaining immunity.

Contents

KIT Supports Small Intestinal Tuft Cell Hyperplasia *1*

Contents *6*

List of figures & tables *9*

Acknowledgements *11*

Chapter 1: Introduction *14*

1.1 The small intestinal epithelium interfaces with the outside environment **14**

1.2 Small intestinal stem cell produces two cellular lineages **15**

1.3 Cellular communication by secreted proteins **19**

1.4 Helminths initiate type 2 immunity in the small intestine **20**

1.5 Tuft cells are rare sentinels that initiate helminth immunity **22**

1.6 KIT expression supports cellular influence **24**

1.7 Dissertation objectives and significance **28**

Chapter 2: KIT supports small intestinal tuft cell hyperplasia *29*

2.1 Introduction **29**

2.2 Results Tuft cells express KIT systemically at homeostasis **32**

Epithelial KIT is dispensable in the homeostatic small intestine 35

IL-4/13 is necessary and sufficient to induce KIT on small intestinal tuft cells. 38

KIT promotes tuft cell hyperplasia during helminth infection 42

KIT is largely dispensable for tuft cell effector function, survival, and migration 46

KIT is required after lineage commitment but before complete maturation of tuft cells 52

KIT ligand is constitutively available in the small intestine 57

Akt phosphorylation in tuft cells does not require KIT 58

2.3 Discussion 65

2.4 Acknowledgements 70

Funding 70

Author Contributions 70

Chapter 3: Material and methods 71

Experimental animals 71

Generation of KIT10 ($Kit^{fl/fl}$) mice 71

Genotyping 72

In vivo stimulation and treatment 72

Helminth infections and analysis 72

Tissue immunofluorescence preparation and analysis by microscopy 73

RNAScope 74

KIT inhibition blocks tuft cell hyperplasia and helminth expulsion 74

Single-cell suspension preparation 75

Flow Cytometry 76

RNA sequencing 76

Monolayer and Enteroid Culture 77

Reverse transcription and quantitative PCR 78

Statistical analysis 78

Chapter 4: Summary, more speculation and future directions 79

Integrating RTK signaling, tissue context, and KIT regulation 79

Significance of KIT10 mice 81

KIT is a growth factor used in response to acute damage 81

Summary 82

References 84

List of figures & tables

Introductory 1. Cellular fate determination into secretory and absorptive lineages. 18

Introductory 2. Schematic overview of the small intestinal epithelium. 26

Introductory 3. KIT and SCF. 27

Figure 1. Tuft cells express KIT systemically at homeostasis. 33

Figure 2. Epithelial KIT is dispensable for cell proliferation and secretory cell emergence in the homeostatic small intestine. 36

Figure 3. IL-4/13 is necessary and sufficient to induce KIT on small intestinal tuft cells. 39

Figure 4. KIT promotes tuft cell hyperplasia during helminth infection. 44

Figure 5. KIT promotes the generation of tuft cells rather than their effector function. 49

Figure 6. KIT is required early in committed tuft cells to support hyperplasia. 54

Figure 7. KIT is dispensable for tuft cell Akt phosphorylation, yet KIT inhibition impairs the tuft-ILC2 circuit. 60

Supplement 1 (Related to Figure 1). 34

Supplement 2 (Related to Figure 2). 37

Supplement 3 (Related to Figure 3). 41

Supplement 4 (Related to Figure 4). 46

Supplement 5 (related to figure 5). 51

Supplement 6 (related to Figure 6). 57

Supplement 7 (Related to Figure 7). 62

Table S 1. RNA sequencing data of *Il4ra*;*Pou2f3-CreERT2*. 42

Table S 2. Mouse lines. 62

Table S 3. Oligonucleotides. 63

Table S 4. Antibodies. 64

Table S 5. Reagents and software. 65

Acknowledgements

The collaboration between poet Ross Gay and artist Justin Vernon (Bon Iver), “Catalog of Unabashed Gratitude” became some kind of early cornerstone in my time with the lab. There’s a line in it that gave me a child-like joy: “It makes me squirm like a worm, I am so grateful.” I would be watching parasitic worms squirm around on top of freshly fileted small intestines and that line struck me with a feeling I couldn’t immediately articulate. Squirming, a visceral reaction from pent-up energy, can come from discomfort, but in its usage here, it’s a reaction to communal hard work paying off. An appreciation for the way generational contributions can build a more inviting, loving, nurturing and, generally, better world for those inhabiting it. It’s overflowing gratitude coming from overcoming challenges and engaging in hard work.

This Ph.D. was not easy for me. Part of the challenge was being pushed to confront areas in my life where I want to grow. What do I want to do with my interests? How much care do I need to take on myself? And how do I do all that? Where big questions—maybe too big at times— but they gradually took shape. And in the months leading up to writing this, I have felt deep gratitude. It feels really special to reflect back on something I committed to do in my early twenties and feel not only a sense of accomplishment, but also that I’ve grown in ways I was hoped to, and beyond what I expected. The work in this dissertation is the fruit of the past six years, but more than that, it is the product of the people who shared this time of life with me. I mean that with full sincerity.

Jakob— or in honor of my early attempts to sway the lab “J”, “J-dawg”, and “J-man”— has been a generous mentor and adviser throughout this process. I may have initially been influenced by our shared appreciation of Bon Iver when deciding to join the lab, but it turned out to be an excellent fit. Jakob prioritized mentorship: he read and thoughtfully edited my grants and manuscript, and he met me wherever I was in my scientific development, adapting his guidance as I grew. He was timely and attentive, even while in Germany studying naked mole rats as we were resubmitting our manuscript. He supported my creatively and was patient

with both my learning and natural fluctuations in productivity over the years. He taught me how to infect a mouse and make enteroids. And, in celebration of finishing our TA-ship, he showed up to my (and the other TAs') doorstep with a cocktail and a sweet treat—a gesture that felt especially warm during a gloomy autumn day sometime in COVID isolation. He celebrated with each of us whenever we accomplished something. And, to my genuine surprise given my "discerning" palate, he made the lab one of the best whiskey sours I've ever had. Jakob, thank you for your care, your attention, your consistency and your mentorship. You've inspired me to be a better leader and a better scientist.

To the Moltke lab—both the one I joined and the one it has become— thank you for the community we made together. To Jack, for modeling what it looks like to be an engaged and critical scientist in meetings. To Marija, for your mentorship and warm company— for looking out for the younger lab members and brining in excitement and cheer to my day-to-day. To Tyler, for our shared culinary and outdoor adventures, and for conversations about science, meaning and art over lunch. To Aloe, for sharing dreams, being a fun and supportive desk mate, and exemplifying strength and resilience. To Macy, for your friendship during COVID times, the summer before you left for med school, and that one time after my general where you got me a hotdog and I dropped it. To Shan, for science discussions, sharing your knowledge and experience and making Thigh Guy Summer 2022 a reality. To Margaret, for cultivating enthusiasm for science and supporting the lab so thoughtfully. To Thornton, for your curiosity of questions and appreciation of play in life. To Lily for, your good company, our conversations about music, letting me complain about journal club and being a wonderful desk neighbor. To Maddie, for your thorough and thoughtful help in the last stage of the paper—it would not be as strong or as considered without your help. To Shealyn, for your eagerness and help in some of the last steps of the revision. To Deb, for your enthusiasm for learning and the incredible food you share. To the fifth floor, especially Tighe and Alejandra who have made these last year's welcoming, playful and enjoyable. To the broader immunology student community, for sharing our frustrations, ideas, our fun late nights, making an

impromptu puppet show play, jumping into lake union and supporting each other throughout the years. And to the department, for the support and continuing to grow.

I've been so fortunate to have many good people around me. There's more to say than space allows, so I'll be brief. Curtis and Jenna, thank you for your continued friendship, care, sharing of art, letters and poems. To those in Seattle, who have been great support throughout the years with a special shout out to Marlena, Evan, Rachel (RVG), Victoria, and Elya. To the Tucson community, for being there for me when I visit and your continued support these past years. To the quad squad boys—James, Kyle, and Bobby—for the Mondays we'd link up to "get that dub". To my brothers, Alan, Asael and Haziel for that warzone pandemic-era community and the time we carved out to be together. To my parents for emphasizing education and for encouraging me to give up my dreams of being a professional soccer player and pursue higher education. And finally, to the many people who shaped my learning, patience, gentleness, curiosity, sense for adventure, bravery, courage to oppose those who hurt the disparaged, and empathy—in college, in childhood, and the less established passing moments. Thank you…oh, and thank you to the ant, for inspiring me to look closely and stay curious.

Chapter 1: Introduction

1.1 The small intestinal epithelium interfaces with the outside environment

The small intestinal epithelium (SIE) is a single-cell barrier tissue that balances nutrient absorption, microbial tolerance and pathogenic clearance. This balance is maintained by the rapid turnover of the intestinal epithelium and its constituent cell types. The SIE cells can be broadly divided into two categories that balance the contradictory functions of the SIE: absorptive enterocytes facilitate nutrient uptake while secretory cells such as the Paneth, enteroendocrine, goblet and tuft cells facilitate microbial tolerance and pathogenic clearance. Microbial tolerance and protection are primarily mediated by the secretory compartment. Goblet cells secrete mucus that forms an additional physical and biochemical barrier while also contributing to antigen uptake [2–5]. Paneth cells, residing in the crypt base, secrete antimicrobial peptides (AMPs) that shape the composition of the intestinal microbiota and can additionally defend against pathogenic microbes [6]. The spatial organization of the small intestine is seemingly designed to guard and protect the progenitor cells: stem and progenitor cells reside deep within the pocket-like crypts, where they are sheltered from the lumen yet positioned to respond rapidly to damage or inflammatory cues. As these cells differentiate, cells migrate upward along the crypt-villus axis to repopulate the surrounding villi that project into the lumen. This architecture not only ensures the regenerative capacity of the barrier but also provides rapid and dynamic remodeling in response to infection.

For both human and mice, the small intestine (SI) represents one of the largest surface areas in direct contact with the external environment. Despite its name, the small intestine is long; it was named small only because its diameter is narrower than that of the large intestine (colon). Along its length, the SI is highly vascularized, supporting efficient nutrient absorption and rapid dissemination of those nutrients. While the organ performs a

unified function, its regions are structurally and physiologically diverse. Historically the SI has been divided into three regions listed in order from proximal (near the stomach) to distal (by the cecum): duodenum, jejunum and ileum. While a widely adopted nomenclature, these divisions are anatomically vague and suggest divided anatomical and functional sections as opposed to continuous gradients[7]. Recent advances in single-cell RNA sequencing have now resolved five, sometimes overlapping, regions with distinct cellular programing [8]. Additionally, proximal-distal variation in villus length and microbial load further supports the presence of spatially organized functional compartments within the SI [5]. Taken together, these spatial and functional zones underscore that the SI is not a static tissue, but one dynamically maintained. This dynamism is in large part due to the continual generation and differentiation of epithelial cells.

1.2 Small intestinal stem cell produces two cellular lineages

The small intestinal epithelium is one of the fastest self-renewing tissues in mammals and must withstand constant mechanical and chemical stress while remaining the primary site for metabolite and water uptake[9]. This unique resilience is partly dependent on the high proliferative rate of epithelial cells. In the pocket-like crypts, adult stem cells (ASCs) divide frequently collectively producing an estimated 32 grams of cellular mass every 80 days in a 70 kg adult human making for one of the highest rates of cellular turnover in mammals[10].

Early widely-adopted concepts of ASC were shaped by the study of hematopoietic stem cells (HSCs), whose importance became evident when reductions in white blood cell counts were noted after the atomic bombing of Hiroshima[11]. The hematopoietic system, one of circulating cells, fostered a view of ASCs as rare, quiescent cells that divide asymmetrically and undergo strictly hierarchical unidirectional differentiation. However, this framework does not fully apply to solid tissue ASCs, including those in the SIE, which are integrated within a structural niche, receiving continuous mechanical and biochemical signals from the extracellular matrix and surrounding stromal cells [9]. More generally, ASCs are undifferentiated cells defined by their capacity for self-renewal, proliferation, and generation of differentiated progeny, as well as their ability to

regenerate tissue after injury[12]. In the SIE, abundant ASCs marked by expression of leucine-rich repeat-containing G-protein coupled receptor 5 (LGR5), divide daily and are thought to divide symmetrically[13,14]. While $LGR5^{+}$ stem cells can self-renew and generate fully differentiated epithelium in vitro, the resulting organoids (enteroids) lack villus structures and require exogenous growth factors. These limits likely reflect the absence of key signals normally provided by the extracellular matrix and stromal cells [15].

Although the established model holds that $LGR5^{+}$ cell divide symmetrically to maintain the stem cell pool, an emerging body of literature suggests additional complexity. Symmetric division of small intestinal stem cells (SISC)—where a stem cell generates two stem progeny—is supported by the observation that confetti-labeled crypts drifted towards clonality, but this concept has been challenged by a mathematically-derived asymmetric model [16–19]. Moreover, evidence that cells in the isthmus, the region between the crypt base and villus base, can repopulate $LGR5^{hi}$ cells suggests the presence of a more plastic precursor population [13,20,21]. Further support for an isthmus-residing ASC comes from observations that epithelial regeneration persists after acute ablation of $LGR5^{hi}$ cells, and that $LGR5^{+}$ cells alone do not consistently give rise to organoids [20–24]. These findings have led to two prevailing paradigms: either 1) a stem cell population resides within the crypt isthmus, distinct from the $LGR5^{hi}$ crypt base columnar (CBC) cell, or 2) the $LGR5^{hi}$ CBC is the primary homeostatic stem cell and isthmus residing cells can return to a stem cell state under certain conditions such as irradiation or tissue injury. While the precise organization and hierarchy of the ASC(s) in the SIE remains under active investigation, the central principle is consistent: crypt-resident ASCs continuously divide to replenish the villus epithelium, and the balance of differentiated cells that emerge is shaped by both SIE intrinsic and extrinsic factors.

Induction of cellular division of the stem cell begins with the accumulation of β-catenin supported by Wnt signaling, LGR5, and R-spondins[25]. After division, the first determinant of cell fate lies in Notch signaling: Notch ligands, DLL1 and DLL4, are provided by Paneth cells and if a cell receives the ligand by close proximity to the Paneth cell it is fated towards the absorptive lineage. Notch signaling promotes differentiation

towards the absorptive lineage by inducing Hairy and enhancer of split 1 (*Hes*1) which in turn represses ATOH1[26]. This is a type of lateral inhibition where Notch-activated cells adopt one fate and simultaneously prevent neighboring cells from adopting the same fate[27]. In the absence of Hes1-mediated repression, ATOH1 drives differentiation towards a secretory lineage with the notable exception of tuft cells, which can differentiate even in an ATOH1 knockout (**In. 1**) [28,29]. As cells differentiate, they reduce LGR5 expression and most cells migrate upwards towards the villus with exception of Paneth cells that migrate to the crypt base.

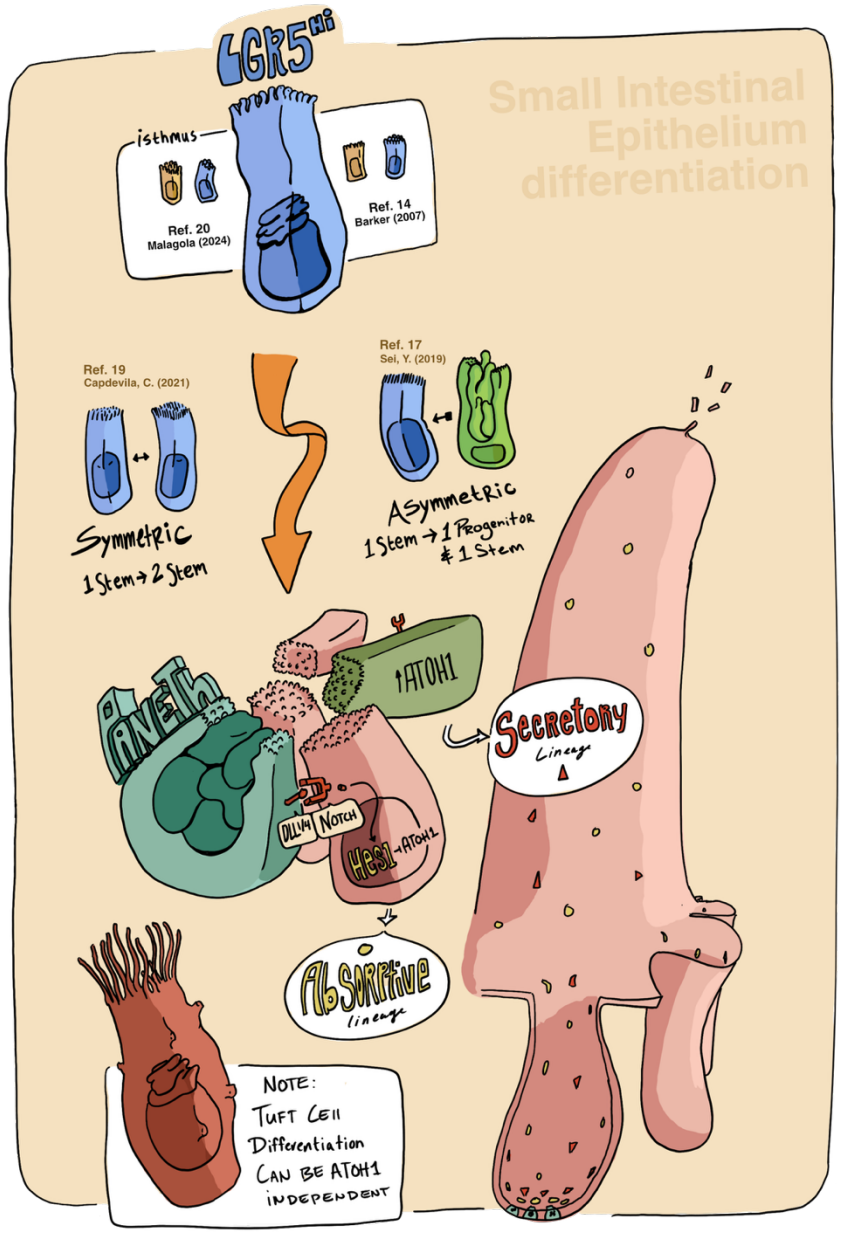

Introductory 1. Cellular fate determination into secretory and absorptive lineages.

Small intestinal epithelial cells that receive Notch ligands, DLL1 or DLL4, upregulate Hes1 that inhibits ATOH1. Hes1 fates a cell towards the absorptive lineage while ATOH1 initiates secretory cell differentiation. Notably, in ATHO1 knockouts, tuft cells can still differentiate, suggesting additional complexity.

1.3 Cellular communication by secreted proteins

The word cytokine was initially coined in appreciation for the broader impact that soluble polypeptides can have on not just lymphocytes (lymphokines), but non-lymphatic compartments[30]. Cytokines are diverse, pleiotropic and potent extracellular signals that drive inflammatory and immune responses. They can promote cell proliferation, differentiation, migration, modulate receptor expression, and even induce cell death. Among their effects, a specialized group known as growth factors (GFs) represent signals that support cellular, proliferation, differentiation and survival [31]. Growth factors are not defined by association with inflammation or immunity, but rather their ability to drive cellular growth programs. Nonetheless, many GFs act as critical supports to inflammatory and immune responses. Growth-promoting signals often act through receptor tyrosine kinases (RTKs) that enable complex and pleotropic intracellular kinase cascades that ultimately integrate environmental cues to guide cell fate[32]. Other major classes of secreted proteins include interleukins (ILs), chemokines, hormones and neuropeptides—each descriptive of their primary source, dominate function, or cellular communication partners. For example, interleukins signal between leukocytes, whereas chemokines induce chemotaxis [33]. Together, these secreted mediators create dynamic intercellular communication networks that regulate homeostasis and coordinate immune responses.

Importantly, cytokines rarely function in isolation. Rather they operate within layered signaling networks in which the receptor expression, spatial positioning, ligand availability, and timing collectively determine cellular—and consequently tissue level— responses. While cytokines can be produced by many cell types, a major conceptual shift in immunology came with the identification of helper T (T_h) cell subsets (type 1 and 2) defined by their cytokine profiles (interferon-gamma and IL-4, respectively) [34]. This solidified the idea that distinct cytokine programs could drive distinct immune responses. Understanding what activates these T cell subsets, when and how long they take to secrete cytokines, and how their signals are integrated to direct an immune response has been key to our understanding of immunity. Subsequently, the discovery of innate counter

parts to T_h cells provided further insight [35]. Innate lymphoid cells (ILCs) can rapidly produce signature cytokines in the absence of antigen receptor signaling, enabling timely, antigen-independent initiation of "types" of immune responses. Among them, group 2 ILCs (ILC2s) are the innate analogs of T_{h2}s. The identification of activators of ILC2s, IL-25 and IL-33, marked a turning point in understanding type 2 immunity[36]. Thus, at this point in history, type 2 immunity (among the other types) is recognized as a multi-cellular circuit in which cell producing "alarmin" cytokines like IL-25 or IL-33 activate ILC2s, ILC2-derived cytokines shape the early tissue response and adaptive T_{h2} cells reinforce and extend this immune response, while also providing immune memory.

1.4 Helminths initiate type 2 immunity in the small intestine

Helminths are a type of nematode (roundworm) that is infectious and parasitic. They can be transmitted by an insect vector (like a mosquito), ingested through the consumption of an infected host, crawl into the skin when stepped on, and ingested through fecal-contaminated soil; the latter two routes define soil transmitted helminths (STHs). STHs alone are among the most infectious agent worldwide with recent estimates at 1.5 billion people infected, and if left untreated these can pose a major health burden, especially on children[37]. Helminth infections are often chronic, and host immunity is rarely complete, and when left undertreated in children cognitive impairment can happen along with increased risk of vitamin A deficiency and forms of inflammatory bowel disease (IBD)[38,39].

Mouse models remain our most tractable and well-characterized systems for studying the immune response to helminths. Two infection models dominate the field: *Heligmosomoides polygyrus bakeri* (HPB), a chronic model native to the mouse, and *Nippostrongylus brasiliensis* (NB) which isn't native to the mouse, but provides an acute model with an infectious course of about a week in control, wild-type animals [38]. In both models, STHs ultimately reside in the small intestine where they enter adulthood and reproduce. While HPB is ingested through fecal contaminated material, NB is primarily acquired transcutaneously, though oral infection

is possible. NB is a hookworm that begins as a rhabditiform larvae (L1) hatchling feeding on bacteria in warm and moist soil where it moults twice to develop into its infective strongyloid larve (L3)[40,41]. L3 larvae penetrate the skin or enter by hair follicles, migrating via the blood stream to the lungs, where they mature into L4 larvae. These are then coughed up, swallowed, and enter the small intestinal lumen, where they mature into adulthood (L5).

Although type 2 immune responses to helminths occur in the lung, the small intestine is the major site of type 2 inflammation to these parasitic worms[42]. There, tuft cells, a rare epithelial cell and secretory family member, sense helminths and release IL-25 and cysteinyl leukotrienes (CysLTs) that activate ILC2s inducing their proliferation and release of type 2 cytokines, IL-13 and IL-5[43–45]. IL-13 can increase muscle sensitivity to acetylcholine, making it hypercontractile, and signals on the epithelium to bias differentiation towards goblet and tuft cell fates (**In. 2**)[44,46,47]. As smooth muscle contracts, goblet cells increase mucus production, and tuft cell release acetylcholine that induces fluid secretion and reduces helminth fitness[48,49]. Together, these responses amplify the protective effects of mucus in this coordinated process known as "weep and sweep" which is effective at clearing some intestinal helminths.

Type 2 immunity, however, is not restricted to helminths. Over a century ago, in their attempt to induce tolerance to toxins, Charles Richet and Paul Portier instead uncovered an unexpected "contrary protection" termed anaphylaxis. Unlike the protection achieved through early vaccination attempts against pathogenic microbes, animals sensitized to a toxin responded to re-exposure with a heighted, sometimes lethal, reaction that exceeded their initial response. This distinct form of sensitization revealed an unfamiliar arm of immunity, labeled allergy or "other work"[50,51]. Decades later, these reactions were connected to type 2 cytokines, ILC2s and Th2 cells. Today, type 2 immunity is understood to be induced by a wide range of stimuli including pollen, heavy metals, peanuts, antibiotics, crystals, and dust mites. Broadly, these triggers fall into two categories: macro-parasites and allergens[52]. Type 2 immunity is biologically ancient. Characteristic molecular signatures

are detectable in early jawed vertebrates such as teleost fish[53], suggesting that this program evolved from wound-healing pathways. Because wound-healing relies on coordinated signaling among stem cell compartments and diverse cell types, this evolutionary origin may explain why type 2 immunity coordinates responses not only across individual cells but across entire organ systems. Unlike type 1 and 3 (ILC3/Th17) immunity, type 2 immune activation does not follow classical structural recognition theory in which pathogen-associated molecular patterns (PAMPs) engage pattern recognition receptors (PRRs) to trigger immune responses [54,55]. Instead, many type 2 stimuli exert shared functional effects on the tissue environment—such as protease activity and cellular damage— suggesting a more context-dependent mode of recognition. Damage associated molecular patters (DAMPs), including IL-25, IL-33, and thymic stromal lymphopoietin (TSLP), are central initiators of type 2 immune responses and signal extracellular stress or injury, reinforcing this context-dependent recognition theory[56]. Recent findings further support this framework. A pore-forming complex (Aeg-S/Aeg-L) derived from the mold allergen *Alternaria alternata* was identified as a key inducer of allergic responses to this fungus, with pore formation enabling the release of IL-33 in the airway[57]. Although this is a major advance in the field, not all allergens—including house dust mites and pollen— possess pore-forming activity. Thus, how these allergens are sensed and which cells mount the allergic cascade in the lung remain important open questions.

1.5 Tuft cells are rare sentinels that initiate helminth immunity

Initiators of immune responses, whether adaptive or innate, are constrained by rare specificities, signal integration, and tissue context. Naïve antigen-specific T cells are numerically scarce and require coordinated T-cell receptor (TCR), costimulatory, and cytokine signals for productive activation[58–60]. In parallel, innate sentinels such as dendritic cells and ILCs rely on regulated access to microbial and damage-associated patterns, complex assembly of PRR signaling, and tissue-derived cytokines, growth factors, and metabolites[61,62]. Together, these layers ensure that both arms of immunity are only engaged when multiple cues are received,

adding tiers of regulation that prevent aberrant immune responses to benign environmental antigens or self-antigens . This concept remains true in type 2 immunity and is highlighted in the immune response to helminths. Tuft cells are homeostatically rare epithelial cells and though in the SIE they are uniquely poised to produce potent activating signals including IL-25, acetylcholine, cysLTs, and prostaglandins, these signals require coordination with other cells to take effect[63].

Tuft cell differentiation is a tightly regulated process that depends on the transcription factor (TF) POU2F3, the only TF known to be necessary for tuft cell development[47,63]. POU2F3 does not act alone; instead, it operates with the co-factors POU2AF2 (OCT-T1) and POU2AF3 (OCA-T2/COLCA2), which enhance its transcriptional activity[64–67]. POU2AF2 (C11orf53/OCA-T1) is required for tuft cell differentiation in the small intestine as mice with a homozygous deletion of *Pou2af2* fail to develop tuft cells. The requirement of POU2AF3 for tuft cell development remains incompletely understood [65]. Together, POU2F3 and its cofactors are thought to induce the tuft cell transcriptional signature that includes *Dclk1*, *Il25*, *Il4ra*, *Il13ra*, and *Kit*[68].

Tuft cells share this POU2F3-dependent development and, largely, this transcriptional program across all tissues in which they develop, yet their function seems to be tissue dependent. Tuft cells develop across many hollow organs—including the small and large intestine, gallbladder, upper airways, urethra and thymus—where they act as chemosensory cells. In the airway (brush cell/solitary chemosensory) they act as innate immune sensors triggering protective reflexes and recruiting innate cells[69,70]. In the gallbladder and extrahepatic biliary tree, tuft cells can induce a weep and sweep response upon sensing a bacterial metabolite or act as regulator of immunity dampening neutrophilic infiltration [71,72]. In the small intestine, tuft cells induce a type 2 immune response when they detect succinate released as a metabolite from bacteria or protists. While tuft cells commonly sense and help coordinate an organ-level response, the response isn't always uniformly inflammatory. Their-tissue dependent roles, cellular network, and environmental context shape the outcome of tuft cell activation and can result in remarkably different responses.

Although tuft cells can develop in the lung after injury, their most dramatic expansion occurs in the helminth-infected small intestine[44,73,74]. Tuft cell hyperplasia (expansion) requires IL-4RA/IL-13R1/STAT6 signaling, and even in enteroids IL-4/13 can selectively promote the differentiation of tuft cells[44]. Activation of this pathway promotes STAT6 *O*-GlcNAcylation optimizing tuft cell expansion[75]. In the absence of tuft cells, or even when tuft cell hyperplasia is impaired, worm burden is increased and clearance is dramatically delayed, underscoring the central role of tuft cells and their expansion in type 2 immunity[44,47]. While some negative regulators of tuft cell hyperplasia have been identified such as CRTH2 and Spi-B, the upstream signals that coordinate the expansion of tuft cells remain unknown[76,77].

1.6 KIT expression supports cellular influence

KIT (c-KIT, SCFR, CD117) is a type III receptor tyrosine kinase (RTK) placing it within the same structural and functional family as platelet-derived growth factor receptors (PDGFRA & PDGFRB), FLT3, and macrophage colony-stimulating growth factor receptor (CSF1R). Like other type III RTKs, KIT contains five extracellular immunoglobulin-like domains, a single transmembrane domain (encoded by exon 10), and an intracellular split tyrosine kinase domain that becomes activated though ligand-induced dimerization and auto phosphorylation (**In. 3**). Ligand-induced KIT dimerization occurs rapidly[78]— and triggers four well established signaling routes: phosphatidylinositol 3'-kinases (PI3Ks), Src family kinases, mitogen-activated protein kinase (MAPK) pathways (MAPK), and phospholipases. These pathways are highly integrated and do not act in isolation. Collectively, they promote cell proliferation, growth, survival and differentiation, and can even support specialized effector functions such as priming mast cells for degranulation[79]. For example, PI3K generates the second messenger phosphatidylinositol 3,4,5-trisphosphate (PIP 3) which serves as a membrane scaffold that recruits proteins with a pleckstrin homology (PH) domain, including the serine/threonine kinase Akt. Akt is a key pro-survival factor that suppresses apoptosis initiation and activates the mTOR complex[80].

KIT signaling can be attenuated by intracellular degradation, serine phosphorylation-mediated inactivation of the kinase domain, and tyrosine dephosphorylation.

KIT's primary ligand, SCF (Stem cell factor/Steel factor/Kit ligand/Kitl), is a homodimeric protein that exists in both membrane-bound and soluble forms. Both isoforms are encoded by *Kitl* and generated by alternative splicing: inclusion of exon 6 introduces a proteolytic cleavage that yields soluble SCF, whereas skipping exon 6 produces the membrane-bound form[81]. SCF is produced by endothelial cells, fibroblasts, keratinocytes, and smooth muscle cells[79]. Its expression can be upregulated by diverse stimuli, including UVB light in human epidermis, follicle stimulating hormone (FSH) in Sertoli cells (via cAMP), and inflammatory cues in small intestinal epithelial cells in humans with colitis and mice with DSS-induced colitis[82–85]. Subcutaneous administration of recombinant SCF to humans induces melanocyte hyperplasia, increased local pigmentation, and mast cell activation [86]. For further details on SCF- KIT biology and expanded discussion of these pathways, see reference 81 for an excellent review.

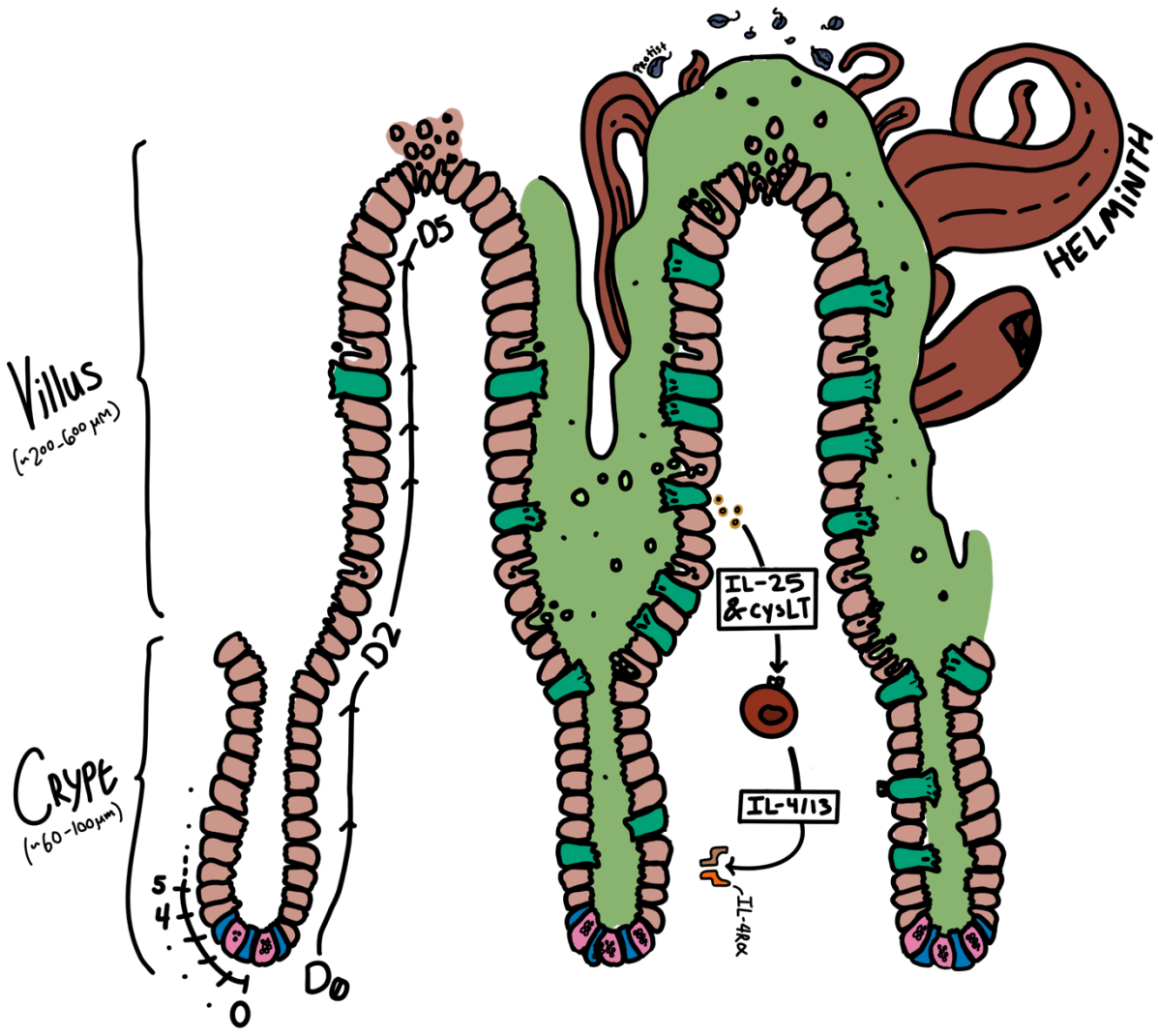

Introductory 2. Schematic overview of the small intestinal epithelium.

Small intestinal epithelial cells are generated in the crypt and populate the villi with a turnover of 3-5 days [14]. This turnover is unchanged between homeostatic (left) and type 2 inflamed (green, right), but with IL-4/13 secreted from ILC2s (red) tuft cells, labeled as the green cells, expand.

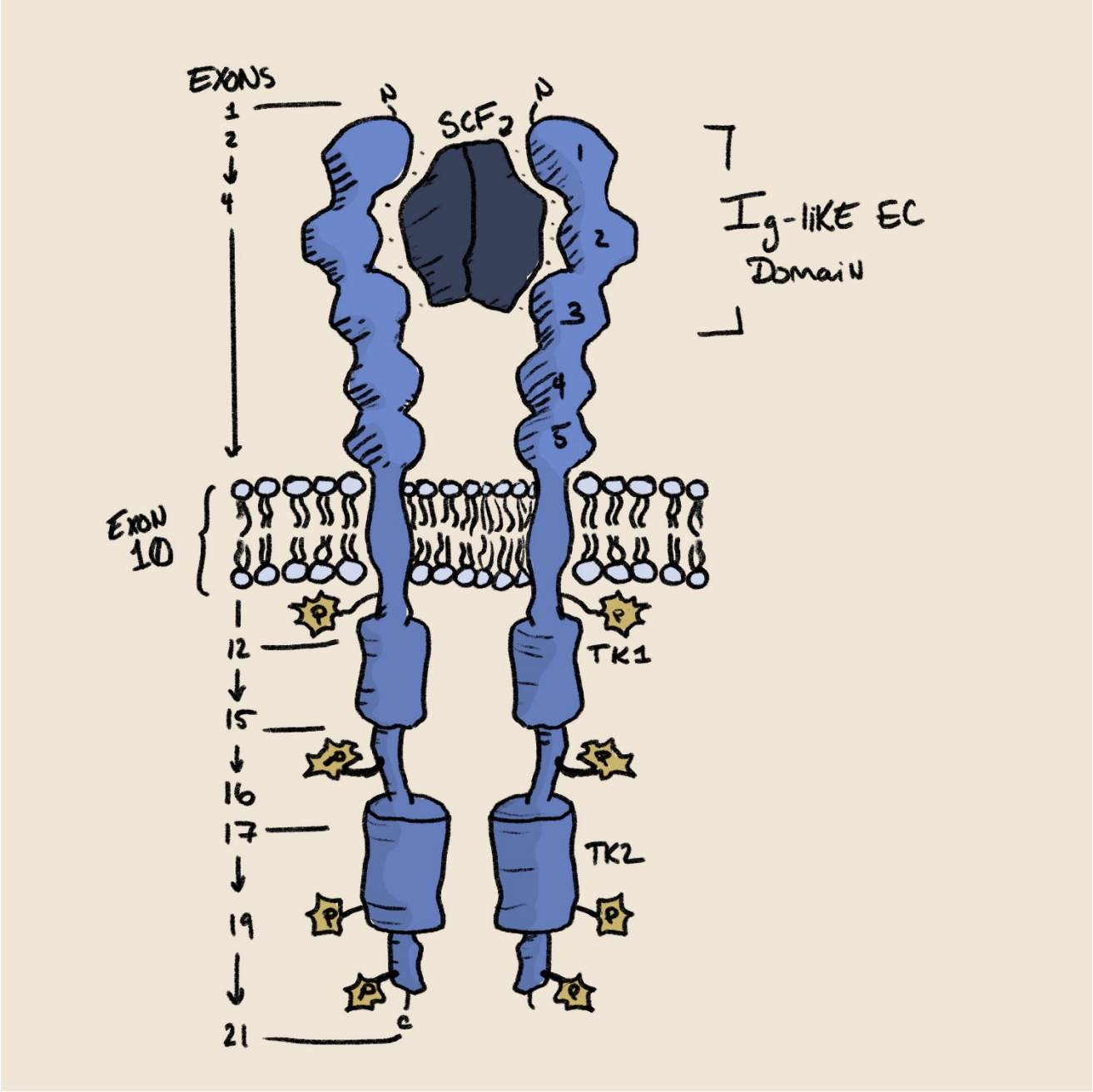

Introductory 3. KIT and SCF.

Kit is comprised of 21 exons that are translated in the indicated regions of KIT (see left). Protein translation begins at the immunoglobulin-like (Ig-like) extracellular (EC) domain then into transmembrane domain (exon

10) and finally the intracellular tyrosine kinase (TK) domain. Both KIT and SCF function as homodimeric proteins where SCF enables KIT homodimer to form and auto phosphorylate to induce its cellular programing.

1.7 Dissertation objectives and significance

This project was conceptualized from the RNA sequencing data presented as Fig. S3A-C. In this dataset, we observed differential gene expression specifically when tuft cells lacked IL-4/13 signaling, (using a POU2F3-driven deletion system). This finding suggested that tuft cells continue to receive IL-4/13 signaling even after commitment to the tuft cell lineage. Among the genes changed, *Kit* emerged as a compelling candidate, as KIT is a growth factor receptor known to regulate cell proliferation and differentiation. *Kit* induction by IL-4/13 suggested a potential mechanism for the dramatic cell expansion in tuft cell hyperplasia characteristic of type 2 immunity. We explored that possibility and I describe the outcome of these efforts here.

The central focus of this dissertation is to define the role of KIT in type 2-induced small intestinal tuft cell hyperplasia and to place this mechanism in the broader framework of how cytokines cooperate to establish an effective immune response. Helminth infection offers a powerful and rich model for this work. Understanding anti-helminth immunity carries direct relevance for the nearly one quarter of the global population infected with soil-transmitted helminths. Moreover, the type 2 immune pathways engaged during a helminth infection overlap extensively with those underlying allergic disease, providing a tractable system in which to study cellular coordination driving hypersensitivity responses. Finally, because helminth immunity requires dramatic remodeling of small intestinal epithelial, this model system can also provide insight into epithelial cell biology, with implication for conditions characterized by altered epithelial turnover or growth factor signaling, including like inflammatory bowel disease (IBD) and gastrointestinal stromal tumor (GIST).

Chapter 2:

KIT supports small intestinal tuft cell hyperplasia

This chapter is adapted from the following publication:

Lara HI, Bell MR, O'Connor S, von Moltke J. KIT supports tuft cell hyperplasia. Science Advances. (Under resubmission)

2.1 Introduction

The SIE is a single-cell layer that separates the intestinal lumen from the lamina propria and mediates nutrient absorption, microbial tolerance and exclusion of pathogens. Balancing these diverse functions requires careful coordination of cellular differentiation that tune the cellular composition, and thus, the function of the SIE. During type 2 immune responses triggered by helminth infection, IL-4 and/or IL-13 drive a 10-fold expansion of the epithelial tuft cell lineage that is required for immune protection [44,47]. Despite the magnitude of this tissue remodeling, the mechanisms that initiate and sustain tuft cell hyperplasia remain poorly defined.

The SIE is folded into two anatomically distinct repeated cellular compartments: small, pocket-like crypts and large villi that extend into the lumen. Stem and progenitor cells reside within the crypts where they proliferate and replenish the surrounding villi[14,87]. The mouse SIE is populated by five major cell types, each of which can be assigned to the absorptive or secretory lineage. Absorptive enterocytes facilitate nutrient and fluid uptake and comprise about 80% of the SIE at homeostasis[88]. Secretory enteroendocrine, Paneth, goblet, and tuft cells are defined by their specialized secreted products such as hormones, mucus, and cytokines[14].

Cell division and differentiation occur in the crypts after which most lineages migrate to the villus tips and are expelled into the lumen. Paneth cells are the exception as they remain at the crypt base[11]. The balance between absorptive and secretory cells is largely determined by growth and patterning factors that direct the daily proliferation, differentiation and maintenance of the five major cell lineages. Wnt and epidermal growth factor (EGF) drive cell division at the crypt base, while bone morphogenetic protein (BMP) antagonizes Wnt signaling to allow cellular differentiation and specialization in the upper crypt region[28,89]. Other growth factors including glucagon-like peptide 2 (GLP-2) and granulocyte colony stimulating factor (G-CSF) have been linked to epithelial repair and can be induced by chemical or mechanical stress[90].

The small intestinal (SI) villus epithelium is replaced every 3-5 days, allowing for rapid adaptations through shifts in cellular composition[14]. For example, during parasitic worm (helminth) infection, the frequency of goblet and tuft cells increases, the latter by as much as 10-fold[44,47]. Goblet cells secrete mucus and RELMβ to reduce helminth attachment and fitness[38,91]. Tuft cells, commonly identified by their expression of doublecortin-like kinase 1 (DCLK1), function as both sentinels that detect helminths in the lumen and, once tuft cell hyperplasia occurs, as effectors that help to expel helminths from the intestine[44,47–49].

Both skin-penetrating hookworms, like *Nippostrongylus brasiliensis* (*N.b.*), and orally transmitted helminths like *Heligmosomoides polygyrus bakeri* (*Hpb)* settle in the SI lumen, where they mature and mate [38]. Here, tuft cells sense the worms and initiate type 2 immunity by secreting IL-25 and leukotriene C_4 (LTC_4) to activate group 2 innate lymphoid cells (ILC2s) in the SI lamina propria [44,45,47]. Activated ILC2s secrete IL-13, which signals crypt epithelial cells to promote differentiation into more tuft and goblet cells, thus completing a feed-forward “tuft-ILC2 circuit”. Tuft cell (and type 2 taste receptor cell) differentiation selectively depends on the transcription factor POU2F3 as *Pou2f3*$^{-/-}$ mice lack all tuft cells, but non-tuft epithelial lineages are unaffected[47,92]. In these mice, SI remodeling is reduced, and worm clearance is delayed.

How tuft cells sense helminths remains unknown, but during colonization with *Tritrichomonas* protists and in certain states of bacterial dysbiosis, the tuft-ILC2 circuit is activated when tuft cells sense luminal accumulation of succinate[93–96]. Tuft cell hyperplasia can also be induced by injecting recombinant IL-25 to directly activate ILC2s or by administering succinate in drinking water to directly activate tuft cells [44,94–96]. In all cases, tuft cell hyperplasia is dependent on IL-4 or IL-13 signaling directly on epithelial cells. These cytokines use a shared heterodimeric receptor consisting of IL4RA and IL13RA1 and are sufficient to induce tuft cell hyperplasia in SI-derived organoids (enteroids)[44,93,95,97]. Consistently, tuft cell hyperplasia does not occur when mice lack *Il4ra* selectively in epithelial cells [44]. BMP and butyrate can restrain tuft cell hyperplasia, while epithelial RANK signaling promotes tuft cell differentiation[98–100]. Other signals that act on the epithelium to support IL-4/13-induced tuft cell hyperplasia have not been identified.

KIT (c-Kit/CD117) is a transmembrane receptor tyrosine kinase that supports cell growth, function, and survival. Following dimerization of KIT by its ligand, stem cell factor (SCF), transphosphorylation at tyrosine residues can activate multiple signaling pathways including the phosphatidylinositol 3-kinase (PI3K) signaling cascade[81,101,102]. KIT is expressed by both stem and differentiated cells across multiple tissue types and organs. In the SI, it is constitutively expressed by neuronal pacemaker cells (interstitial cells of Cajal; ICCs) and Paneth cells[103,104]. KIT has been shown to act as a regenerative factor in dextran sulfate sodium (DDS)-induced colitis, during which it is thought to induce stem cell-like reprograming of Paneth cells[84]. Some colonic crypt epithelial cells lacking the Wnt receptor and stem cell marker LGR5 also express KIT and can repopulate the epithelium, especially in regenerative states [105].

Mast cells, key effectors of type 2 immunity, rely on KIT, as demonstrated by the lack of mast cells in mice with hypomorphic *Kit* alleles (e.g. $Kit^{W\text{-}sh/W\text{-}sh}$)[106]. Type 2 immunity defects in $Kit^{W\text{-}sh/W\text{-}sh}$ mice have generally been interpreted to result from this lack of mast cells, but the pleiotropic functions of KIT make such conclusions difficult in the context of germline mutations that affect all cells[79,107–110]. *Kit* expression has also

been noted in mouse and human tuft cells, but its function in this context remains unclear[111,112]. Here, we generated KIT floxed mice ("KIT10") to characterize the SIE-specific role of KIT. We show that while epithelial KIT is dispensable for SIE homeostasis, during a type 2 immune response it is upregulated by IL-4/13 and required in committed tuft cells to achieve full tuft cell hyperplasia.

2.2 Results

Tuft cells express KIT systemically at homeostasis

Having previously identified IL-4/13 signaling and alternative splicing of *Pou2af2* as small intestinal epithelium (SIE)-intrinsic regulators of tuft cell differentiation and hyperplasia [44,66], we searched for additional regulators of these processes. We and others noted *Kit* expression in datasets from human and murine tuft cells as well as tuft cell-like carcinomas[112–115]. Reanalysis of our previously published bulk RNA sequencing data revealed *Kit* expression in homeostatic tuft cells across all tissues surveyed, with the highest transcript reads in the gallbladder and trachea, and the lowest in the SI and its non-tuft epithelium (Fig. 1A)[95]. Immunofluorescence labeling confirmed KIT protein expression on at least some tuft cells (identified as $DCLK1^+$) in all tissues tested (Fig. 1B). We also confirmed previous reports that some $DCLK1^-$ cells in the colonic crypt epithelium express KIT[104,105].

Given the critical role of SI tuft cells in helminth infection, their unique ability to expand during SI type 2 inflammation, and a body of literature linking KIT to anti-helminth immunity[107,109], we focused further analysis on SIE KIT. Consistent with prior reports, we found that Paneth cells constitutively express KIT, whereas $LGR5^+$ stem cells do not (Fig. S1A)[84]. Flow cytometry analysis revealed that proximal (defined here as the first 5-12 cm from the stomach) and distal (last 5-12 cm before the cecum) regions of the SIE contained similar frequencies of tuft cells, but KIT expression was significantly higher in distal tuft cells by proportion and per-cell expression (Fig. 1C-F). Altogether, a subset of tuft cells homeostatically expresses KIT protein in all tissues examined.

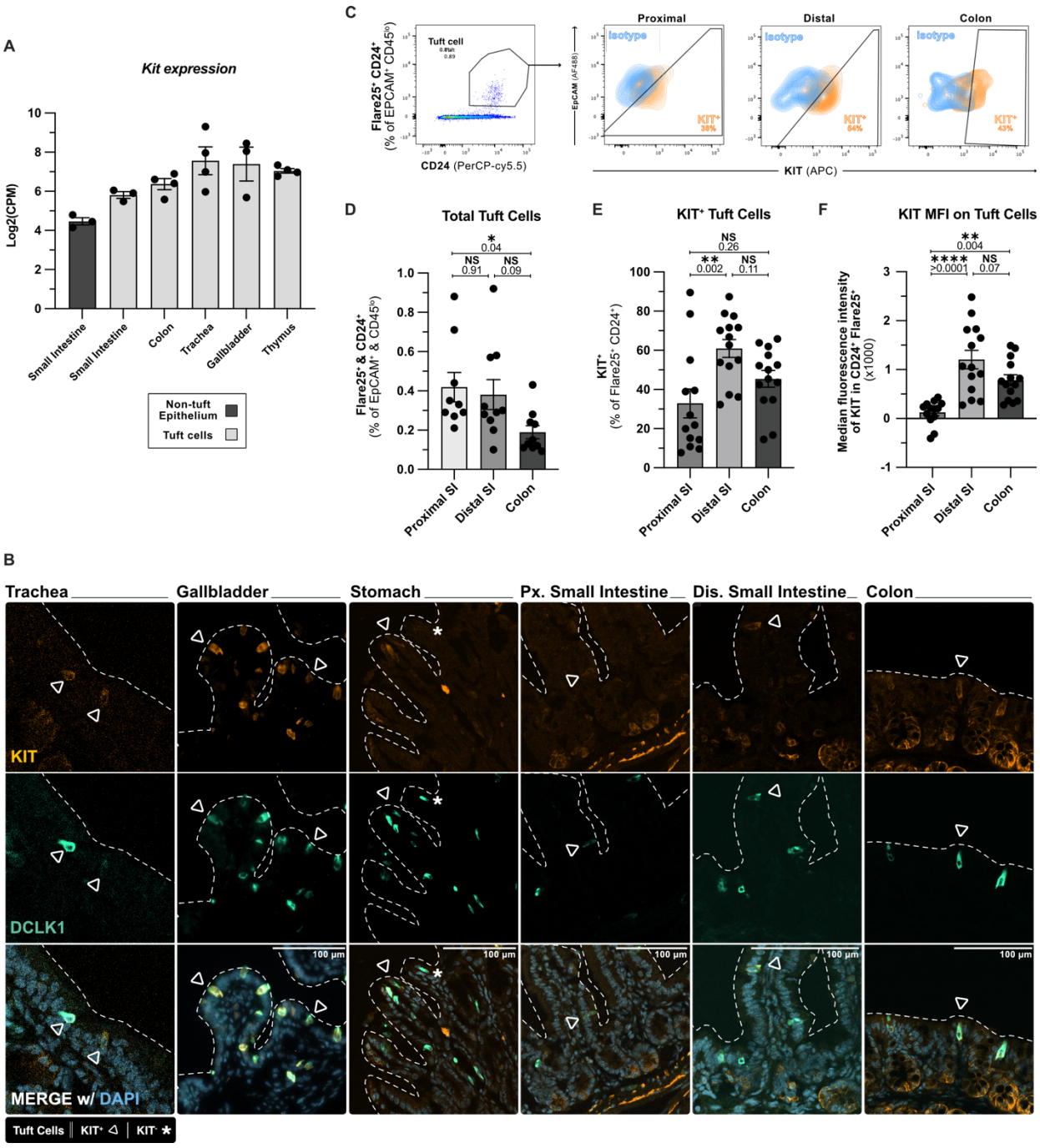

Figure 1. Tuft cells express KIT systemically at homeostasis.

(**A**) Normalized RNA transcript reads in tuft cells and non-tuft epithelium sorted from indicated tissue of unmanipulated Flare25 (Il25RFP/RFP) mice. Adapted from Ref #95. (**B**) Immunofluorescent images of

indicated tissues from unmanipulated wildtype C57BL/6 mice stained as indicated. (**C-F**) Flow cytometry analysis of intestinal epithelium taken from the proximal 5 cm of small intestine, distal 5 cm of small intestine and proximal 5 cm of colon of unmanipulated Flare25 (Il25RFP/RFP) mice. (C) Representative tuft cell gating and KIT expression. (D) Total tuft cell frequency. (E) Frequency of KIT+ tuft cells. (F) Median fluorescent intensity (MFI) of KIT among tuft cells. MFI of the tissue isotype control was subtracted from the sample. In graphs, each datapoint represents a biological replicate. Data are pooled from at least 2 experiments (A, D-F) or representative of at least 3 experiments (B, C). Statistics: ordinary one-way ANOVA (D-F).

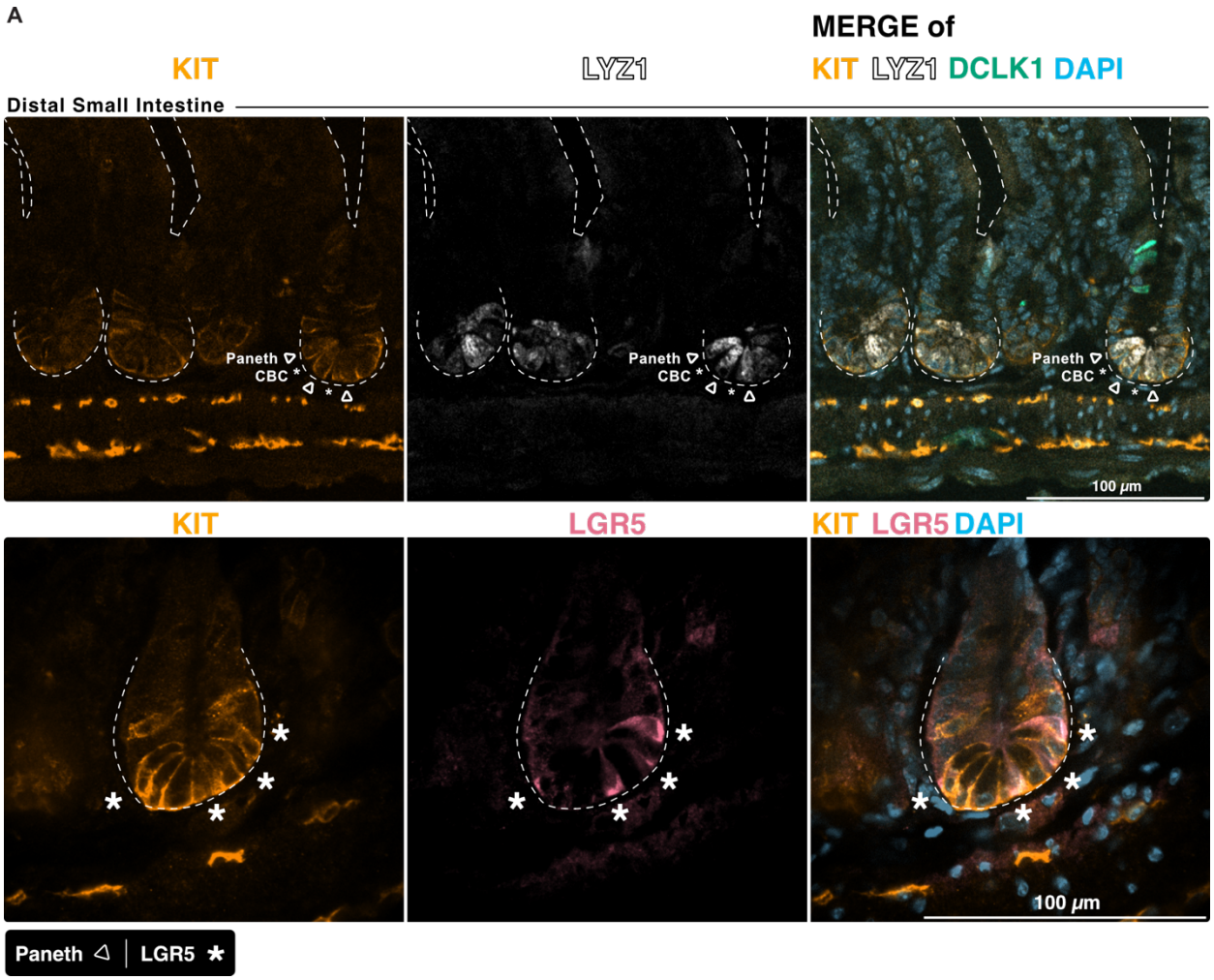

Supplement 1 (Related to Figure 1).

(**A**) Immunofluorescent imaging of indicated proteins in distal (last 10 cm) small intestine from unmanipulated wildtype mice. * = examples of Lysozyme 1 (LYZ1)$^{+}$ Paneth cells; arrowheads = examples of CBC by absence of LYZ1 (upper) or presence of LGR5 (lower). CBC = crypt base columnar cell. Data are representative of 2 experiments.

Epithelial KIT is dispensable in the homeostatic small intestine

KIT inhibitors and mice carrying loss of function *Kit* mutations have demonstrated that KIT contributes to the division, migration, and/or survival of many cells[79]. For example, stem-like function of Paneth cells was reduced in mice treated with a KIT inhibitor[84]. One limitation of these studies, however, is the indiscriminate and/or incomplete targeting of KIT. To genetically test the function of KIT specifically in the SIE, we used CRISPR/Cas9 editing of mouse embryos to insert *loxP* sites flanking exon 10, which encodes the transmembrane domain of KIT (Fig. 2A; S2A). We call this the "KIT10" mouse line. We first crossed KIT10 mice with *Vil1-Cre* mice to delete KIT from SIE stem cells and all differentiated progeny. We validated the deletion by immunofluorescence staining of homeostatic SI tissue and flow cytometry analysis of tuft cells from the SI and SI-derived enteroids (Fig. 2B-D; S2B). Mice lacking SIE KIT had no difference in body weight, SI length and overnight 5-ethynyl-2'-deoxyuridine (EdU) uptake (Fig. 2E-G). Furthermore, *Vil1*-Cre^{+} KIT10 mice had no homeostatic defects in secretory cell differentiation as tuft, Paneth and goblet cell frequencies were identical to wildtype littermates (Fig. 2H-J). Thus, SIE-expressed KIT is dispensable for SI function, cellular turnover, and differentiation at homeostasis.

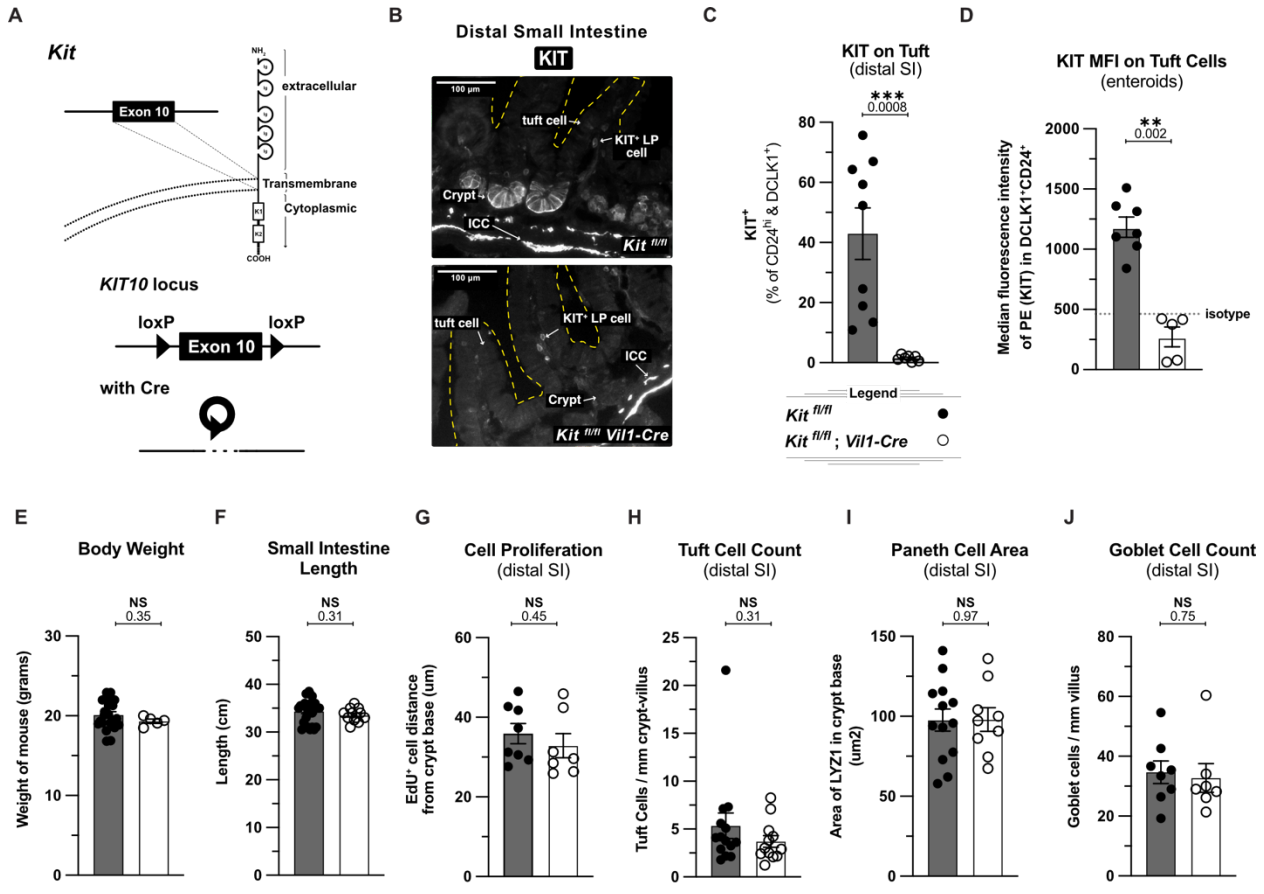

Figure 2. Epithelial KIT is dispensable for cell proliferation and secretory cell emergence in the homeostatic small intestine.

(**A**) Schematic of Cre-Lox targeting of *Kit*. (**B**) Immunofluorescent (IF) imaging of KIT in distal (last 10cm) small intestine from unmanipulated mice of indicated genotypes. ICC = interstitial cell of Cajal; LP = lamina propria. (**C**) Flow cytometric quantification of KIT on tuft cells ($DCLK1^+$ $CD24^+$) relative to an isotype control for KIT. Data from distal SI (10 cm section before the cecum) of unmanipulated mice of indicated genotypes. (**D**) Flow cytometric quantification of KIT median fluorescence intensity (MFI) on tuft cells from proximal (first 10cm) small intestine-derived enteroids maintained in culture for 7 days. (**E-J**) Analysis of indicated parameters in unmanipulated $Kit^{fl/fl}$ and $Kit^{fl/fl}$*;Vil1-Cre* littermates. In (G), mice were injected intraperitoneally

with EdU 17-20 hrs before analysis. In (H), tuft cells were identified by IF staining for DCLK1. In (I), Paneth cells were identified by IF staining for LYZ1. In (J), goblet cells were identified by IF staining with WGA. In graphs, each datapoint represents a biological replicate. Data are representative of 3 experiments (B) or pooled from at least 2 experiments (C-J). Statistics: unpaired t-test (C-J).

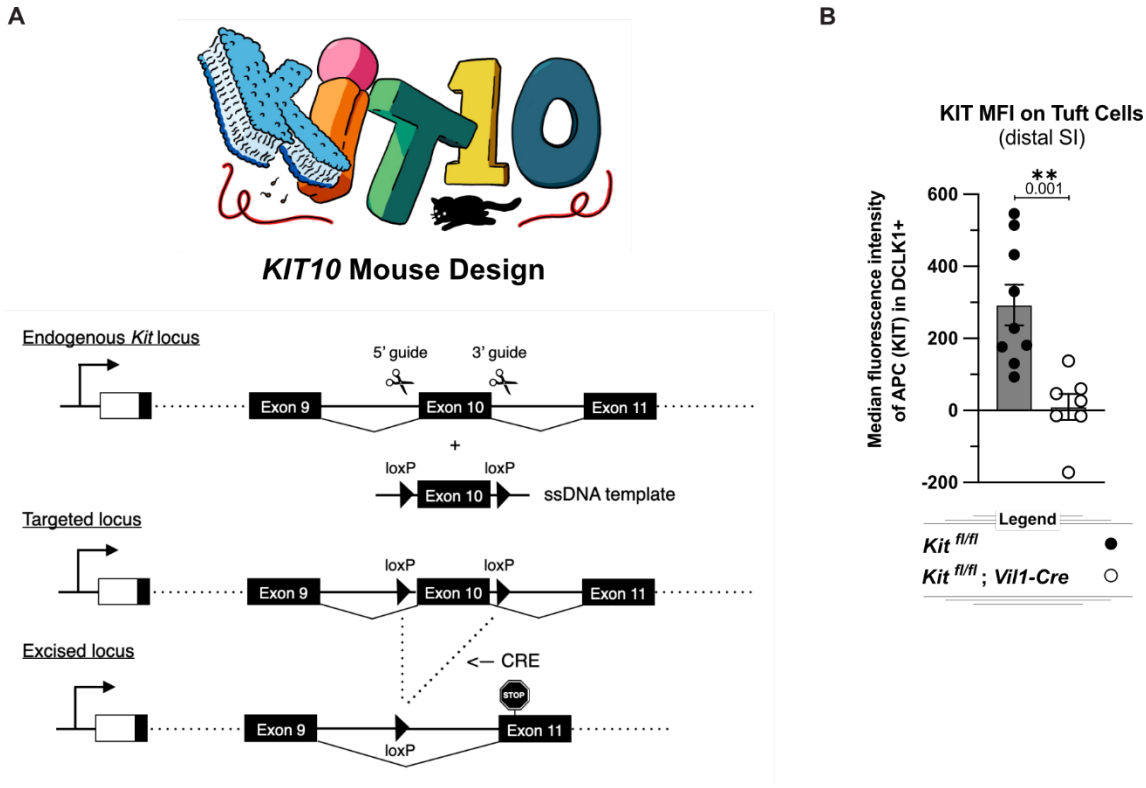

Supplement 2 (Related to Figure 2).

(**A**) Diagram of CRISPR/Cas9 targeting strategy to insert *loxP* sites flanking the transmembrane domain-encoding exon 10 of *Kit*. Splicing of exon 9 to exon 11 (if it occurs) gives rise to a stop codon. (**B**) Flow cytometric quantification of KIT MFI on tuft cells ($DCLK1^+$ $CD24^+$) from jejunum (10 cm section starting 20 cm before the cecum) of unmanipulated mice of indicated genotypes. Average isotype MFI was subtracted from each sample. Data are pooled from 2 experiments. Statistics: unpaired t-test (B).

IL-4/13 is necessary and sufficient to induce KIT on small intestinal tuft cells.

Given the central role of IL-4/13 in tuft cell expansion[44] and the high transcript expression of IL-4/13 receptor (*Il13ra1* + *Il4ra*) in tuft cells[113], we tested whether IL-4/13 modulates KIT on tuft cells. We first bulk sequenced SI tuft cells from mice with tuft cell-specific deletion of IL-4/13 receptors (*Il4ra*$^{fl/fl}$;*Pou2f3*$^{Cre\text{-}ERT2/+}$) and littermate controls. To enhance differences between the two groups, all mice were given tamoxifen 6 days prior to harvest to activate CRE function (and drive ablation of functional Kit) and stimulated with recombinant IL-4 complexed with anti-IL-4 antibody for the final 8 hours (Fig. S3A). *Kit* was the most significantly reduced transcript in the Cre^{+} (*Il4ra*-negative) tuft cells, suggesting upregulation of *Kit* by IL4RA/IL-13RA1 signaling in wildtype tuft cells (Fig. S3B-C; Table S1).

Next, we used immunofluorescence to label KIT protein in the SI of mice given succinate in their drinking water, infected with *N. brasiliensis* or *H. polygyrus bakeri*, or injected with recombinant IL-25 (rIL25), all of which are known to induce IL-4/13. Consistent with our bulk *Il4ra*-deficient tuft cell sequencing data, tuft cell KIT was upregulated when compared to naïve littermates (Fig. 3A; S3D). Indeed, during type 2 inflammation, KIT is present on tuft cells, Paneth cells and some DCLK1^{-} cells just above the crypt base, which could be immature tuft cells that do not express detectable DCLK1 or LGR5^{-} stem cells that reside in this region[20]. In the villi, KIT was detectable only on tuft cells and all tuft cells were marked by KIT. Using enteroids, we found that 10 ng/ml IL-13 was sufficient to induce KIT on >95% of tuft cells (Fig. 3B-D).

We also tested if IL-4/13 signaling is necessary for KIT upregulation on tuft cells using *Il4ra*$^{fl/fl}$;*Vil1-Cre* mice and littermate controls infected with *N. brasiliensis* or given succinate-treated water for 7 days. As previously reported, tuft cells failed to expand in the absence of *Il4ra* (Fig. S3E)[44]. Compared to controls, a smaller proportion of the remaining tuft cells expressed detectable KIT and the MFI of KIT on these cells remained at baseline in both helminth-infected and succinate treated mice (Fig. 3E-F; S3F). Together, IL-4/13 is both necessary and sufficient to induce KIT on tuft cells and perhaps Paneth cells and other crypt epithelial cells.

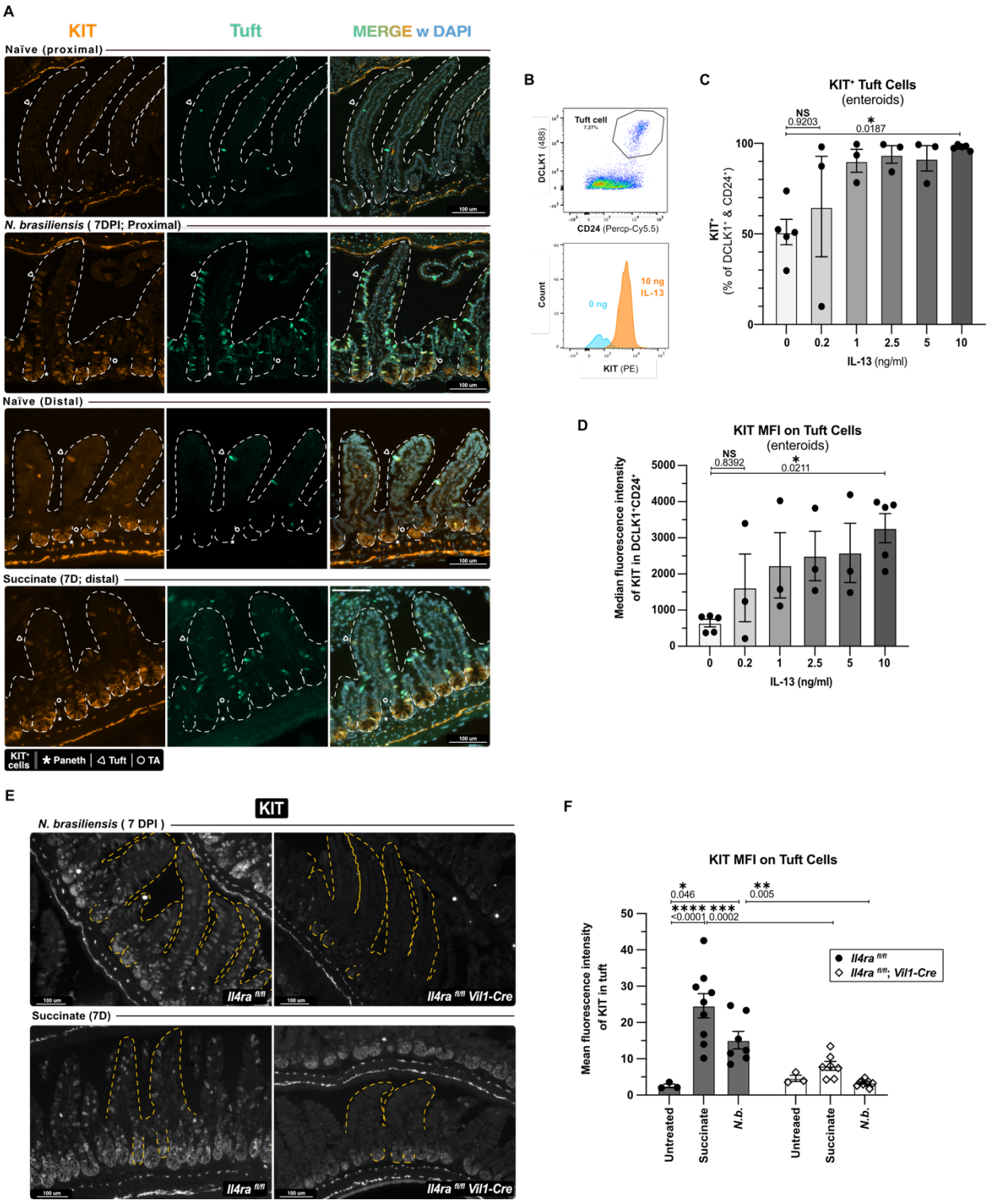

Figure 3. IL-4/13 is necessary and sufficient to induce KIT on small intestinal tuft cells.

(**A**) Immunofluorescent staining for indicated proteins in small intestine of wildtype mice treated as indicated. Proximal 12cm of the small intestine used for *N. brasiliensis* and distal 12cm for succinate. TA = non-tuft transit amplifying cell. (**B-D**) Flow cytometric analysis of small intestinal enteroids from wildtype mice treated for 7 days as indicated. (B) Representative gating of tuft cells and KIT expression. (C) Frequency of tuft cells ($DCLK1^+$ $CD24^+$). (D) MFI of KIT on tuft cells. (**E**) Immunofluorescent imaging of KIT in proximal small intestine of mice of indicated genotypes treated as indicated. (**F**) Mean fluorescence intensity (MFI) of KIT on tuft cells ($DCLK1^+$) from images in (E). D = days; DPI = days post infection. *N.b.* = *N. brasiliensis*. In graphs, each datapoint represents a biological replicate. Data are representative of at least 3 (A-B) or at least 2 (E) experiments or pooled from at least 2 (C-D, F) experiments. Statistics: ordinary one-way ANOVA (C, D) or two-way ANOVA (F).

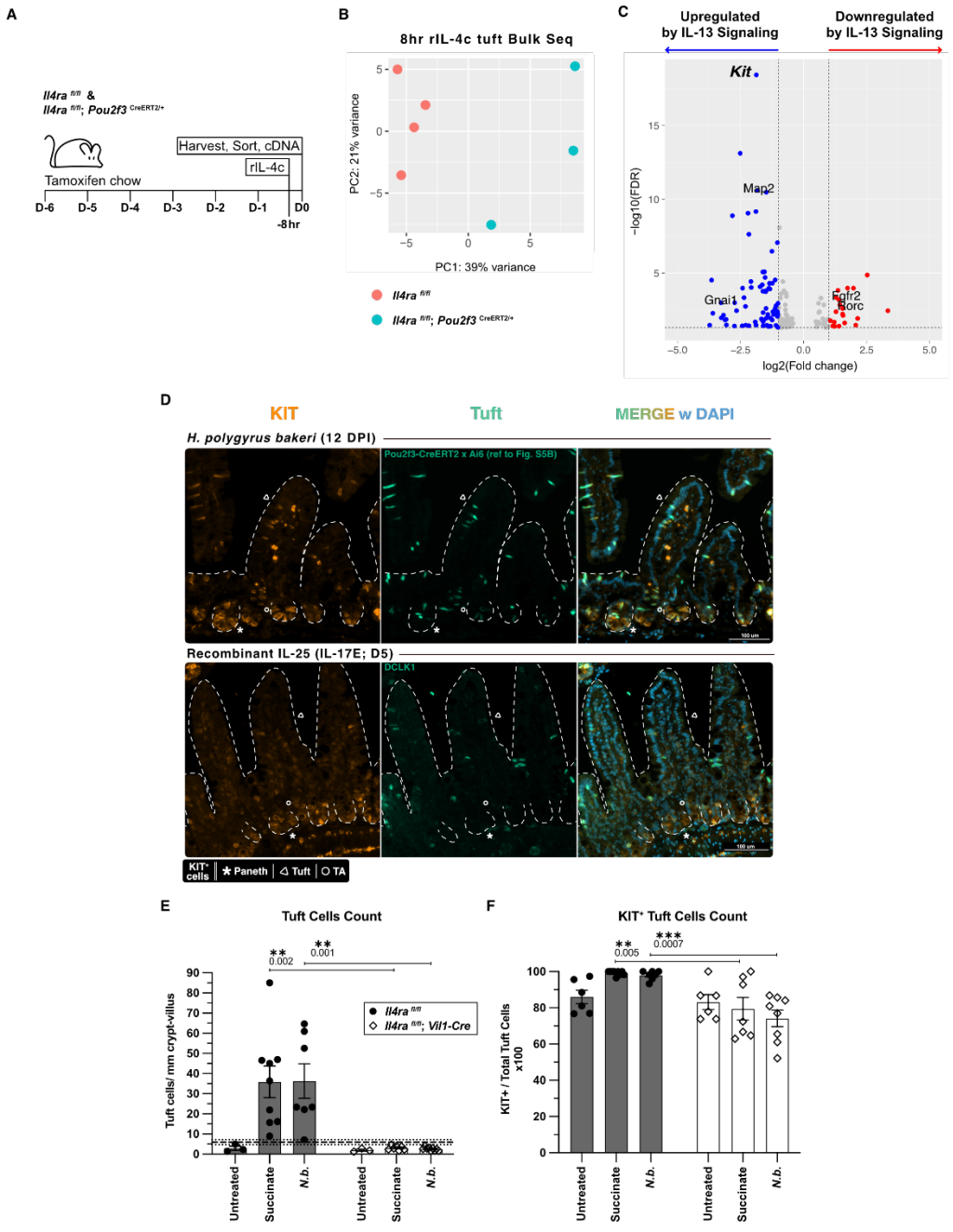

Supplement 3 (Related to Figure 3).

(**A**) Experimental schematic for RNA sequencing experiment. (**B**) Principal component analysis of samples generated in (A). (**C**) Volcano plot of differentially expressed genes from samples generated in (A). (**D**) Immunofluorescent imaging of indicated proteins in small intestine of wildtype mice treated as indicated. TA =

non-tuft transit amplifying cell**.** (**E-F**) Quantification of total tuft cells (DCLK1$^+$) (E) and KIT$^+$ tuft cells (F) in mice from Figure 3E-F. D = days; DPI = days post infection. *N.b.* = *N. brasiliensis*. In graphs, each datapoint represents a biological replicate; thick dashed line represents homeostatic tuft cell baseline calculated from a large cohort of unmanipulated wild-type mice with ± 1SEM (thin dashed line). Data are from 1 experiment (B-C), representative of 2 experiments (D), or pooled from at least 2 experiments (E, F). Statistics: Ordinary two-way ANOVA (E, F).

geneid	gene symbol	baseMean	log2FoldChange	lfcSE	stat	pvalue	padj
ENSMUSG00000005672	*Kit*	248.2499135	-1.873111951	0.18905273	-9.907881171	3.85E-23	3.71E-19
ENSMUSG00000085180	*AI838599*	98.061229	-2.512427387	0.29481352	-8.522090007	1.57E-17	7.56E-14
ENSMUSG00000030729	*Pgm2l1*	192.5101353	-1.82367596	0.23460953	-7.773238915	7.65E-15	2.46E-11
ENSMUSG00000015222	*Map2*	184.2345089	-1.479034234	0.1920904	-7.69967801	1.36E-14	3.29E-11
ENSMUSG00000108105	*Gm5340*	100.2189694	-1.889847108	0.25978168	-7.27475139	3.47E-13	6.70E-10
ENSMUSG00000027562	*Car2*	177.8382959	-2.199950012	0.30491749	-7.214902782	5.40E-13	8.68E-10
ENSMUSG00000028194	*Ddah1*	66.35026652	-2.820994206	0.39503925	-7.141047849	9.26E-13	1.28E-09
ENSMUSG00000030560	*Ctsc*	698.6072668	-0.956263911	0.13937231	-6.861218723	6.83E-12	8.24E-09
ENSMUSG00000060681	*Slc9a6*	56.86750418	-2.167605929	0.3238127	-6.69401148	2.17E-11	2.33E-08
ENSMUSG00000028657	*Ppt1*	409.8735329	-1.036967972	0.15991958	-6.484309007	8.91E-11	8.60E-08

Table S 1. RNA sequencing data of *Il4ra*;*Pou2f3-CreERT2*.

List of top 10 differential expressed genes.

KIT promotes tuft cell hyperplasia during helminth infection

We began testing the function of epithelial KIT in vitro by using enteroids. We treated enteroids derived from KIT10;Vil1-*Cre*$^+$ mice and littermate controls with rIL-13 and found equivalent tuft cell frequencies (Fig. S4A-B). Although an excellent model, enteroids do not fully recapitulate the complexities of the in vivo environment. Notably, enteroid cultures eliminate coordination between the SIE and non-epithelial cells [116] thereby disrupting endogenous growth factor gradients, which are replaced with high concentrations of exogenous growth factors such as EGF[117]. Moreover, enteroids lack spatial niches such as fully developed villi

and basal tensile interactions that influence SIE differentiation[118]. Therefore, we returned to in vivo models to further test the function of epithelial KIT.

We infected KIT10;*Vil1-Cre* mice and littermate controls with *N. brasiliensis* for 7 days and quantified tuft cells in the proximal SI by immunofluorescence microscopy. KIT was absent from all epithelial cells in Cre^+ mice (Fig. S4C), which had a partial (~ 35%) yet significant defect in tuft cell hyperplasia (Fig. 4A-B). This defect was more pronounced in the proximal SI—where the worms reside—than in the distal SI (Fig. 4C). Goblet cell hyperplasia, SI length, and total body weight were unaffected (Fig. 4D; S4D-E). We also did not find a change in worm burden, indicating that although they were reduced, tuft cell hyperplasia and associated type 2 inflammation remained above the threshold required for worm clearance (Fig. 4E).

To begin to define when KIT is needed and to minimize potential compensatory effects induced by deleting SIE KIT constitutively, we utilized *Vil1-Cre-ERT2* mice. Cre was activated 6 and 4 days prior to infection by tamoxifen gavage to acutely delete KIT (Fig. 4F; S4F). Here, tuft cell hyperplasia was reduced ~ 44% (Fig. 4G-H). As before, SI length and body weight were unchanged (Fig. S4G-H). There was a trend toward increased worm burden, though not statistically significant (Fig. 4I).

During succinate treatment, type 2 inflammation is predominantly localized to the distal SI and tuft cell hyperplasia does not reach the magnitude observed in helminth-infected mice[95]. In mice given succinate, constitutive deletion of KIT with *Vil1*-Cre caused no significant defects (Fig. S4I-L); however, there was a significant defect in tuft cell hyperplasia following inducible deletion (*Vil1-Cre-ERT2*) (Fig. S4M-N). Thus, KIT contributes to IL-4/13-induced tuft cell hyperplasia, especially in the proximal SIE of a helminth-infected mice, and this dependency is more pronounced following acute KIT deletion.

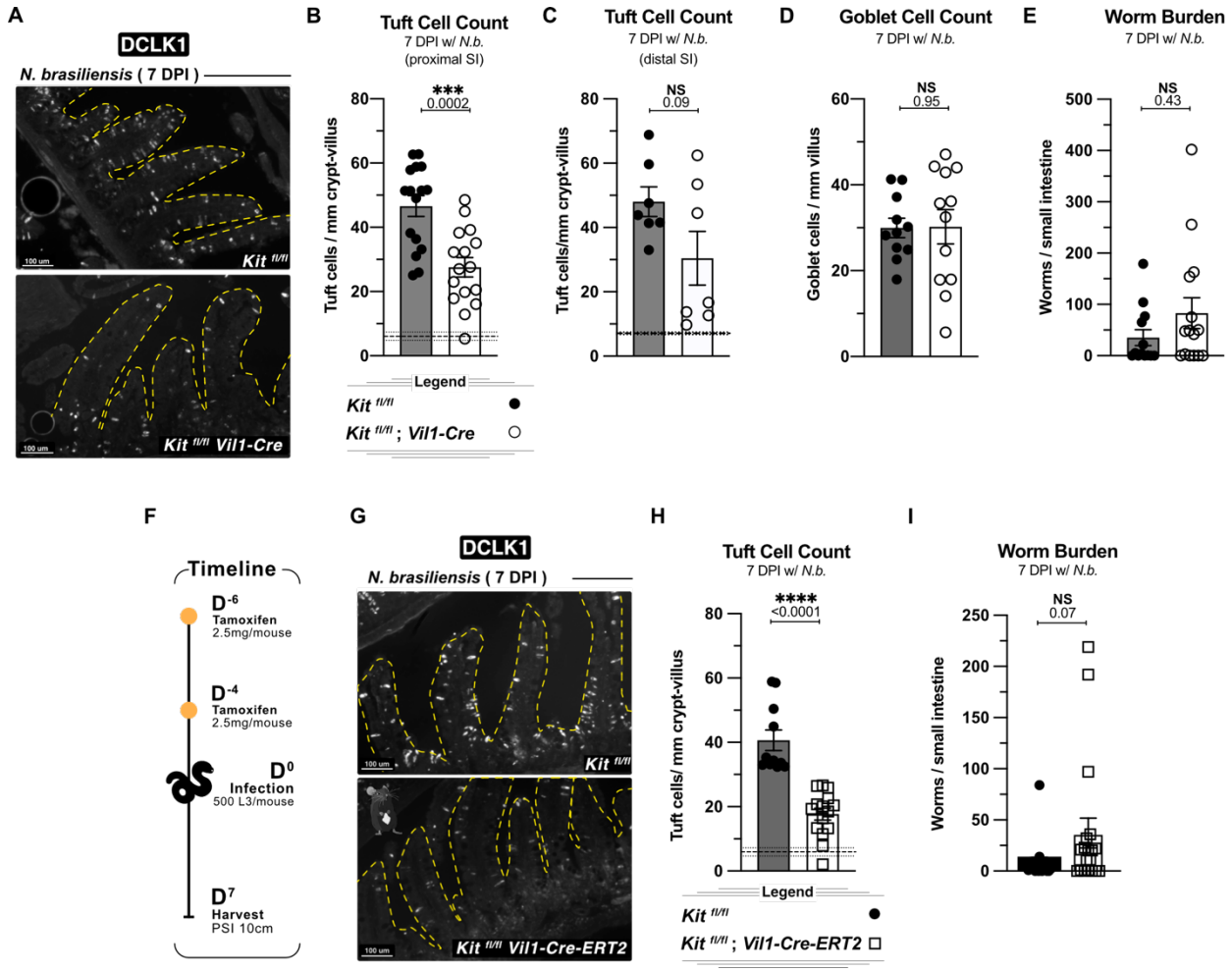

Figure 4. KIT promotes tuft cell hyperplasia during helminth infection.

(**A-E**) Analysis of *Kit*$^{fl/fl}$ and *Kit*$^{fl/fl}$*;Vil1-Cre* mice 7 days post *N. b.* infection. (A) Immunofluorescent. (IF) staining of tuft cells (DCLK1^{+}) in proximal small intestine. (B) Quantification of tuft cells from imaging in (A). (C) Quantification of distal (last 10-12 cm before the cecum) tuft cells from mice included in (B). (D) Quantification of goblet cells by IF staining (WGA^{+}). (E) Total worms counted in the small intestine. **(F-I)** Analysis of *Kit*$^{fl/fl}$ and *Kit*$^{fl/fl}$*;Vil1-Cre-ERT2* mice 7 days post *N. b.* infection. (F) Experimental schematic. (G) IF staining of tuft cells (DCLK1^{+}) in proximal small intestine. (H) Quantification of tuft cells from imaging in (G). (I) Total worms counted in the small intestine. D = days; DPI = days post infection. *N.b.* = *N. brasiliensis*. In graphs, each datapoint represents a biological replicate; thick dashed line represents homeostatic tuft cell

baseline calculated from a large cohort of unmanipulated wild-type mice with ± 1SEM (thin dashed line). Data are representative of at least 3 experiments (A, G) or pooled from at least 3 experiments (B-E, H-I). Statistics: unpaired t-test (B-D, H), Mann-Whitney test (E, I).

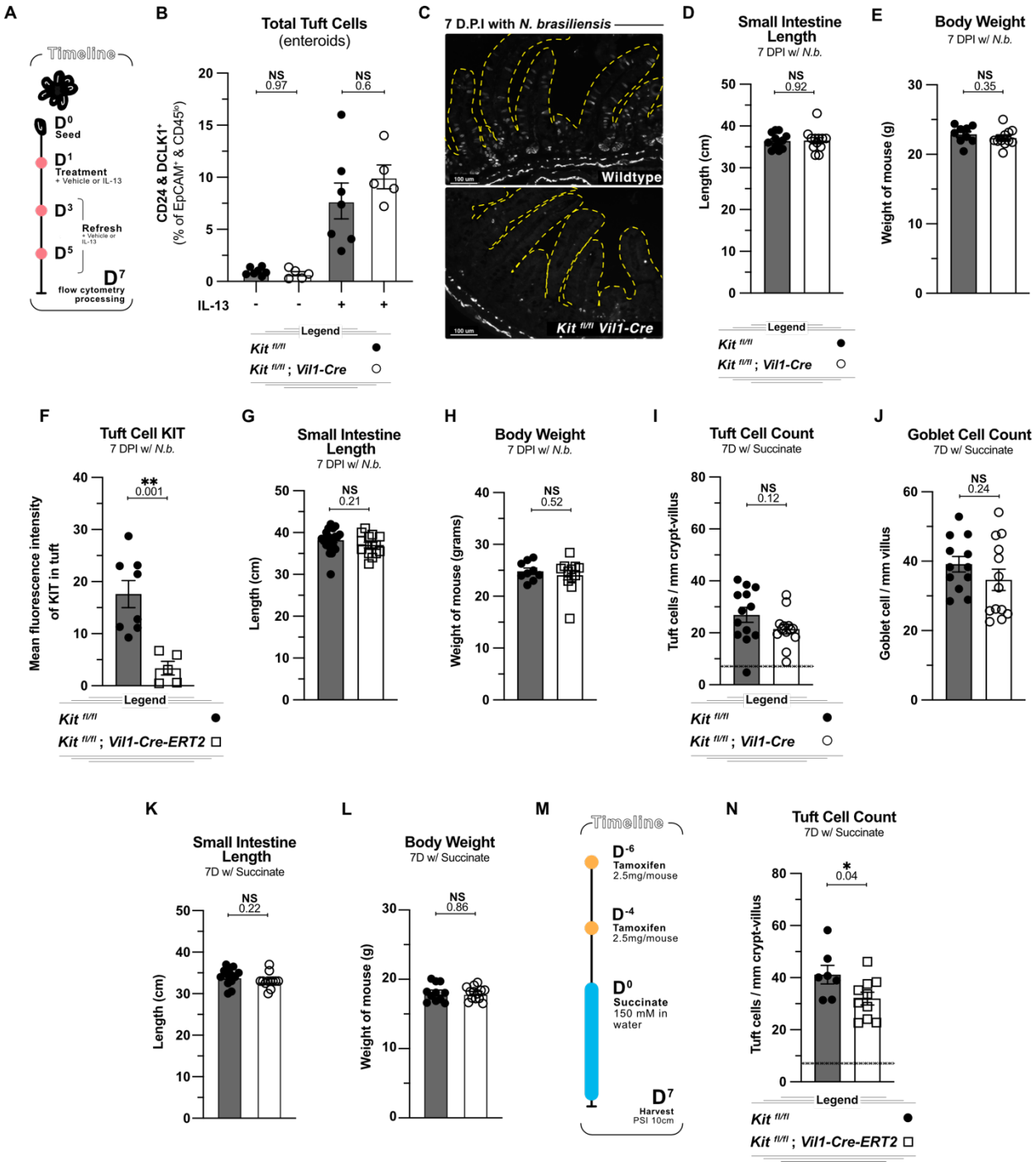

Supplement 4 (Related to Figure 4).

(A) Experimental schematic for proximal-derived enteroids in which "refresh" indicates a media change, with DMSO as the vehicle and IL-13 dosed at 10 ng/ml. **(B)** Flow cytometric quantification of tuft cells ($DCLK1^+$ $CD24^+$) in enteroids derived from the proximal small intestine of indicated mice and treated as indicated for ~1 week. (**C-E**) Analysis of $Kit^{fl/fl}$ and $Kit^{fl/fl}$*;Vil1*-Cre littermates 7 days after *N. brasiliensis* infection. (C) Immunofluorescent (I) staining of KIT in proximal small intestine. (D) Small intestinal length. (E) Mouse body weight. (**F-H**) Analysis of $Kit^{fl/fl}$ and $Kit^{fl/fl}$*;Vil1-Cre-ERT2* littermates 7 days after *N. brasiliensis* infection. (F) Mean fluorescence intensity quantification of KIT on tuft cells by flow cytometry. **(G)** Small intestinal length. (H) Mouse body weight. (**I-L**) Analysis of $Kit^{fl/fl}$ and $Kit^{fl/fl}$*;Vil1-Cre* littermates after 7 days of succinate administration. (I) Quantification of tuft cells by IF staining ($DCLK1^+$). (J) Quantification of goblet cells by IF staining (WGA^+). (K) Small intestinal length. (L) Mouse body weight. (**M-N**) Analysis of $Kit^{fl/fl}$ and $Kit^{fl/fl}$*;Vil1-Cre-ERT*2 littermates after 7 days of succinate administration. (M) Experimental schematic. (N) Quantification of tuft cells by IF staining ($DCLK1^+$). D = days. In graphs, each datapoint represents a biological replicate; thick dashed line represents homeostatic tuft cell baseline calculated from a large cohort of unmanipulated wild-type mice with ± 1SEM (thin dashed line). Data are representative of 3 experiments (C) or pooled from at least 2 experiments (B, D-L, N). Statistics: unpaired t-test (D-L, N), ordinary two-way ANOVA (B).

KIT is largely dispensable for tuft cell effector function, survival, and migration

KIT signaling has been linked to cell division, survival, migration and effector function across various cell types. Defects in any of these processes could be non-mutually exclusive explanations for the reduction in hyperplasia when tuft cells lack KIT. For example, decreased survival would directly reduce tuft cell frequency

while less IL-25 and LTC_4 release would indirectly reduce tuft cell hyperplasia by lowering ILC2 secretion of IL-13.

To test if KIT supports tuft cell production of LTC_4 in vitro, we cultured epithelial monolayers from KIT10;*Vil1-Cre*$^+$ mice overnight with or without rIL-13 and then stimulated for 30 minutes with ionomycin or vehicle to induce LTC_4 synthesis and release. rIL-13 stimulated monolayers produced more LTC_4, but there was no significant decrease in LTC_4 production from KIT-deficient monolayers, suggesting KIT is dispensable for LTC_4 production (Fig. S5A).

Because we have never been able to measure IL-25 release from tuft cells and LTC_4 release is difficult to measure quantitatively in vivo, especially at early timepoints, we used downstream ILC2 activation as a proxy for tuft cell effector function. *N. brasiliensis* larvae arrive in the SI about 2 days post infection (DPI) and ILC2s upregulate PD-1, Ki-67 and KIT starting 4 DPI (Fig. S5B-F). Using KIT10;*Vil1-Cre-ERT2* mice, we found that KIT and PD-1 upregulation were unchanged in KIT-deficient mice, while Ki-67 was partially decreased (Fig. 5A-C, S5G). Because reduced ILC2 proliferation may indicate reduced tuft cell effector potential, this result suggested that KIT might influence the release of tuft cell effectors that specifically regulate ILC2 replication. At the same time, it is difficult to identify proximal causes of defects in the feed-forward tuft-ILC2 circuit. For example, a defect in tuft cell differentiation from day 2-3 of infection could also result in reduced ILC2 activation on day 4 since there would be fewer tuft cells available to produce IL-25 and LTC_4. Thus, we sought to isolate epithelial effects by normalizing ILC2 activation. After four daily rIL-25 injections to hyper-stimulate ILC2s, *Il13* expression was induced at least as well in KIT-deficient mice as in littermate controls, yet *Pou2f3* transcript and tuft cell count were again decreased in the absence of KIT (~25%; Fig. 5D-F; S5H). Thus, while our results do not definitively rule out a role for KIT in tuft cell effector functions, it appears that KIT can influence tuft cell abundance even when ILC2 activation is normalized.

Within the epithelium, the extent of tuft cell hyperplasia is determined both by the generation of new tuft cells and by their survival within villi. To determine at which stage KIT supports tuft cell hyperplasia, we performed in vivo pulse-chase experiments using EdU, which is stably incorporated into the DNA of dividing cells. Because *N. brasiliensis* reach the intestine around 2 days post infection (DPI), we injected KIT10;*Vil1-Cre* mice and littermate controls with EdU 5 DPI, a timepoint when tuft cells are actively expanding and tuft cell hyperplasia is just emerging at the base of villi. One (6 DPI) or three (8 DPI) days later, we quantified total EdU^+ $DCLK1^+$ tuft cells (Fig. 5G-N). Although not statistically significant ($p = 0.14$ and 0.07, respectively) compared to littermate controls, we found an ~18% decrease in EdU^+ tuft cells in KIT-deficient mice at both timepoints. Since the defect was already apparent after the one-day chase period and did not increase two days later, we hypothesized that KIT is more likely to promote the generation of new tuft cells than the survival of mature tuft cells.

Of note, while analyzing these pulse-chase experiments, we found that EdU-labeled tuft cells were always found closer to the crypts than other EdU-labeled SIE cells, suggesting that tuft cells migrate up the villi more slowly and thus have a longer lifespan than other migrating SIE cells. Indeed, after a 5-day chase, tuft cells were the only EdU-labeled cells found in lower regions of the villi (Fig. 5O-P). In sum, while our experiments did not definitively rule out a role for KIT in tuft cell survival or effector function, they were consistent with a role for KIT during tuft cell differentiation.

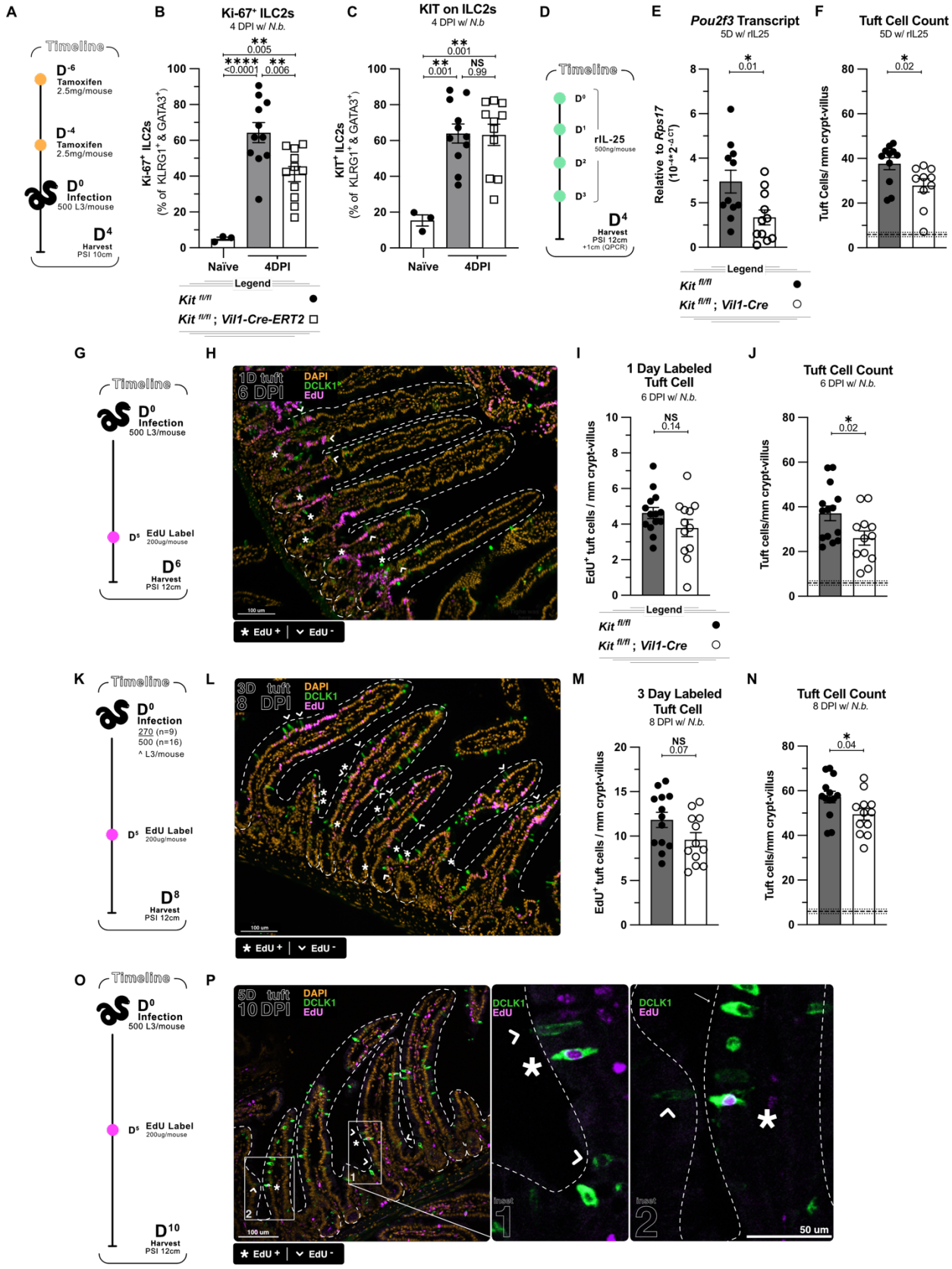

Figure 5. KIT promotes the generation of tuft cells rather than their effector function.

(**A-C**) Analysis of *Kit*$^{fl/fl}$ and *Kit*$^{fl/fl}$*;Vil1-Cre-ERT2* littermates 4 days after *N. brasiliensis* infection. (A) Experimental schematic. (B) Flow cytometric quantification of Ki-67^{+} group 2 innate lymphoid cells (ILC2s). (C) KIT quantification. (**D-F**) Analysis of *Kit*$^{fl/fl}$ and *Kit*$^{fl/fl}$*;Vil1-Cre* littermates after 4 daily injections of recombinant IL-25. (D) Experimental schematic. (**E**) Quantitative PCR analysis of *Pou2f3* in 1cm of proximal small intestinal tissue. (F) Quantification of tuft cells (DCLK1^{+}) by immunofluorescent (IF). **(G-J)** Analysis of *Kit*$^{fl/fl}$ and *Kit*$^{fl/fl}$*;Vil1-Cre* littermates 6 days after *N. brasiliensis* infection and 1 day after EdU injection. (G) Experimental schematic. (H) IF imaging of DAPI, DCLK1 and EdU in proximal small intestine. (I) Quantification of EdU^{+} DCLK1^{+} tuft cells from (H)**.** (J) Quantification of total DCLK1^{+} tuft cells from (H). **(K-N)** Analysis of *Kit*$^{fl/fl}$ and *Kit*$^{fl/fl}$*;Vil1-Cre* littermates 8 days after infection and 3 days after EdU injection. (K) Experimental schematic. (L) IF imaging of DAPI, DCLK1 and EdU in proximal SI. (M) Quantification of EdU^{+} DCLK1^{+} tuft cells from (L). (N) Quantification of total DCLK1^{+} tuft cells from (L). **(O-P)** Analysis of wildtype mice 10 days after infection and 5 days after EdU injection. (O) Experimental schematic. (P) IF imaging of DAPI, DCLK1 and EdU. ***** = examples of EdU^{+} tuft cells; arrowheads = examples of EdU^{-} tuft cells. D = days; DPI = days post infection; *N.b. = N. brasiliensis*. Each datapoint represents a biological replicate; thick dashed line indicates homeostatic tuft cell baseline from unmanipulated wild-type mice with ± 1SEM (thin dashed line). Data represent 2 (P) or 3 experiments (H, L) or are pooled from at least 2 experiments (B, C, E, F, I, J, M, N). Statistics: unpaired t-test (E, F, I, J, M, N), ordinary one-way ANOVA (B, C)

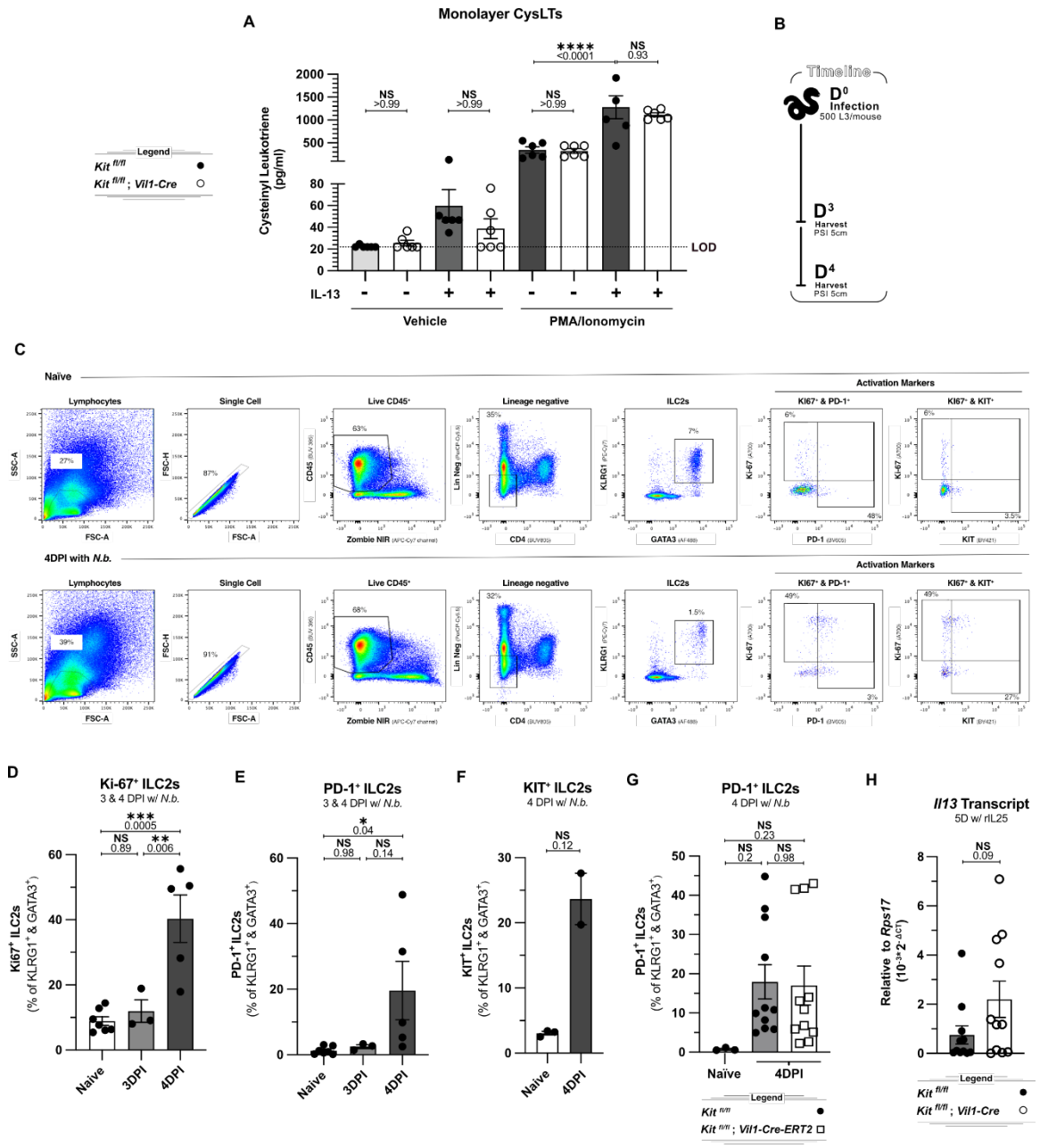

Supplement 5 (related to figure 5).

(A) Epithelial monolayers derived from proximal intestine of *Kit*$^{fl/fl}$ and *Kit*$^{fl/fl}$*;Vil1-Cre* littermates, cultured in the indicated conditions and analyzed for LTC_4 by ELISA. LOD= limit of detection (22 pg/ml). Readings below 22 were set to 22 pg/ml while those outside the standard curve (>2000 pg/ml) were discarded. (**B-F**) Flow cytometric analysis of lamina propria group 2 innate lymphoid cells (ILC2s) 3 and 4 days after *N. brasiliensis*

infection of wild-type mice. (B) Experimental schematic. (C) Representative gating strategy to identify ILC2s in wildtype mice by flow cytometry. Naïve is shown on top and 4 days after N. brasiliensis infection at the bottom. (D) Ki-67 quantification. (E) PD-1 quantification. (F) KIT quantification. (**G**) PD-1 quantification of lamina propria ILC2s 4 days after *N. brasiliensis* infection of $Kit^{fl/fl}$ and $Kit^{fl/fl}$*;Vil1-Cre-ERT2* littermates. (**H**) Quantitative PCR analysis of *Il13* in 1cm of proximal small intestinal tissue from rIL-25 stimulated mice. Data are representative of 2 experiments (C) or pooled from at least 2 experiments (A, D, E, F, G, H). Statistics: unpaired t-test (F, H) ordinary one-way ANOVA (D, E, G), ordinary two-way ANOVA (A).

KIT is required after lineage commitment but before complete maturation of tuft cells

To further assess when KIT is needed during the tuft cell lifecycle, we turned back to genetic approaches. Previous lineage-tracing experiments demonstrated that SI epithelial cells expressing *Dclk1* become tuft cells, except in very rare exceptions when a "ribbon" of $DCLK1^-$ traced cells appears in a single villus [119]. We found the same is true for *Pou2f3* using *Rosa26::STOP*$^{fl/fl}$*::zsGreen*;*Pou2f3*$^{Cre\text{-}ERT2/+}$ mice given tamoxifen; except for very rare exceptions, lineage-traced cells were $DCLK1^+$ (Fig. S6A-B). Thus, it appears that both *Dclk1-Cre* and *Pou2f3-Cre-ERT2* overwhelmingly target cells that have exclusively committed to a tuft cell fate.

At the same time, we found a key difference between these two CRE drivers. When we gave KIT10;*Pou2f3*$^{Cre\text{-}ERT2/+}$ mice tamoxifen every other day for 6 days and then quantified KIT^+ tuft cells by immunofluorescence and flow cytometry (Fig. 6A), we could not detect KIT on any tuft cells, including those newly generated in the crypts (Fig. 6B; S6C-D). In contrast, in KIT10;*Dclk1-Cre* mice we found that many newly generated $DCLK1^+$ tuft cells in the crypt and villus base still expressed KIT, while all tuft cells in the upper villi were KIT-deficient (Fig. 6B; S6C-D).

This distinction provided the opportunity to selectively test the function of KIT on committed, but newly generated tuft cells. We therefore combined *Pou2f3*- and *Dclk1*-mediated KIT deletion with *N. brasiliensis* infection. Because of the continuous generation of tuft cells, we dosed *Pou2f3-Cre-ERT2* mice with tamoxifen every other day 6 days prior to infection and during the infection (Fig. 6C). In KIT10;*Pou2f3*$^{Cre\text{-}Ert2/+}$ mice, KIT was again deleted from all tuft cells and similar to the results of *Vil1-Cre* mice with complete KIT deletion in all epithelial cells, there was a defect in tuft cell hyperplasia and an increase in worm burden even when only tuft cells lacked KIT (Fig. 6D-F). By contrast, in KIT10;*Dclk1-Cre* mice we again found that KIT was retained on many crypt tuft cells during *N. brasiliensis* infection and there was no change in tuft cell hyperplasia or worm clearance (Fig. 6G-J). As before, neither *Pou2f3*- nor *Dclk1*-mediated KIT deletion altered body weight or SI length (Fig. S6E-I). Collectively, our data support a model in which KIT predominantly supports tuft cell hyperplasia by acting on early tuft cells that reside in the crypts and villus base. Furthermore, these data suggest that KIT is utilized for tuft cell hyperplasia after *Pou2f3* commitment but before migration to the base of villi. In other words, KIT supports the differentiation and/or division of an early IL-4/13-sensitive and *Pou2f3*-commited progenitor.

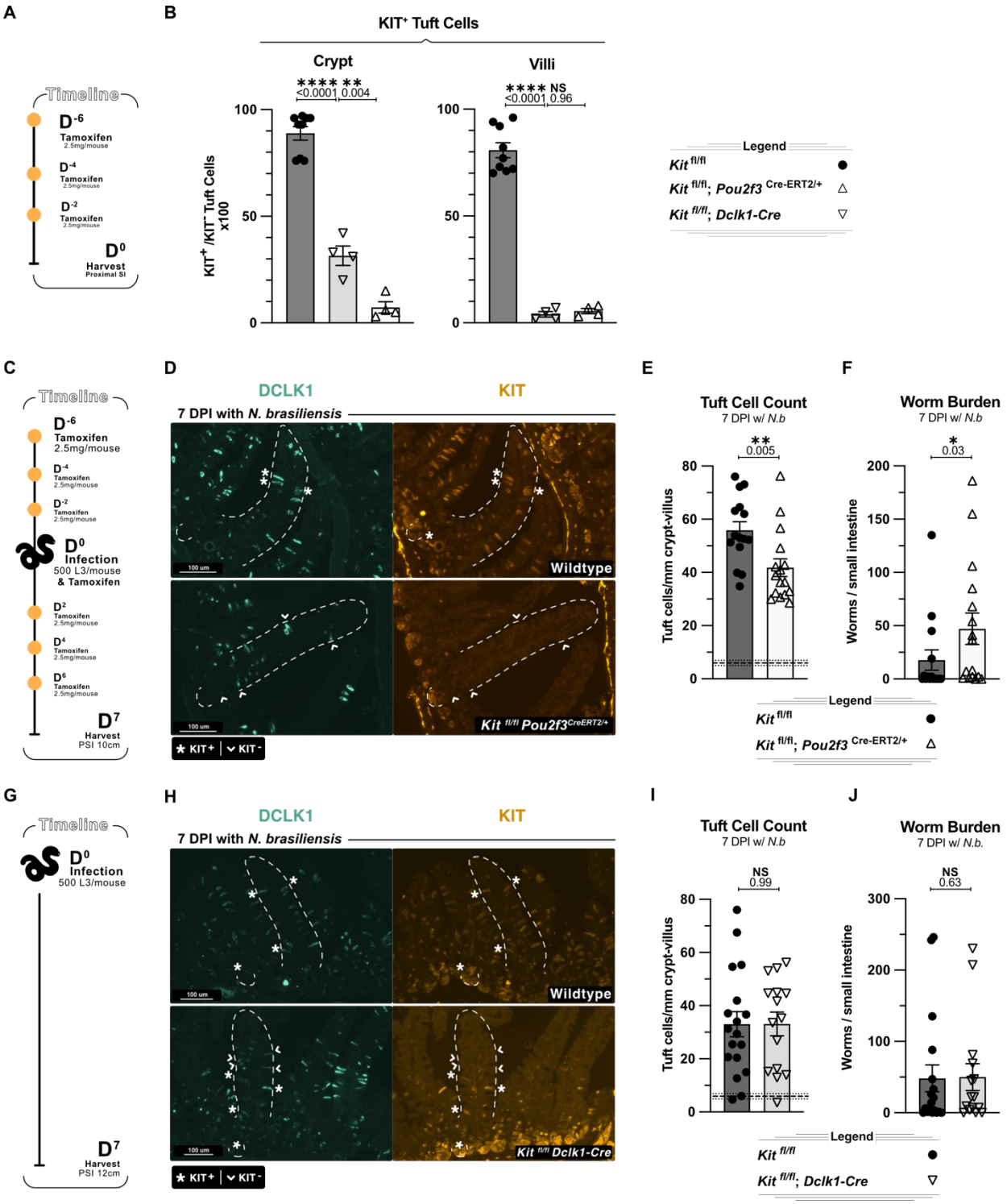

Figure 6. KIT is required early in committed tuft cells to support hyperplasia.

(**A-B**) Immunofluorescence (IF) imaging analysis of naïve *Kit*$^{fl/fl}$, *Kit*$^{fl/fl}$*;Pou2f3*$^{Cre\text{-}ERT2/+}$ and *Kit*$^{fl/fl}$*;Dclk1-Cre* mice. (A) Experimental schematic. (B) Quantification of KIT^{+} tuft cells (DCLK1^{+}) at indicated location. (**C-F**) Analysis of *Kit*$^{fl/fl}$ and *Kit*$^{fl/fl}$*;Pou2f3*$^{Cre\text{-}ERT2/+}$ littermates 7 days post *N. b.* infection. (C) Experimental schematic. (D) IF staining of DCLK1 and KIT in proximal small intestine. (E) Quantification of tuft cells (DCLK1^{+}) from imaging in (D). (F) Worms counted in the small intestine. **(G-J**) Analysis of *Kit*$^{fl/fl}$ and *Kit*$^{fl/fl}$*;Dclk1-Cre* littermates 7 days post *N. b.* infection. (G) Experimental schematic. (H) IF staining of DCLK1 and KIT in proximal small intestine. (I) Quantification of tuft cells (DCLK1^{+}) from imaging in (H). (J) Worms counted in the small intestine. D = days; DPI = days post infection. *N.b. = N. brasiliensis.* In graphs, each datapoint represents a biological replicate; thick dashed line represents homeostatic tuft cell baseline calculated from a large cohort of unmanipulated wild-type mice with ± 1SEM (thin dashed line). Data are representative of at least 3 experiments (D, H) or pooled from at least 2 experiments (B, E-F, I-J) Statistics: unpaired t-test (E, I) ordinary one-way ANOVA (B) Mann-Whitney test (F, J).

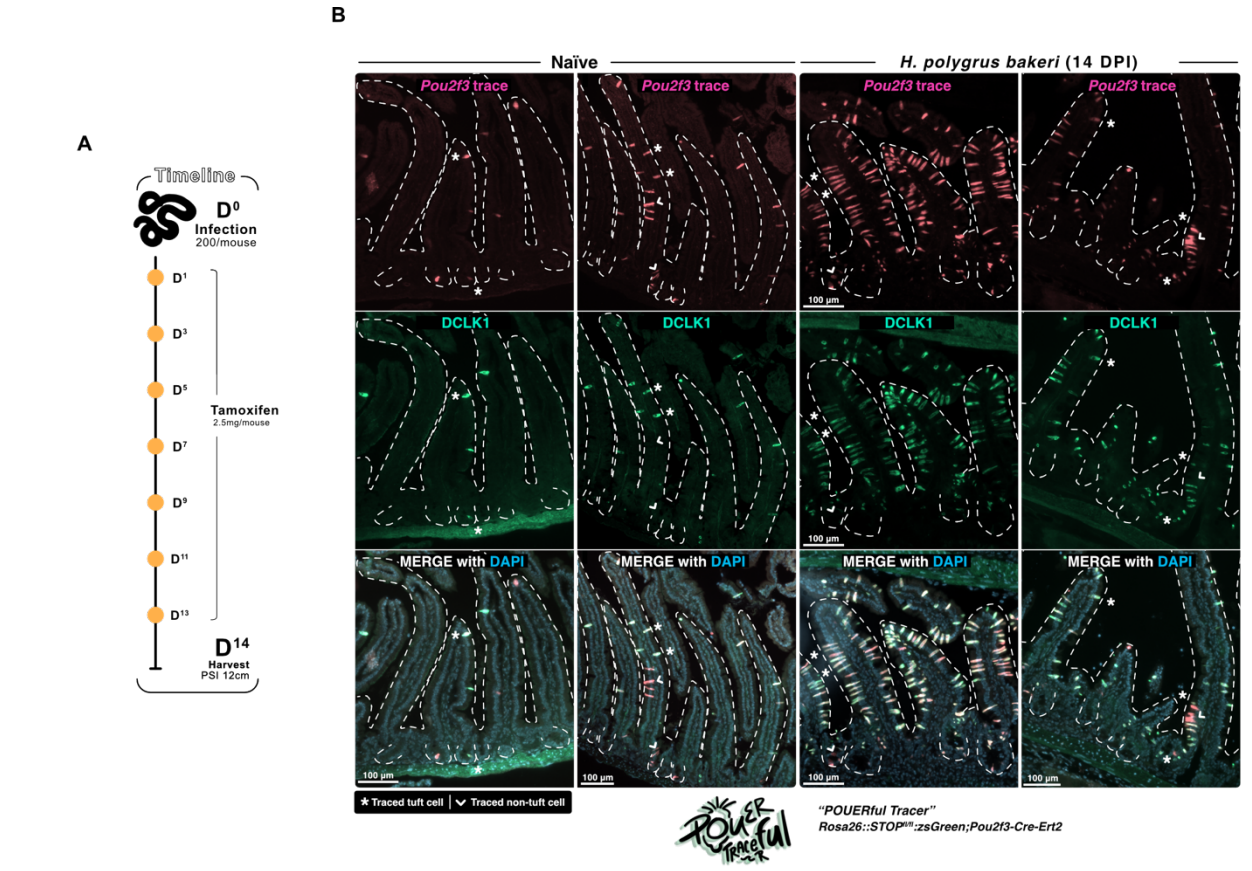
A
Timeline
D0
Infection
200/mouse
D1
D3
D5
Tamoxifen
2.5mg/mouse
D7
D9
D11
D13
D14
Harvest
PSI 12cm
B
Naïve
H. polygrus bakeri (14 DPI)
Pou2f3 trace
DCLK1
MERGE with DAPI
100 µm
* Traced tuft cell | v Traced non-tuft cell
"POUERful Tracer"
Rosa26::STOPfl/fl:zsGreen;Pou2f3-Cre-Ert2

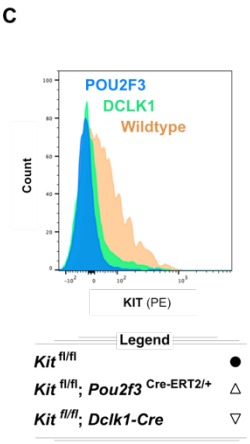
C
POU2F3
DCLK1
Wildtype
Count
KIT (PE)
Legend
Kit fl/fl
Kit fl/fl; Pou2f3 Cre-ERT2/+
Kit fl/fl; Dclk1-Cre

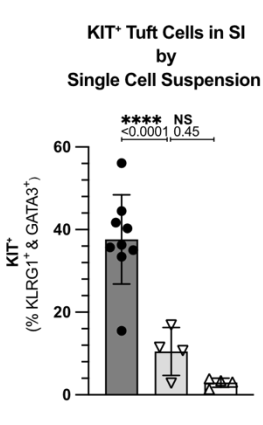
D
KIT+ Tuft Cells in SI
by
Single Cell Suspension
**** NS
<0.0001 0.45
KIT+
(% KLRG1+ & GATA3+)

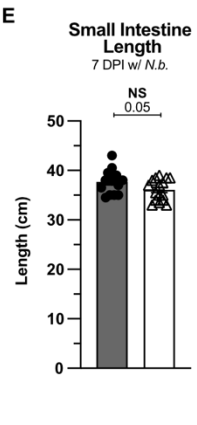
E
Small Intestine
Length
7 DPI w/ N.b.
NS
0.05
Length (cm)

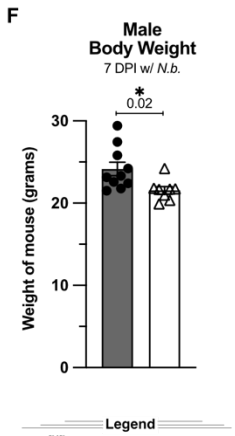
F
Male
Body Weight
7 DPI w/ N.b.
*
0.02
Weight of mouse (grams)

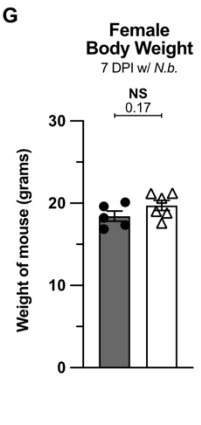
G
Female
Body Weight
7 DPI w/ N.b.
NS
0.17
Weight of mouse (grams)


Legend
Kit fl/fl
Kit fl/fl; Pou2f3 Cre-ERT2/+
Legend
Kit fl/fl
Kit fl/fl; Dclk1-Cre

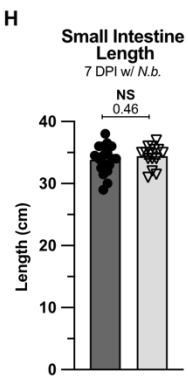
H
Small Intestine
Length
7 DPI w/ N.b.
NS
0.46
Length (cm)

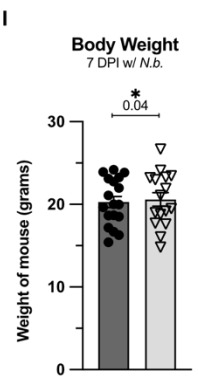
I
Body Weight
7 DPI w/ N.b.
*
0.04
Weight of mouse (grams)

Supplement 6 (related to Figure 6).

(**A**) Experimental schematic for *Pou2f3-Cre-ERT2* lineage tracing i.e. "POUERful tracer". (**B**) Immunofluorescent (IF) imaging of small intestine from Rosa26:STOP$^{fl/fl}$:zsGreen;*Pou2f3*$^{Cre\text{-}ERT2}$ mice treated as indicated. (**C-D**) Flow cytometric analysis of naïve *Kit*$^{fl/fl}$, *Kit*$^{fl/fl}$*;Pou2f3*$^{Cre\text{-}ERT2/+}$ and *Kit*$^{fl/fl}$*;Dclk1-Cre* mice (C) Representative histogram of KIT expression on tuft cells. (D) Frequency of KIT$^+$ tuft cells (DCLK1$^+$ CD24$^+$). **(E-G)** Analysis of *Kit*$^{fl/fl}$ and *Kit*$^{fl/fl}$*;Pou2f3*$^{Cre\text{-}ERT2/+}$ littermates 7 days post *N. b.* infection. Tamoxifen administration as in Figure 6C. (E) Small intestinal length. (F) Male and (G) female mouse body weight. (**H-I**) Analysis of *Kit*$^{fl/fl}$ and *Kit*$^{fl/fl}$*;Dclk1-Cre* littermates 7 days post *N. b.* infection. (H) Small intestinal length. (I) Mouse body weight. D = days; DPI = days post infection. *N.b.* = *N. brasiliensis*. In graphs, each datapoint represents a biological replicate. Data are representative of 2 experiments (B, C) or pooled from at least 2 experiments (D-I). Statistics: unpaired t-test (E-I), ordinary one-way ANOVA (D).

KIT ligand is constitutively available in the small intestine

To better understand the regulation of KIT signaling in tuft cells, we examined expression of *Kitl*, which encodes stem cell factor (SCF), the primary ligand for KIT[120]. By alternative splicing, SCF can be both membrane-bound and secreted and is produced by stromal, endothelial and some KIT$^+$ cells, including POU2F3$^+$ taste cells[81,121]. Using our tuft cell mRNA transcript dataset, we observed broad *Kitl* expression across the tissues surveyed (Fig. S7A).

Our experiments using *Pou2f3-Cre-ERT2* and *Dclk1-Cre* indicated a role for KIT signaling while tuft cells are still in the crypt. To assess the spatial distribution of SCF, we performed in-situ hybridization for *Kitl* and found that it was expressed throughout the SI epithelium and in many lamina propria cells of both naïve and

N. brasiliensis-infected mice (Fig. 7A). We next asked whether *Kitl* is upregulated during helminth-induced inflammation. Whole SI tissue transcript analysis targeting both membrane-bound and secreted forms, again revealed high *Kitl* expression at baseline and there was no further increase with *N. brasiliensis* infection (Fig. 7B). Given the abundance of *Kitl*, it appears that KIT signaling is regulated primarily by variable expression of the receptor rather than the ligand.

Akt phosphorylation in tuft cells does not require KIT

We also sought to identify downstream targets of KIT signaling in tuft cells. Because KIT is known to induce the phosphoinositide 3-kinase (PI3K) signaling pathway that activates Akt by phosphorylation, and mice lacking raptor (*Rptor*), a downstream target of Akt, have impaired tuft cell hyperplasia[122], we used immunofluorescence to detect phosphorylated Akt (pAkt) in the SI. We found that tuft cells were the only pAkt-positive cell in the SIE, with ~ 50% of tuft cells positive for pAkt at baseline (Fig 7C-D). The MFI of pAkt in tuft cells did not significantly change in the presence of *N. brasiliensis* or in the absence of KIT. However, the frequency of $pAkt^+$ tuft cells increased with infection in a KIT-independent manner (Fig. 7C-D; S7B).

Many receptor tyrosine kinases (RTKs) can induce the phosphorylation of Akt and could therefore act redundantly with KIT. For example, epidermal growth factor receptor (EGFR) is known to be constitutively phosphorylated in SI tuft cells; thus, we examined the effect of EGFR inhibition with or without KIT deletion[123,45]. KIT10;*Vil1-Cre* mice and littermate controls received the EGFR inhibitor erlotinib or vehicle control daily during *N. brasiliensis* infection (Fig. 7E). While KIT deletion reduced tuft cell hyperplasia as expected, we did not find an effect of erlotinib alone or a further reduction of tuft cells or pAkt in tuft cells when erlotinib was combined with KIT deletion, although we could not quantify the efficiency of EGFR inhibition (Fig. 7F; S7C-F).

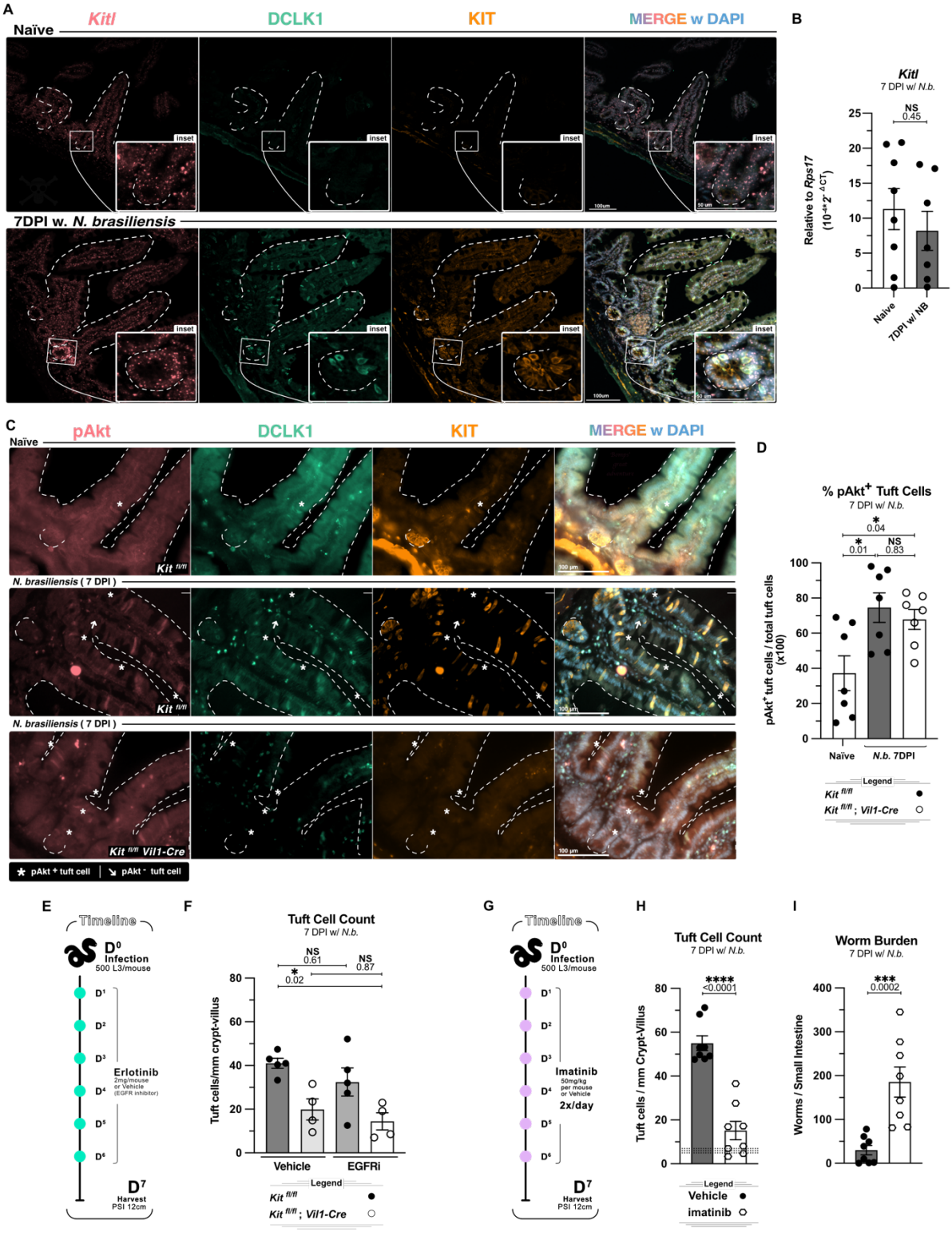
A
Naïve
Kitl
DCLK1
KIT
MERGE w DAPI
inset
7DPI w. N. brasiliensis
B
Kitl
7 DPI w/ N.b.
NS
0.45
Relative to Rps17
Naive
7DPI w/ NB
C
Naïve
pAkt
DCLK1
KIT
MERGE w DAPI
Kit fl/fl
N. brasiliensis (7 DPI)
Kit fl/fl Vil1-Cre
pAkt + tuft cell
pAkt - tuft cell
D
% pAkt+ Tuft Cells
7 DPI w/ N.b.
0.04
0.01
NS
0.83
pAkt+ tuft cells / total tuft cells (x100)
Naïve
N.b. 7DPI
Legend
Kit fl/fl
Kit fl/fl ; Vil1-Cre
E
Timeline
D0
Infection
500 L3/mouse
Erlotinib
2mg/mouse or Vehicle (EGFR inhibitor)
D7
Harvest
PSI 12cm
F
Tuft Cell Count
7 DPI w/ N.b.
NS
0.61
NS
0.87
0.02
Tuft cells/mm crypt-villus
Vehicle
EGFRi
Legend
Kit fl/fl
Kit fl/fl ; Vil1-Cre
G
Timeline
D0
Infection
500 L3/mouse
Imatinib
50mg/kg per mouse or Vehicle
2x/day
D7
Harvest
PSI 12cm
H
Tuft Cell Count
7 DPI w/ N.b.
****
<0.0001
Tuft cells / mm Crypt-Villus
Legend
Vehicle
imatinib
I
Worm Burden
7 DPI w/ N.b.
***
0.0002
Worms / Small Intestine

Figure 7. KIT is dispensable for tuft cell Akt phosphorylation, yet KIT inhibition impairs the tuft-ILC2 circuit.

(**A-B**) Analysis of proximal small intestinal tissue from wildtype naïve mice or mice infected for 7 days with *N. brasiliensis*. (A) RNAscope (In-situ hybridization) of *Kitl* and immunofluorescent (IF) staining of indicated proteins. (B) Quantitative PCR analysis of *Kitl* in 1cm of SI. (**C-D**) Analysis of $Kit^{fl/fl}$ and $Kit^{fl/fl}$*;Vil1-Cre* littermates left untreated or infected for 7 days with *N. b*. (C) Representative IF staining of DAPI, KIT, DCLK1, and phosphorylated Akt (pAkt) in proximal small intestine. (D) Frequency of $pAkt^+$ $DCLK1^+$ tuft cells from imaging in (C). (**E-F**) Analysis of $Kit^{fl/fl}$ and $Kit^{fl/fl}$*;Vil1-Cre* littermates infected for 7 days with *N. brasiliensis* and treated with EGFR inhibitor erlotinib or vehicle control. (E) Experimental schematic. (F) Quantification of tuft cells by IF staining ($DCLK1^+$). (**G-I**) Analysis of wild-type mice infected for 7 days with *N. brasiliensis* and treated with KIT inhibitor imatinib or vehicle control. (G) Experimental schematic. (H) Quantification of tuft cells by IF staining ($DCLK1^+$). (I) Worms counted in the small intestine. *N.b. = N. brasiliensis*. D = days. DPI = days post infection. In graphs, each datapoint represents a biological replicate. Data are representative of at least 2 experiments (A, C) or pooled from at least 2 experiments (B, D, F, H, I). Statistics: unpaired t-test (B, H), ordinary two-way ANOVA (D, F), Mann-Whitney test (I).

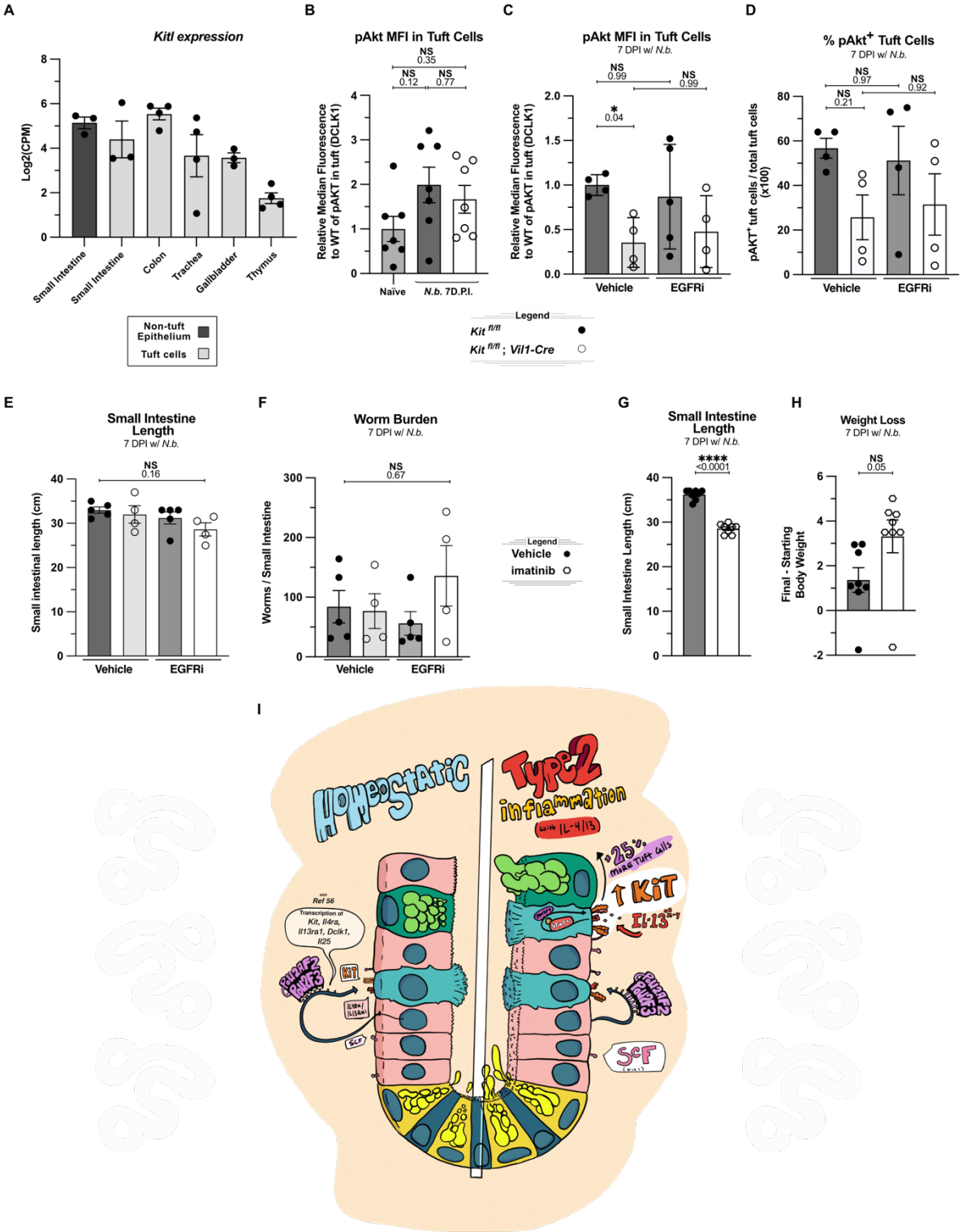
A
Kitl expression
Log2(CPM)
Small Intestine
Small Intestine
Colon
Trachea
Gallbladder
Thymus
Non-tuft Epithelium
Tuft cells
B
pAkt MFI in Tuft Cells
NS 0.35
NS 0.12
NS 0.77
Relative Median Fluorescence to WT of pAKT in tuft (DCLK1)
Naïve
N.b. 7D.P.I.
C
pAkt MFI in Tuft Cells
7 DPI w/ N.b.
NS 0.99
NS 0.99
* 0.04
Relative Median Fluorescence to WT of pAKT in tuft (DCLK1)
Vehicle
EGFRi
D
% pAkt+ Tuft Cells
7 DPI w/ N.b.
NS 0.97
NS 0.92
NS 0.21
pAKT+ tuft cells / total tuft cells (x100)
Vehicle
EGFRi
Legend
Kit fl/fl
Kit fl/fl ; Vil1-Cre
E
Small Intestine Length
7 DPI w/ N.b.
NS 0.16
Small intestinal length (cm)
Vehicle
EGFRi
F
Worm Burden
7 DPI w/ N.b.
NS 0.67
Worms / Small Intestine
Vehicle
EGFRi
Legend
Vehicle
imatinib
G
Small Intestine Length
7 DPI w/ N.b.
**** <0.0001
Small Intestine Length (cm)
H
Weight Loss
7 DPI w/ N.b.
NS 0.05
Final - Starting Body Weight
I
Homeostatic
Type2 inflammation
with IL-4/13
~25% more Tuft cells
KIT
Il-13
Ref 56
Transcription of Kit, Il4ra, Il13ra1, Dclk1, Il25
KIT
Il4Rα/ Il13Rα1
SCF
SCF

Supplement 7 (Related to Figure 7).

(**A**) Normalized RNA transcript reads in tuft cells and non-tuft epithelium sorted from indicated tissue of unmanipulated Flare (*Il25*$^{RFP/RFP}$) mice. Adapted from Ref #95 (**B**) Mean fluorescence intensity (MFI) by immunofluorescent (IF) imaging of pAKT in tuft cells (DCLK1^{+}) from images in Figure 7C. (**C-F**) Analysis of *Kit*$^{fl/fl}$ and *Kit*$^{fl/fl}$*;Vil1-Cre* littermates infected for 7 days with *N. b.* and treated with EGFR inhibitor erlotinib or vehicle control. (C) Mean fluorescence intensity (MFI) by IFF imaging of pAKT on tuft cells (DCLK1^{+}). (D) Frequency of pAKT^{+} DCLK1^{+} tuft cells. (E) Small intestinal length. (F) Worms counted in the small intestine. (**G-H**) Analysis of wild-type mice infected for 7 days with *N. b.* and treated with KIT inhibitor imatinib or vehicle control. (G) Small intestinal length. (H) Weight difference from starting to final weight. (**I**) Proposed model where left represents a homeostatic small intestinal epithelial crypt and the right a type 2 inflamed crypt. *N.b. = N. brasiliensis*. DPI = days post infection. In graphs, each datapoint represents a biological replicate. Data are pooled form at least 2 experiments (A-H). Statistics: unpaired t-test (G, H) ordinary two-way ANOVA (B-F).

Mouse Strains	Common name	Source	Strain number
C57BL/6J	**B6**	Jackson Laboratoires	000664
B6.Cg-Gt(ROSA)26Sortm6(CAG-ZsGreen1)Hze/J	**Ai6**	Jackson Laboratoires	007906
Kit f/f	**KIT10**	see "Generation of KIT10 (Kitf/f) mice"	n/a
B6.Cg-Kit tm1.1Sraf/Mmjax	**c-Kit lox66-71**	Jackson Laboratoires	042035-JAX
B6.Cg-Tg(Vil1-cre)1000Gum/J	**Vil1-Cre**	Jackson Laboratoires	021504
B6.Cg-Tg(Vil1-cre/ERT2)23Syr/J	**Vil1-Cre-ERT2**	Jackson Laboratoires	020282
B6(129S4)-Pou2f3tm1.1(cre/ERT2)Imt/J	**POU2F3-Cre-ERT2**	Jackson Laboratoires	007911
	DCLK1-Cre-IRES-GFP	T. Wang; see PMID 24487592	n/a
B6.129P2-Lgr5tm1(cre/ERT2)Cle/J	**Lgr5-EGFP-IRES-creERT2**	Tissue sections from E. Tait Wojno	008875

Table S 2. Mouse lines.

A summary of all mouse strains used in this study and their sources.

Kit LoxP insertion for KIT10 (5'-NNN-3')					
5' gRNA	GTTCCCTGAATGTGCCATGAGGG				
3' gRNA	TCTTCCTGGGGACGCCAAGGCGG				
ssDNA template	GGGAGAGGGAGAGATGATGTATTTGAATACCAAGAGAAAGCTTTGTTCCCTGAATGTGCCAATAACTTCGTATAATG TATGCTATACGAAGTTATTGAGGGAAATGGTTTAGTTTGGGATAGGTGGTGGTGGCGGCGAGGCTGTTGTCCTGCGC CTGCTGGCTCACAATCATGGTTCCCTTCCTTGCAGAGCAAATCCAGGCCCACACTCTGTTCACGCCGCTGCTCATT GGCTTTGTGGTTGCAGCTGGCGCGATGGGGATCATTGTGATGGTGCTCACCTACAAATATTTGCAGGTGAGCATTGA ATTGTTCTCTTCCTGGGGACGCCAATAACTTCGTATAATGTATGCTATACGAAGTTATAGGCGGCAGGGCAGGCACT GATTGTTCAGCGGGTGACACATCTTTCTTTTCCTTTCTCCTCCAGAAACCCA				
Genotyping					
Target	Forward primer (5'-NNN-3')	reverse primer (5'-NNN-3')	PCR program	Aproximate Amplifcaiton (Base pair)	
				Mutant	Wildtype
KIT 5' loxP	ACCAAGAGAAAGCTTTGTTCCCTG	ATGAGCAGCGGCGTGAACAGAG	Touchdown (55C-65C) with 1	201	167
KIT 3' loxP	GCAGAGCAAATCCAGGCCCACA	AACAATCAGTGCCTGCCCTGCC	Touchdown with 1C steps	206	172
General Cre	TTCCCGCAGAACCTGAAGATG	CCCAGAAATGCCAGATTACG	"Genotype"	300	na
Ai6 wildtype	AAG GGA GCT GCA GTG GAG TA	CCG AAA ATC TGT GGG AAG TC	"Genotype"	na	297
Ai6 transgene	GGC ATT AAA GCA GCG TAT CC	AAC CAG AAG TGG CAC CTG AC	"Genotype"	199	na
il4ra flox	ACGGCACGCTGATCTACAAGGT	CACAGACTGATCTCTAGGAAACCAG	"Genotype"	279	185
QPCR					
Target	Forward primer (5'-NNN-3')	reverse primer (5'-NNN-3')			
Rps17	CGCCATATCCCCAGCAAG	TGTCGGGATCCACCTCAATG			
Il13	CCTGGCTCTTGCTTGCCTT	GGTCTTGTGTGATGTTGCTCA			

Table S 3. Oligonucleotides.

A summary of all DNA oligonucleotides used in this study.

Immunofluorescence					
Target	Supplier	Catalogue #	Host	Concentration used	Fluorophores
cKIT (KIT)	R&D	AF1356	Goat	1:200	594, 647
DCAMK1 (DCLK1)	Abcam	ab31704	Rabbit	1:500	488, 594
Anti-human Lysozyme EC.2.2.1.17 (LYZ1)	Dako	A099	Rabbit	1:1000	594, 647
Phospho-Akt (Ser473) Antibody #9271 (pAKT)	Cell Signaling	9271S	Rabbit	1:20	594
Secondares					
Donkey anti-Rabbit IgG (H+L) Highly Cross-Adsorbed Secondary Antibody, Alexa Fluor™ 488	Thermofisher	A-21206	Donkey	1:1000	
Donkey anti-Rabbit IgG (H+L) Highly Cross-Adsorbed Secondary Antibody, Alexa Fluor™ 594	Thermofisher	A-21207	Donkey	1:1000	
Donkey anti-Goat IgG (H+L) Cross-Adsorbed Secondary Antibody, Alexa Fluor™ 594	Thermofisher	A-11058	Donkey	1:1000	
Donkey anti-Goat IgG (H+L) Cross-Adsorbed Secondary Antibody, Alexa Fluor™ 647	Thermofisher	A-21447	Donkey	1:1000	
Flow Cytometry					
Target	supplier	Catalogue #	Clone	Concentration used (1: #)	Fluorophores
KIT (CD117)	Biolegend	105811	2B8	100	APC
(isotype for APC)	Biolegend	400612	RTK4530	100	APC
KIT (CD117)	Biolegend	105807	2B8	100	PE
(isotype for PE)	Biolegend	400607	RTK4530	100	PE
CD24	Biolegend	101824	M1/69	200	PerCP-Cy5.5
CD45	Biolegend	103155	30F11	200	BV605
EpCAM (CD326)	Biolegend	118210	G8.8	200	Alexa Fluor 488
EpCAM (CD326)	Biolegend	118215	G8.8	200	PE-Cy7
Siglec-F	BD	562680	E50-2440	100	AF647
CD45	BD Biosciences	564279	30-F11	400	BUV395
CD4	Biolegend	589193	RMA4-5	500	BUV805
PD-1 (CD279)	BD	563059	J43	100	BV605
KIT (CD117)	Biolegend	105827	2B8	100	BV421
CD1.d	Biolegend	123514	1B1	200	PerCP-Cy5.5
CD3e	Biolegend	100328	145-2C11	100	PerCP-Cy5.5
CD8a	Biolegend	100734	56.6.7	100	PerCP-Cy5.5
CD19	Biolegend	152406	1D3	250	PerCP-Cy5.5
FceR1	Biolegend	134320	MAR-1	200	PerCP-Cy5.5
GR1 (Ly-6G/Ly-6C)	Biolegend	108433	RB6-8C5	200	PerCP-Cy5.5
NK1.1	Biolegend	108728	PK136	100	PerCP-Cy5.5
GATA3	BD Biosciences	560163	L50-823	100	AF488
KLRG1 (MAFA)	Biolegend	138416	2F1	250	PE-Cy7
Ki67 (SolA15)	Invitrogen	14-5698-82	SolA15	200	A700
Human CD4	Biolegend	300508	RPA-T4	100	PE

Table S 4. Antibodies.

A summary of all antibodies used in this study and their sources.

Reagent or Resource	Source	Identifier
mouse recombinant carrier-free IL-4	Biolegend	574304
azide-free (LEAF)–purified anti-mouse IL-4 antibody (clone 11B11)	Biolegend	504121
SMART-Seq v4 Ultra Low Input RNA Kit	Takara	Cat#634894
Superscript II reverse transcriptase	Thermo	Cat#18064014
PowerUp SYBR green master mix	Thermo	A25742
Gibco™ Mouse IL-13 Recombinant Protein, PeproTech	Fisher	210-13
Recombinant mouse IL-17e (IL-25)	R&D Systems	1399-IL-025
Sodium succinate hexahydrate, 99%	Fisher	AA41983A1
DNase I	Sigma-Aldrich	D4513
Collagenase A	Sigma-Aldrich	10103578001
Tween-80	Sigma-Aldrich	P1754-25
UltraPure™ 0.5M EDTA, pH 8.0	Invitrogen	15575020
HEPES (1M)	Thermo	15630080
Vectashield	Vector Labs	H-1000
Normocin	Life Technologies	ant-nr-1
Recombinant mouse EGF (mEGF)	Peprotech	315-09
Glutamine	Thermo	25030081
Penicillin-streptomycin	Thermo	15140122
N2 supplement	Life Technologies	17502048
B27 supplement	Life Technologies	17504044
R-spondin	10% supernatants from R-spondin secreting cells	In house
Noggin	10% supernatant from Noggin secreting cells	In house
N-acetylcysteine	VWR	102433-518
Y27632	Stemcell	72304
Normocin	InvivoGen	ant-nr-05
DMEM/F12	Thermo	12634-010
RPMI 1640	Fisher	21870092
Hanks' balanced salt solution (HBSS) no Ca2+/Mg2+	Fisher	14-190-250
Click-iT™ Plus EdU Cell Proliferation Kit for Imaging, Alexa Fluor™ 555 dye	Invitrogen	C10638
EdU (5-ethynyl-2'-deoxyuridine)	Invitrogen	A10044
Triton x-100	VMR	97062-208
Fetal Bovine Serum, qualified, USDA-approved regions	VWR	8030501796 (discontinued)
Newborn calf serum (Fetal Calf Serum; FSC)	BioWest USA	S0700
eBioscience™ Foxp3 / Transcription Factor Staining Buffer Set	Invitrogen	00-5523-00
eBioscience™ IC Fixation Buffer	Invitrogen	00-8222-49
Donkey Serum	Sigma	D9663
Wheat Germ Agglutinin (WGA)-488	Invitrogen	W11261
4',6-diamidino-2-phenylindole (DAPI)	Biolegend	422801
RNAscope Multiplex Fluorescent Detection Reagents v2	ACD (Bioteche)	323110
RNAscope Multiplex Fluorescent v2 Assay	ACD (Bioteche)	323100
RNAscope™ 3-plex Positive Control Probe- Mm	ACD (Bioteche)	32881
3-Plex Negative Control Probe (dapB)	ACD (Bioteche)	320871
RNAscope™ Probe- Mm-Kitl	ACD (Bioteche)	423401
ProLong Gold Antifade Mountant	Thermo Fisher Scientific	P36930
Imatinib (mesylate)	Cayman Chemical	13139
Erlotinib hydrochloride	Sigma	SML2156
Zombie NIR™ Fixable Viability Kit	Biolegend	423106
Cysteinyl Leukotriene Express ELISA- 96 strip well	Cayman	10009291
Phorbol 12-myristate 13-acetate (PMA)	Sigma	P8139
Ionomycin	Sigma	I0634
Software and algorithms		
GraphPad Prism 10 v10.4.0	GraphPad Software	http://www.graphpad.com/
FlowJo v10.10.0	BD	https://www.flowjo.com/
Affinity Publisher 2 v2.6.2	Serif	https://affinity.serif.com/en-us/publisher/

Table S 5. Reagents and software.

A summary of all reagents and software used in this study and their sources.

2.3 Discussion

Tuft cell hyperplasia—a striking feature of small intestinal helminth infection—promotes worm clearance[48,49]. IL-4/13 signaling in epithelial cells is required for this hyperplasia and, when provided

exogenously, also sufficient[44]. How IL-4/13 signals are translated into tuft cell expansion and whether other signals support this process is largely unknown. Here, we have shown that epithelial KIT is dispensable at homeostasis, but during type 2 inflammation cooperates with IL-4/13 signaling to promote tuft cell hyperplasia. Transcript expression of the KIT ligand SCF (*Kitl*) is widespread at baseline and does not change with helminth infection. Instead, IL-4/13 induces expression of KIT itself. Without KIT in tuft cells, tuft cell hyperplasia is reduced, and worm burden is increased. While we were preparing this manuscript, another study reported that deletion of KIT from the SIE reversed the spontaneous type 2 inflammation and tuft cell hyperplasia induced by deletion of epithelial *SpiB*, further demonstrating the importance of KIT in tuft cells[77].

Our findings provide specific insight into the timing of KIT signaling events that lead to tuft cell hyperplasia. First, we found the same decrease in tuft cell hyperplasia and modest increase in helminth burden when KIT was deleted from all epithelial cells (*Vil1-Cre, Vil1-Cre-Ert2*) or only from tuft cells (*Pou2f3-Cre-Ert2*), indicating that KIT is required after tuft cell lineage commitment for expansion and that KIT expression in non-tuft epithelial cells (e.g. Paneth) is dispensable in this context. At the same time, there was no change in tuft cell hyperplasia when KIT was deleted using *Dclk1-Cre* mice. Unlike *Pou2f3-Cre-Ert2*, which deletes KIT from all DCLK1$^+$ tuft cells, in KIT10;*Dclk1-Cre* mice, KIT is deleted in the upper villi but still expressed on most tuft cells in the crypts and the lower villi. Also, increasing the “chase” period from 1 to 3 days did not reduce the frequency of EdU-labeled tuft cells. Together, these data demonstrate that KIT predominantly supports the generation of tuft cells in crypts, rather than their survival in the villi.

Although likely KIT-independent, we were surprised to observe that migration of EdU$^+$ tuft cells up the villi is slower than other epithelial lineages and that some EdU$^+$ tuft cells remain 5 days after EdU injection. Thus, it appears that the turnover of tuft cells is slower than the 2.3-4.0 days reported for enterocytes, goblet cells, and enteroendocrine cells[88]. This slower migration may preferentially support tuft cell accumulation in

longer villi of the proximal SI, an effect less apparent in the shorter distal SI villi or in enteroids lacking defined villi.

Whether tuft cells arise exclusively from multipotent progenitors or if committed tuft cells can further divide in crypts, as has been observed in human enteroids[112], is not fully resolved. Tuft cell division has, however, not been observed in the villi[44]. In our experiments, we found a 2.5-fold increase of total EdU-labeled tuft cells from 1 day to 3 days post EdU injection, supporting the model that tuft cells divide after picking up EdU and before exiting crypts. Further studies will be needed to test this model, to delineate the molecular events that lead to tuft cell hyperplasia, and to determine how IL-4/13 promotes goblet cell hyperplasia, as we did not find a role for KIT in the latter process. Because the percent increase in goblet cells is much smaller than tuft cells, perhaps IL-4/13 signals in different progenitors (e.g. $DLL1^+$ secretory progenitor) to promote goblet cell differentiation.

We did not study the molecular mechanisms regulating *Kit* expression, but a recent ChIP-Seq analysis of POU2F3 found binding near Il4ra, *Il13ra1* and *Kit*, suggesting direct regulation[68]. Moreover, we note that there is a canonical STAT6 (TTCTCCAGAA) binding site just 13 bases from a POU2F3 (ATGCAAAT) binding site in a 3' enhancer region located between exons 1 and 2 of the *Kit* gene, suggesting the possibility of cooperative binding[124,125]. KIT itself has been suggested to directly dimerize with cytokine receptors like IL-4RA and to induce downstream signals that synergize with cytokines like IL-6[126,127]. IL-4/13 is a necessary upstream signal for KIT induction; however, we have not ruled out potential synergy that could also occur between KIT and the IL-4/13 receptor.

We propose the following model (Fig. S7I): first, yet unknown mechanisms lead to the induction of *Pou2f3* in epithelial progenitors, committing them to a tuft cell fate. POU2F3 then induces expression of *Il4ra* and *Il13ra1*, rendering early tuft cells responsive to IL-4/13; it also induces *Kit* expression at a low level. In the absence of type 2 inflammation, these cells do not receive an IL-4/13 signal; they complete their differentiation

into tuft cells and exit the crypts at low frequency. When IL-4/13 is present however, such as during helminth infection, signaling through the IL-4RA/IL-13RA1 heterodimer leads to STAT6 activation and STAT6 and POU2F3 cooperatively induce *Kit* expression. SCF, which is constitutively available, then signals through KIT to support the further differentiation and/or proliferation of early tuft cells in the crypt, giving rise to tuft cell hyperplasia.

Although our data clearly demonstrate a role for KIT during early tuft cell differentiation, we cannot exclude an additional role for KIT in tuft cell effector functions. LTC_4 secretion in vitro and upregulation of KIT and PD-1 on ILC2s in vivo were KIT-independent. On the other hand, ILC2 replication, as measured by Ki-67, was decreased 4 days post *N. brasiliensis* infection in the absence of SIE KIT, suggesting decreased tuft cell effector production. While quantification of IL-25 release remains impossible in our hands, the combination of cytokine reporter alleles (e.g. Smart13) with $Kit^{fl/fl}$ and epithelial CRE should eventually allow us to quantify ILC2 activation at earlier timepoints, before the feed-forward nature of the tuft-ILC2 circuit confounds our interpretations.

Interestingly, KIT is largely dispensable during succinate-induced hyperplasia, which predominantly occurs in the distal SI. Even during *N. brasiliensis* infection, KIT deletion had less of an impact on tuft cell hyperplasia in the distal SI, suggesting that KIT is generally more important in the proximal SI. Inherent differences between helminth- and succinate-induced tuft cell hyperplasia may also contribute. For example, we previously found that only helminth infection requires tuft cell derived leukotrienes for synergistic activation of ILC2s[45]. How context dependent use of effector functions could integrate with KIT signaling is a topic for future study.

Although RTK signaling is important for all cells, within the SIE it appears to be uniquely central to tuft cell biology. Previous studies demonstrated that tuft cells are the only SIE cells constitutively marked by an antibody for phosphorylated EGFR[123,45,111]. We now show that tuft cells are also the only mature villi epithelial

cells that express KIT and the only cells marked by pAkt, a downstream target of both KIT and EGFR. About 40% of tuft cells were pAkt^{+} at homeostasis and this increased to about 80% during helminth infection, but this was not consistently KIT-dependent. These observations, combined with the overall modest impact of epithelial KIT deletion, the evidence for compensation when KIT is constitutively deleted, and the lack of requirement for KIT in enteroids, where EGF is provided at high concentrations, led us to hypothesize that EGFR can compensate for loss of KIT. Our efforts to both delete KIT and inhibit EGFR did not, however, reveal a further loss of pAkt or tuft cell hyperplasia, although we could not validate the effectiveness of our EGFR inhibitor. Additional studies will be needed to determine why Akt and EGFR are uniquely phosphorylated in tuft cells and how their functions overlap.

Another interpretation of our EGFR inhibitor study is that additional tyrosine kinases might be involved. Indeed, when we used imatinib, which has particular specificity for KIT and the ABL kinase[128], we found a nearly complete loss of tuft cell hyperplasia and a defect in helminth clearance. As with all inhibitor studies, it is difficult to determine which cells are the key target(s) of this therapeutic. Of note, we found that ILC2s also upregulate KIT during helminth infection; thus, the combined inhibition of ILC2s and tuft cells may explain the more profound phenotype compared to tuft- or epithelium-specific KIT deletion. Nonetheless, our results suggest that KIT inhibitors and RTK inhibitors more generally, which are commonly used in the clinic, can substantially alter type 2 immunity. Relatedly, a separate study found that the ageusia (loss of taste) reported by many patients taking RTK inhibitors is likely caused by KIT inhibition. Using KIT10 mice, the authors demonstrated a role for KIT in sweet-sensing type II taste receptor cells (TRCs), which are closely related to tuft cells[47,92,129]. Unlike intestinal tuft cells, type II TRCs require KIT under homeostatic conditions, as both the number of these cells and the ability to taste sweet ligands was reduced when *Kit* was deleted with *Pou2f3*-Cre-ERT2 or mice were treated with RTK inhibitors.

2.4 Acknowledgements

We thank members of the Moltke lab for helpful discussion and insightful feedback. A. Lee and H. Dhaliwal of the Berkeley Gene Targeting Facility for their help in the making of the KIT10 mice strain and D. Kasal for help in the design; T. Christopher for providing tissue from Lgr5-EGFP-IRES-Cre-ERT2 mice; J. (swizzle) Balolong for running the CysLT ELISA; D.W. Hailey and the Institute for Stem Cell & Regenerative Medicine (ISCRM) Lynn & Mike Garvey Imaging core for microscopy support; M. F. Fontana for helpful comments on the manuscript; and the staff of the University of Washington's Cell Analysis Facility Shared Resource Lab and mouse husbandry staff in the UW 3.1 vivarium.

Funding

H.I.L. was supported by a ISCRM fellows grant along with a University of Washington Cellular and Molecular Biology T32 grant 5T32GM007270-46. Work at the University of Washington was supported by R01AI167923 (J.v.M.) and R01AI145848 (J.v.M.). J.v.M. is a Burroughs Wellcome Investigator in the Pathogenesis of Infectious Disease.

Author Contributions

Conceptualization: HIL, H-AT, JvM

Methodology: HIL, JvM

Investigation: HIL, MRB, H-AT, SO

Visualization: HIL

Supervision: JvM

Writing—original draft: HIL, JvM

Writing—review & editing: HIL, MRB, SO, H-AT, JvM

Chapter 3:

Material and methods

Experimental animals

Mice aged between 6 and 14 weeks were used for all experiments and age-matched within each experiment. Littermates (e.g. CRE-negative mice) were used as controls in all experiments. Unless otherwise noted, all data represent pooled results from at least 2 experiments and include both male and female mice. All mice were maintained in specific pathogen–free conditions at the University of Washington and were confirmed to be free of Tritrichomonas by qPCR (39). All procedures were conducted within University of Washington Institutional Animal Care and Use Committee guidelines under approved protocols (4390-01). See Table S2 for details about the mouse strains used in this study.

Generation of KIT10 (*Kit*$^{fl/fl}$) mice

Guide RNAs (IDT) targeting either side of exon 10 of the Kit gene were micro-injected into the pro-nucleus of C57BL/6 embryos together with Cas9 protein and a single-stranded DNA template (IDT) containing 5' and 3' homology arms as well as exon 10 and flanking loxP sites (see Table S3 for guide and template sequences). Embryos were transferred to pseudopregnant dams and resulting offspring were screened for insertion of both loxP sites by Sanger sequencing (see Table S3 for PCR primers).

Heterozygous founders were bred to generate homozygous offspring, and further genotyping was performed by PCR (see Table S3 for genotyping primers). Homozygous KIT10 (*Kit*$^{fl/fl}$) mice were crossed with various Cre

drivers. Cre-mediated disruption of protein expression was confirmed by flow cytometry or immunofluorescence microscopy.

Genotyping

Offspring of homozygous KIT10 gene-targeted mice were tested for the KIT10 modification with the 5' *loxP* primers using a touch-down PCR with annealing temperatures ranging from 65C to 55C in 1C steps. Amplified products were run on 1.5% agarose (Fisher) gels. All mice from Jackson Laboratories were genotyped according to Jackson protocols.

In vivo stimulation and treatment

For succinate experiments, mice were given 150 mM sodium succinate hexahydrate (Thermo Fisher Scientific) ad libitum in drinking water for the indicated amount of time (*39*). IL-4 complexes were generated by incubating 2 μg of mouse recombinant carrier-free IL-4 (Biolegend) with 10 μg of low endotoxin, anti-mouse IL-4 antibody (BioLegend) per mouse for 30 min at room temperature. rIL-4 complex or 500 ng of rIL-25 (R&D systems) was given for 4 consecutive days intraperitoneally in 200 μl of phosphate-buffered saline (PBS) (*39*). Tissue was harvested on the fifth day. For cellular turnover and pulse-chase experiments, mice were injected intraperitoneally with 200ug of 5-ethynyl-2'-deoxyuridine (EdU; Invitrogen) reconstituted in DMSO and diluted in PBS. Imatinib (Caymen) was resuspended in acetate buffer (Ph 5.5) and administered intraperitoneal twice daily, morning and evening, at 50 mg/kg based on starting body weight. Erlotinib (Sigma-Aldrich) was resuspended in DMSO and delivered intraperitoneally once daily at a constant 2mg per mouse.

Helminth infections and analysis

Heligmosomoides polygyrus bakeri (also known *as H. polygyrus*) and *Nippostrongylus brasiliensis* larvae were raised and maintained as previously described[130,131]. Mice were infected by oral gavage with 200 *H. polygyrus bakeri* L3 or subcutaneously at the base of the tail with 500 *N. brasiliensis* L3. Mice were weighed shortly after

euthanasia and the small intestines were flushed and laid out without stretching for total length quantification (39). For *N. brasiliensis* infection, the entire SI was then flushed with PBS and the effluent collected in a petri dish to count worms. SI was fileted open and all worms remaining in the tissue were enumerated using a dissecting microscope before tissue fixation.

Tissue immunofluorescence preparation and analysis by microscopy

Intestines, trachea, stomach, thymus and gallbladder were excised, flushed with PBS and fixed in 4% paraformaldehyde (Electron Microscopy Sciences) with gentle rocking for 3-4 hours at 4°C, followed by 30% (w/v) sucrose overnight at 4°C. Samples were then embedded in Optimal Cutting Temperature Compound (OCT; Tissue-Tek), and sectioned at 8 μm on a CM1950 cryostat (Leica). Small and large intestine samples were coiled into "Swiss rolls" for embedding.

Unless otherwise noted, immunofluorescent staining was performed in PBS with 1% bovine serum albumin (BSA; Fisher Bioreagents) at room temperature as follows: 1 hour 5% donkey serum, 1 hour with primary antibody (Table S4), 40 min to an hour with secondary antibody against host of primary (Table S4). In some cases, primary antibody incubation was overnight at 4°C. For WGA staining slides were washed in 0.1% Tween (Sigma) for the last wash. Then slides were stained 5 min with 4′,6-diamidino-2-phenylindole (DAPI) in PBS at 1:1000 concentration. EdU staining (Life Technologies) followed manufacture's protocol. After tissue rehydration with PBS and before serum blocking, the Click-it reaction (Life Technologies) was followed by the staining detailed above to combine multiple fluorophores. For phospho-Akt staining, sections were washed with PBS and then permeabilized with 0.05% Triton X-100 (VMR) in PBS (v/v) for 20 min at room temperature. Remaining staining steps were as described above with 3% BSA in PBS (w/v) substituted in washes. Tissue was mounted with Vectashield (Vector Laboratories). Images were acquired on a Zeiss Axio Observer A1, Nikon A1R confocal microscope, Nikon inverted widefield epifluorescence microscope, or Leica Sp8 microscope with 10x or 20x objectives.

All counts and measurements were calculated using FIJI (ImageJ) software. DCLK1$^+$ cells were counted manually and normalized to the distance per crypt-villus axis they occupied (mm). Goblet cell counts were calculated by counting WGA$^+$ cells in the villi and normalizing to villus length. Paneth cell area was quantified by outlining the LYZ1$^+$ area per crypt and crypts were averaged within image and mice. EdU$^+$ "height" was measured from the base of all in-plane crypts to the farthest EdU$^+$ nucleus in the villus. Mean fluorescence intensity (MFI) of KIT and pAkt were captured in FIJI using the ROI tool to store tuft cell outlines by DCLK1. DCLK1 outlines were applied to KIT or pAkt channel where the mean intensity was measured. These means were made relative to surrounding epithelium. For each replicate four 10x images of the Swiss roll were analyzed and at least 20 total villi/crypts were counted, except for pAkt quantification that used 20x images and at least a total of 10 tuft cells per replicate.

RNAScope

Small intestinal tissue was immediately flushed with ice-cold 4% PFA after harvest and fixed in 4% PFA for an additional 4hrs gently rocking at 4°C. Following fixation, tissue was submerged 4% PFA with 30% sucrose for 16-24 hrs, embedded in OCT and placed in -80c. Tissue sections were processed for RNAscope and protein-based antibodies according to manufacturer's protocol (Biotechne; Table S5) using the protease-free sample pretreatment and as described above.

KIT inhibition blocks tuft cell hyperplasia and helminth expulsion

Previous studies of KIT deficiency or inhibition in helminth infection did not assess effects on tuft cell hyperplasia, nor did they utilize clinical KIT inhibitors. Imatinib, also known as Gleevec, is another RTK inhibitor that includes KIT among its targets and is used to treat leukemias, systemic mastocytosis, and gastrointestinal stromal tumors. To test how this chemotherapeutic agent might impact intestinal type 2 immunity we gave imatinib [132,133] during *N.brasiliensis* infection and harvested at 7 days post infection (Fig 7G). Imatinib induced weight loss and SI lengthening normally associated with type 2 inflammation was

impaired. We also found impaired tuft cell hyperplasia and increased worm burden (Fig 7H-I; S7G-H). Since *N. brasiliensis* clearance does not require mast cells [134], this result further underscored the critical importance of KIT and perhaps other RTKs in the tuft-ILC2 circuit.

Single-cell suspension preparation

For single-cell epithelial preparations from SI or colon, tissues were flushed with PBS, and Peyer's patches were removed, opened longitudinally, and rinsed with PBS (*39*). Tissue was cut into small pieces and incubated either rocking at 37°C for 10 min in Ca^{+2}/Mg^{+2}-free Hanks' balanced salt solution (Fisher) supplemented with 3 mM EDTA (Invitrogen) and 1 mM HEPES (Thermo), or shaking at 37°C for 30 min in RPMI 1640 (Fisher) supplemented with 30% fetal bovine serum (VMR), 1 mM Hepes, deoxyribonuclease I (0.05 mg/ml; Sigma-Aldrich), and collagenase A (1 mg/ml; Sigma-Aldrich). Tissues were vortexed, and released epithelial cells were passed through a filter. 10 min incubations were repeated 3x for a total of 30 minutes. Supernatants were pooled and washed before staining for flow cytometry.

For small intestinal lamina propria preparations, the first 5 cm of the proximal SI were isolated, Peyer's patches removed, and the tissue opened longitudinally and cut into 1-2 cm sections. Sections were transferred into 35 mL ice cold HBSS (no Ca^{+2}/Mg^{+2}) containing 10 mM HEPES and shaken vigorously for 30 s. Tissue pieces were filtered through a mesh, stored on ice in RPMI 1640 (Fisher) + 5% FCS then transferred into 15 ml pre-warmed of EDTA [HBSS (no Ca^{+2}/Mg^{+2}) + 10 mM HEPES + 3mM EDTA] and shaken for 10 min at 200 RPM at 37°C. This wash was repeated twice (three washes total) to remove the epithelium, with tissue rinsed between washes with 10ml prewarmed HBSS (no Ca^{+2}/Mg^{+2}) + 10 mM HEPES. Following EDTA washes, tissues were digested in 10 ml prewarmed RPMI 1640 supplemented with 20% fetal calf serum (FCS; Biowest), 1 mg/ml collagenase A (Sigma-Aldrich), 10 mM HEPES, 1 mg/ml DNase I (Sigma-Aldrich) and shaken at 200 rpm at 37°C for 30 min. Digested tissues were vortexed, filtered sequentially through a 100 μm and 40 μm

mesh, and washed with ice-cold PBS + 3% FCS. Cells were pelleted by centrifugation (5 min, 1500 rpm), supernatant discarded, and the cell pellet washed and stained for flow cytometry.

Enteroids were washed in ice cold PBS twice and pelleted. Pellets were resuspended in 1× TrypLE (Gibco) diluted with PBS, sheared with a 28G insulin syringe, incubated for 10 min at room temperature, washed, and then stained for flow cytometry.

Flow Cytometry

Single cell suspensions were stained with Zombie Violet (BioLegend) for live/dead exclusion and then labeled with surface antibodies in PBS + 3% fetal bovine serum (FBS; v/v; VMR). For antibodies used in this study see Table S4. Except for FLARE25 mice (Fig 1), cells were fixed and permeabilized using the eBioscience™ Foxp3 / Transcription Factor Staining Buffer Set following manufacturer's instructions. After fixation and permeabilization, cells were stained for cytosolic DCLK1 (tuft cells) or for GATA 3 (ILC2s). Samples were acquired on a Canto RUO or Symphony A3 (BD Biosciences) and analyzed with FlowJo 10 (Tree Star). Debris was excluded with FSC-A/SSC-A gating and FSC-A/FSC-H were used to select single cell events.

RNA sequencing

Single cell epithelial suspensions were generated and stained as described above and then 500 tuft cells ($CD45^{low}$ $EpCAM^{+}$ $CD24^{+}$ $SigF^{+}$) directly into lysis buffer from the SMART-Seq v4 Ultra Low Input RNA Kit (Takara) and cDNA was generated following manufacturer's instructions. Four biological replicates were collected for each genotype. Each biological replicate represents one mouse. Next-generation sequencing and analysis was performed by the Benaroya Research Institute Genomics Core. Sequencing libraries were generated using the Nextera XT library preparation kit with multiplexing primers, according to manufacturer's

protocol (Illumina), and library quality was assessed using the Tapestation (Agilent). High throughput sequencing was on HiSeq 2500 (Illumina), sequencing dual-indexed and single-end 58 base pair reads. All samples were in the same run with target depth of 5 million reads to reach adequate depth of coverage.

Sequencing was inspected by FASTQC (v0.11.3) and one sample that failed QC was discarded. The following analytic pipeline was managed on the Galaxy platform. Reads were trimmed by 1 base at the 3' end, and then trimmed from both ends until base calls had a minimum quality score of at least 30 (Galaxy FASTQ Trimmer tool v1.0.0). Sequence alignment was performed using STAR aligner (v2.4.2a) with the GRCm38 reference genome and gene annotations from Ensembl release 91. Gene counts were generated using HTSeq-count (v0.4.1). Quality metrics were compiled from PICARD (v1.134), FASTQC (v0.11.3), and HTSeq-count. Raw input from HTseq-count was normalized in DESeq2. Uniquely mapped Ensembl IDs (genes and non-coding RNAs) with a mean normalized read count < 10 were excluded.

Monolayer and Enteroid Culture

Small intestinal crypts were collected from the proximal 10 cm from the stomach and used to establish 2D monolayers on Matrigel in 48-well plates or 3D enteroids in Matrigel domes in 24-well plates, as previously described[45,117]. The following modifications were applied: 100ug/mL Normacin (InvivoGen) was included in the media, R-spondin was replaced with supernatants from R-spondin expressing L-cells, and recombinant Noggin was replaced with supernatants from Noggin expressing cells. Enteroid media was replaced on days 3 and day 5 and enteroids were either treated with 2.5 ng/ml rIL-13 (PeproTech) or as indicated in figures on day 1, 3 and 5. On day 7, organoids were harvested for passage or analysis.

Monolayers were treated with 20 ng/ml rIL-13 or vehicle control at time of plating and media was replaced after overnight culture. 1-3 hours later, monolayers were stimulated with ionomycin (1 μg/ml) in

HBSS containing calcium for 30 minutes. Supernatants were stored at -80C before analysis by Cysteinyl Leukotriene Express ELISA (Cayman Chemical) according to manufacturer's protocol.

Reverse transcription and quantitative PCR

Small intestinal tissue was flushed with ice cold PBS and 1 cm of tissue was placed in a 2 ml microcentrifuge tube. Tubes were then snap-frozen on dry ice to snap freeze and stored at -80C. RLT buffer (Qiagen) was added to snap-frozen tissue and dissociated for 2 min at 60 RPM using TissueLyser II (Qiagen) with a single 5 mm stainless steel bead (Qiagen). RNA was isolated using the Mini Plus RNeasy kit (Qiagen) according to the manufacturer's instructions and reverse-transcribed using SuperScript II (Thermo Fisher Scientific) following the manufacturer's protocol. cDNA was used as a template for qPCR with PowerUP SYBR Green (Thermo Fisher Scientific) on a Viia7 cycler (Applied Biosystems) (*39*). Transcripts were normalized to *Rps17* (40S ribosomal protein S17) expression. See Table S3 for primer sequences.

Statistical analysis

Statistical analysis was performed as noted in figure legends using Prism 10 (GraphPad) software. Graphs show mean values (± SEM). Unless otherwise noted, samples were analyzed by a normality test to determine if they fit a normal distribution and then tested by a two-tailed (unpaired) *t-test*. The following were normally distributed: Tuft and goblet cell counts, Paneth cell area, cell proliferation by EdU, SI length, mouse weight, KIT MFI, and EdU-labeled tuft cells. For non-normal distributions like worm burden, we used the Mann-Whitney two-tailed test. For multiple comparisons we compared means of each column by a one-way ANOVA or by two-way ANOVA. *$p < 0.05$, **$p < 0.01$, ***$p < 0.001$, ****$p < 0.0001$.

Chapter 4:

Summary, more speculation and future directions

As explored throughout this dissertation, KIT is not solely responsible for driving tuft cell hyperplasia. In KIT-deficient mice, tuft cell expansion is attenuated, but not abolished, and worm clearance largely proceeds as in KIT-sufficient mice. Yet this partial phenotype remains insightful: it reveals that KIT contributes specifically to the magnitude and efficiency of tuft cell expansion rather than serving as its sole determinant. This suggests that tuft cell hyperplasia is supported by redundant mechanisms, ensuring that this response is biologically protected even when individual signaling pathways are impaired.

Integrating RTK signaling, tissue context, and KIT regulation

Our findings raise several mechanistic and physiological questions regarding the regulation and function of KIT in tuft cells and across other cell types involved in type 2 immunity. First, our results suggest that tuft cell hyperplasia is not uniformly regulated along the proximal-distal small intestine (SI). We show that distal tuft cells homeostatically express higher levels of KIT than proximal tuft cells and that, during a *N.b.* infection, KIT-deficient SIE exhibits attenuated tuft cell hyperplasia in the proximal SI (PSI), but not the distal SI (DSI). Moreover, KIT deficiency driven by a constitutively active Cre driver (*Vil1*-Cre) similarly impairs tuft cell hyperplasia in the PSI during *N. b.* infection, while tuft cell expansion in the DSI remains intact during succinate-induced type 2 inflammation. These regional differences suggest that the contribution of KIT to tuft cell expansion is context- and location-dependent rather than uniformly required across the SI. Integrating these findings with recently published transcriptional profiles describing tuft cell differentiation states and SI-wide epithelial heterogeneity may help clarify how KIT intersects with tuft cell ontogeny, metabolic readiness, and tissue-derived signals[8,135]. For example, because we show that KIT is important for early committed tuft cell generation, transcriptomic data revealing distinct regulators of KIT between proximal and distal tissue or

defining downstream signaling programs present in the distal and not proximal SI could help explain the biological rationale for KIT dependence and why the SI has evolved pronounced transcriptional differences.

Second, our data suggest potential redundancy among growth factor signaling pathways. We show KIT-independent expression of pAKT, yet its induction with type 2 inflammation. Validation of EGFR inhibition during infection—using erlotinib treatment combined with pEGFR immunofluorescence, established EGFR-dependent readouts, or alternative downstream signaling reporters—will help clarify whether EGFR-derived signals synergize with, or function independently of, KIT signaling to induce tuft cell-specific AKT activation. In parallel, defining the role of pAKT in tuft cell biology and type 2-induced tuft cell hyperplasia may provide insight into key aspects of RTK biochemistry, SIE population maintenance, and type 2 immune programing. These studies may also reveal therapeutic opportunities for helminth infection and for inflammatory diseases of the SI, including inflammatory bowel disease (IBD). For example, in IBD, which includes both Ulcerative colitis, and Crohn's disease, the pathology remains largely unclear; however, it has been shown that patients have increased SCF[84]. This finding not only suggests the necessity of a repair response in resisting disease, but that this repair program involves cKIT.

We found that tuft cells migrate more slowly to the villi apex compared to other SIE cells. This reduced migratory rate may provide a mechanism that enables their dramatic expansion: increased tuft cell generations, coupled with delayed upward migration, would allow accumulating tuft cells to temporarily saturate the villus epithelium during type 2 inflammation. Determining whether slow migration is intrinsic to tuft cell biology or induced by type 2 cytokines will help clarify the cellular bias of tuft cell hyperplasia. These studies may also provide insight into the other unusual epithelial migratory behaviors, such as downward migration of Paneth cells, and more broadly elucidate how epithelial flow is modulated during inflammation.

Significance of KIT10 mice

Studies of KIT's function predate its 1986 viral counterpart (v-KIT) and mammalian cellular (c-KIT*)* identification. These early studies relied on mice with naturally-occurring partial loss-of-function mutations on the dominant-white spotting (*W*) or Steel (*Sl*) locus which were later linked to KIT receptor and its ligand, SCF, respectively[81,136]. As complete deletion of KIT is embryonic lethal, mice with incomplete mutations have provided substantial insight into KIT biology. The Cre-*loxP* system allows for cell type-specific and time-specific deletion of KIT; however, there is a current lack of readily available mouse models using this system. We tested one available *Kit* flox-dependent depletion wherein GFP is expressed upon Cre -mediated gene, and subsequently, protein disruption[137]. However, *Vil1*-Cre was largely ineffective at depleting KIT, as assessed by flow cytometry for GFP and KIT expression and immunofluorescence of KIT expression in the SIE (**data not shown**). We therefore designed a *Kit* flox depletion model in house, wherein we similarly targeted exon 10, the transmembrane region, for the CRIPSR insertion of flanking *loxP* sites, but oriented the *loxP* sites in the same 5' to 3' sequence allowing for gene excision, not reversion[138]. These mice promise a more precise KIT targeting approach and can be easily leveraged to study the role of KIT in other contexts, such as cancer biology and IBD (wherein KIT signaling is heavily implicated)[84].

KIT is a growth factor used in response to acute damage

Responses to both infection and stress broadly require the selective expansion of effector cell types and KIT is often involved in this process. For example, UV exposure induces KIT-dependent expansion of melanocytes to increase melanin production and subsequently protect against further DNA damage[139]. In the context of type 2 immunity, a requirement for KIT on mast cells is well-established[79]. Here we have defined an additional role for KIT in type 2 immunity by demonstrating its epithelium-intrinsic contributions to tuft cell hyperplasia. Cancer is another setting defined by biased heighted cellular proliferation. Many tumors express KIT, and gain of function *Kit* mutations have been implicated in melanoma, thymic carcinoma, and

gastrointestinal stromal tumors (GIST)[140]. Recent studies have revealed a subset of tuft cell-like carcinomas in all tissues that normally contain tuft cells (intestine, thymus, etc.) and most of these cancers express KIT [115]. Thus, our findings suggest that KIT inhibitors approved for GIST and systemic mastocytosis[141] may be of therapeutic benefit in tuft cell-like cancers. Furthermore, although type 2 immune responses in the context of cancer have yet to be fully understood[142–144], the possibility that attenuating a KIT-driven type 2 immune response may provide therapeutic warrants careful, yet promising, investigation.

Summary

Together, these findings highlight KIT as an important epithelial growth factor receptor during type 2-induced remodeling. Although KIT is dispensable for homeostatic SIE turnover, IL-4/13 signaling induces KIT on tuft cells during helminth infections or microbial dysbiosis, positioning it as a context-dependent amplifier of epithelial remodeling. By supporting the generation of newly committed tuft cells in the crypt, KIT integrates cytokine cues with growth-factor signaling to expand a cellular lineage essential for parasitic clearance. This work therefore reframes tuft cell hyperplasia not as a purely cytokine-driven phenomenon but as a coordinated response requiring both immune-derived signals and epithelial growth factor pathways.

More broadly, theses insights exemplify how epithelial tissues deploy layered regulatory mechanisms to meet the demands of infection, injury, and environmental stress. The discovery of a tuft cell-specific function for KIT raises new questions about how growth factor programs intersect with immune circuits across tissues and disease states. Given emerging evidence of tuft cell-like cancers, the widespread clinical use of KIT inhibitors, and growing interest in targeting the IL-13 signaling axis in cancer, understanding the interplay between KIT signaling, epithelial differentiation, and type 2 immunity will be important for future therapeutic exploration. Ultimately, this work provides a framework for dissecting how cytokines and growth factors cooperate to reshape barrier tissues and offers a foundation for defining KIT's broader roles in immunity, epithelial biology, and disease.

References

1. Kaufmann, S. H. E. Immunology's Coming of Age. *Front. Immunol.* **10**, 684 (2019).

2. Pelaseyed, T. *et al.* The mucus and mucins of the goblet cells and enterocytes provide the first defense line of the gastrointestinal tract and interact with the immune system. *Immunol. Rev.* **260**, 8–20 (2014).

3. Rios, D. *et al.* Antigen sampling by intestinal M cells is the principal pathway initiating mucosal IgA production to commensal enteric bacteria. *Mucosal Immunol.* **9**, 907–916 (2016).

4. Gustafsson, J. K. *et al.* Intestinal goblet cells sample and deliver lumenal antigens by regulated endocytic uptake and transcytosis. *eLife* **10**, e67292 (2021).

5. Kulkarni, D. H. & Newberry, R. D. Antigen Uptake in the Gut: An Underappreciated Piece to the Puzzle? *Annu. Rev. Immunol.* **43**, 571–588 (2025).

6. Bevins, C. L. & Salzman, N. H. Paneth cells, antimicrobial peptides and maintenance of intestinal homeostasis. *Nat. Rev. Microbiol.* **9**, 356–368 (2011).

7. San Roman, A. K. & Shivdasani, R. A. Boundaries, junctions and transitions in the gastrointestinal tract. *Exp. Cell Res.* **317**, 2711–2718 (2011).

8. Zwick, R. K. *et al.* Epithelial zonation along the mouse and human small intestine defines five discrete metabolic domains. *Nat. Cell Biol.* **26**, 250–262 (2024).

9. Gehart, H. & Clevers, H. Tales from the crypt: new insights into intestinal stem cells. *Nat. Rev. Gastroenterol. Hepatol.* **16**, 19–34 (2019).

10. Sender, R. & Milo, R. The distribution of cellular turnover in the human body. *Nat. Med.* **27**, 45–48 (2021).

11. Van Der Flier, L. G. & Clevers, H. Stem Cells, Self-Renewal, and Differentiation in the Intestinal Epithelium. *Annu. Rev. Physiol.* **71**, 241–260 (2009).

12. Potten, C. S. & Loeffler, M. Stem cells: attributes, cycles, spirals, pitfalls and uncertainties Lessons for and from the Crypt. *Development* **110**, 1001–1020 (1990).

13. Barker, N. *et al.* Identification of stem cells in small intestine and colon by marker gene Lgr5. *Nature* **449**, 1003–1007 (2007).

14. Barker, N. Adult intestinal stem cells: critical drivers of epithelial homeostasis and regeneration. *Nat. Rev. Mol. Cell Biol.* **15**, 19–33 (2014).

15. Greicius, G. & Virshup, D. M. Stromal control of intestinal development and the stem cell niche. *Differentiation* **108**, 8–16 (2019).

16. Schepers, A. G., Vries, R., van den Born, M., van de Wetering, M. & Clevers, H. Lgr5 intestinal stem cells have high telomerase activity and randomly segregate their chromosomes. *EMBO J.* **30**, 1104–1109 (2011).

17. Sei, Y., Feng, J., Chow, C. C. & Wank, S. A. Asymmetric cell division-dominant neutral drift model for normal intestinal stem cell homeostasis. *Am. J. Physiol.-Gastrointest. Liver Physiol.* **316**, G64–G74 (2019).

18. Capdevila, C. *et al.* Cellular origins and lineage relationships of the intestinal epithelium. *Am. J. Physiol.-Gastrointest. Liver Physiol.* **321**, G413–G425 (2021).

19. Snippert, H. J. *et al.* Intestinal Crypt Homeostasis Results from Neutral Competition between Symmetrically Dividing Lgr5 Stem Cells. *Cell* **143**, 134–144 (2010).

20. Malagola, E. *et al.* Isthmus progenitor cells contribute to homeostatic cellular turnover and support regeneration following intestinal injury. *Cell* **187**, 3056-3071.e17 (2024).

21. Li, M.-L. & Sumigray, K. Redefining intestinal stemness: The emergence of a new ISC population. *Cell* **187**, 2900–2902 (2024).

22. Sato, T. *et al.* Paneth cells constitute the niche for Lgr5 stem cells in intestinal crypts. *Nature* **469**, 415–418 (2011).

23. Tetteh, P. W. *et al.* Replacement of Lost *Lgr5*-Positive Stem Cells through Plasticity of Their Enterocyte-Lineage Daughters. *Cell Stem Cell* **18**, 203–213 (2016).

24. Jadhav, U. *et al.* Dynamic Reorganization of Chromatin Accessibility Signatures during Dedifferentiation of Secretory Precursors into Lgr5+ Intestinal Stem Cells. *Cell Stem Cell* **21**, 65-77.e5 (2017).

25. Clevers, H. & Nusse, R. Wnt/β-Catenin Signaling and Disease. *Cell* **149**, 1192–1205 (2012).

26. Stamataki, D. *et al.* Delta1 Expression, Cell Cycle Exit, and Commitment to a Specific Secretory Fate Coincide within a Few Hours in the Mouse Intestinal Stem Cell System. *PLOS ONE* **6**, e24484 (2011).

27. Kim, T.-H. *et al.* Broadly permissive intestinal chromatin underlies lateral inhibition and cell plasticity. *Nature* **506**, 511–515 (2014).

28. Beumer, J. & Clevers, H. Cell fate specification and differentiation in the adult mammalian intestine. *Nat. Rev. Mol. Cell Biol.* **22**, 39–53 (2021).

29. Gracz, A. D. *et al. Sox4* Promotes *Atoh1*-Independent Intestinal Secretory Differentiation Toward Tuft and Enteroendocrine Fates. *Gastroenterology* **155**, 1508-1523.e10 (2018).

30. Cohen, S., Bigazzi, P. E. & Yoshida, T. Similarities of T cell function in cell-mediated immunity and antibody production. *Cell. Immunol.* **12**, 150–159 (1974).

31. Kungwankiattichai, S. & Maziarz, R. T. The history of cytokines and growth factors development. *Best Pract. Res. Clin. Haematol.* **38**, 101612 (2025).

32. Aaronson, S. A. Growth Factors and Cancer. *Science* **254**, 1146–1153 (1991).

33. Morán, G. A. G., Parra-Medina, R., Cardona, A. G., Quintero-Ronderos, P. & Rodríguez, É. G. Cytokines, chemokines and growth factors. in *Autoimmunity: From Bench to Bedside [Internet]* (El Rosario University Press, 2013).

34. Mosmann, T. R., Cherwinski, H., Bond, M. W., Giedlin, M. A. & Coffman, R. L. Two types of murine helper T cell clone. I. Definition according to profiles of lymphokine activities and secreted proteins. *J. Immunol. Baltim. Md 1950* **136**, 2348–2357 (1986).

35. Eken, A., Johnson, S., Erdem, S. & Hsieh, E. W. Y. Phantom of the immunologic opera: Unmasking the role of innate lymphoid cells (ILC) in inborn errors of immunity (IEI). *J. Hum. Immun.* **1**, e20250045 (2025).

36. Moro, K. *et al.* Innate production of TH2 cytokines by adipose tissue-associated c-Kit+Sca-1+ lymphoid cells. *Nature* **463**, 540–544 (2010).

37. Soil-transmitted helminth infections. https://www.who.int/news-room/fact-sheets/detail/soil-transmitted-helminth-infections.

38. Grencis, R. K. Immunity to helminths: resistance, regulation, and susceptibility to gastrointestinal nematodes. *Annu. Rev. Immunol.* **33**, 201–225 (2015).

39. Weatherhead, J. E., Hotez, P. J. & Mejia, R. The Global State of Helminth Control and Elimination in Children. *Pediatr. Clin. North Am.* **64**, 867–877 (2017).

40. Galán-Puchades, M. T. *et al.* New data on the life cycle of Nippostrongylus brasiliensis (Travassos, 1914) (Nematoda: Heligmosomidae): development of eggs and larval stages in the intestine of naturally infected Rattus norvegicus (Berkenhout, 1769). *Parasitol. Res.* **124**, 20 (2025).

41. Yokogawa, S. The Development of *Heligmosomum muris* Yokogawa, a Nematode from the Intestine of the Wild Rat. *Parasitology* **14**, 127–166 (1922).

42. Nair, M. G. & Herbert, D. R. Immune polarization by hookworms: taking cues from T helper type 2, type 2 innate lymphoid cells and alternatively activated macrophages. *Immunology* **148**, 115–124 (2016).

43. Liang, H.-E. *et al.* Divergent expression patterns of IL-4 and IL-13 define unique functions in allergic immunity. *Nat. Immunol.* **13**, 58–66 (2012).

44. von Moltke, J., Ji, M., Liang, H.-E. & Locksley, R. M. Tuft-cell-derived IL-25 regulates an intestinal ILC2-epithelial response circuit. *Nature* **529**, 221–225 (2016).

45. McGinty, J. W. *et al.* Tuft-Cell-Derived Leukotrienes Drive Rapid Anti-helminth Immunity in the Small Intestine but Are Dispensable for Anti-protist Immunity. *Immunity* **52**, 528-541.e7 (2020).

46. Akiho, H., Blennerhassett, P., Deng, Y. & Collins, S. M. Role of IL-4, IL-13, and STAT6 in inflammation-induced hypercontractility of murine smooth muscle cells. *Am. J. Physiol.-Gastrointest. Liver Physiol.* **282**, G226–G232 (2002).

47. Gerbe, F. *et al.* Intestinal epithelial tuft cells initiate type 2 mucosal immunity to helminth parasites. *Nature* **529**, 226–230 (2016).

48. Billipp, T. E. *et al.* Tuft cell-derived acetylcholine promotes epithelial chloride secretion and intestinal helminth clearance. *Immunity* **57**, 1243-1259.e8 (2024).

49. Ndjim, M. *et al.* Tuft cell acetylcholine is released into the gut lumen to promote anti-helminth immunity. *Immunity* **57**, 1260-1273.e7 (2024).

50. Dworetzky, M., Cohen, S., Cohen, S. G. & Zelaya-Quesada, M. Portier, Richet, and the discovery of anaphylaxis: A centennial. *J. Allergy Clin. Immunol.* **110**, 331–336 (2002).

51. Sokol, C. L. & Rahimi, R. A. Editorial overview: Framing the logic of type 2 immunity. *Curr. Opin. Immunol.* **92**, 102523 (2025).

52. Kopp, E. B., Agaronyan, K., Licona-Limón, I., Nish, S. A. & Medzhitov, R. Modes of type 2 immune response initiation. *Immunity* **56**, 687–694 (2023).

53. Molofsky, A. B. & Locksley, R. M. The ins and outs of innate and adaptive type 2 immunity. *Immunity* **56**, 704–722 (2023).

54. Janeway, C. A. & Medzhitov, R. Innate immune recognition. *Annu. Rev. Immunol.* **20**, 197–216 (2002).

55. Iwasaki, A. & Medzhitov, R. Control of adaptive immunity by the innate immune system. *Nat. Immunol.* **16**, 343–353 (2015).

56. Rahimi, R. A. & Sokol, C. L. Functional Recognition Theory and Type 2 Immunity: Insights and Uncertainties. *ImmunoHorizons* **6**, 569–580 (2022).

57. Shi, K. *et al.* Epithelial cell membrane perforation induces allergic airway inflammation. *Nature* **645**, 475–483 (2025).

58. Corthay, A. A Three-cell Model for Activation of Naïve T Helper Cells. *Scand. J. Immunol.* **64**, 93–96 (2006).

59. Reicher, B. & Barda-Saad, M. Multiple pathways leading from the T-cell antigen receptor to the actin cytoskeleton network. *FEBS Lett.* **584**, 4858–4864 (2010).

60. Jenkins, M. K. & Moon, J. J. The role of naïve T cell precursor frequency and recruitment in dictating immune response magnitude. *J. Immunol. Baltim. Md 1950* **188**, 4135–4140 (2012).

61. Ryu, S., Lim, M., Kim, J. & Kim, H. Y. Versatile roles of innate lymphoid cells at the mucosal barrier: from homeostasis to pathological inflammation. *Exp. Mol. Med.* **55**, 1845–1857 (2023).

62. Stockwin, L. H., McGonagle, D., Martin, I. G. & Blair, G. E. Dendritic cells: Immunological sentinels with a central role in health and disease. *Immunol. Cell Biol.* **78**, 91–102 (2000).

63. Feng, X., Flüchter, P., De Tenorio, J. C. & Schneider, C. Tuft cells in the intestine, immunity and beyond. *Nat. Rev. Gastroenterol. Hepatol.* **21**, 852–868 (2024).

64. Yamashita, J., Ohmoto, M., Yamaguchi, T., Matsumoto, I. & Hirota, J. Skn-1a/Pou2f3 functions as a master regulator to generate Trpm5-expressing chemosensory cells in mice. *PLOS ONE* **12**, e0189340 (2017).

65. Genetic mapping reveals Pou2af2/OCA-T1–dependent tuning of tuft cell differentiation and intestinal type 2 immunity | Science Immunology. https://www-science-org.offcampus.lib.washington.edu/doi/10.1126/sciimmunol.ade5019.

66. Nadjsombati, M. S. *et al.* Genetic mapping reveals Pou2af2/OCA-T1–dependent tuning of tuft cell differentiation and intestinal type 2 immunity. *Sci. Immunol.* **8**, eade5019 (2023).

67. Yamashita, J., Ohmoto, M., Yamaguchi, T., Matsumoto, I. & Hirota, J. Skn-1a/Pou2f3 functions as a master regulator to generate Trpm5-expressing chemosensory cells in mice. *PloS One* **12**, e0189340 (2017).

68. Ankenbauer, K. E. *et al.* Pcdh20 is a POU2F3 target gene required for proper tuft cell microvillus formation. 2025.03.18.644042 Preprint at https://doi.org/10.1101/2025.03.18.644042 (2025).

69. Hollenhorst, M. I. *et al.* Bitter taste signaling in tracheal epithelial brush cells elicits innate immune responses to bacterial infection. *J. Clin. Invest.* **132**, (2022).

70. Abdel Wadood, N. *et al.* Tracheal tuft cells release ATP and link innate to adaptive immunity in pneumonia. *Nat. Commun.* **16**, 584 (2025).

71. Keshavarz, M. *et al.* Cysteinyl leukotrienes and acetylcholine are biliary tuft cell cotransmitters. *Sci. Immunol.* **7**, eabf6734 (2022).

72. O'Leary, C. E. *et al.* Bile acid–sensitive tuft cells regulate biliary neutrophil influx. *Sci. Immunol.* **7**, eabj1080 (2022).

73. Rane, C. K. *et al.* Development of solitary chemosensory cells in the distal lung after severe influenza injury. *Am. J. Physiol.-Lung Cell. Mol. Physiol.* **316**, L1141–L1149 (2019).

74. Barr, J. *et al.* Injury-induced pulmonary tuft cells are heterogenous, arise independent of key Type 2 cytokines, and are dispensable for dysplastic repair. *eLife* **11**, e78074 (2022).

75. Zhao, M. *et al.* Epithelial STAT6 O-GlcNAcylation drives a concerted anti-helminth alarmin response dependent on tuft cell hyperplasia and Gasdermin C. *Immunity* **55**, 623-638.e5 (2022).

76. Oyesola, O. O. *et al.* PGD2 and CRTH2 counteract Type 2 cytokine–elicited intestinal epithelial responses during helminth infection. *J. Exp. Med.* **218**, e20202178 (2021).

77. Wang, J. *et al.* Tuft cells restrain intestinal type 2 immunity through the transcription factor Spi-B. *Sci. Immunol.* **10**, eads5818 (2025).

78. Broudy, V. C., Lin, N. L., Bühring, H. J., Komatsu, N. & Kavanagh, T. J. Analysis of c-kit receptor dimerization by fluorescence resonance energy transfer. *Blood* **91**, 898–906 (1998).

79. Tsai, M., Valent, P. & Galli, S. J. KIT as a master regulator of the mast cell lineage. *J. Allergy Clin. Immunol.* **149**, 1845–1854 (2022).

80. Datta, S. R. *et al.* Akt Phosphorylation of BAD Couples Survival Signals to the Cell-Intrinsic Death Machinery. *Cell* **91**, 231–241 (1997).

81. Lennartsson, J. & Rönnstrand, L. Stem cell factor receptor/c-Kit: from basic science to clinical implications. *Physiol. Rev.* **92**, 1619–1649 (2012).

82. Hachiya, A., Kobayashi, A., Ohuchi, A., Takema, Y. & Imokawa, G. The paracrine role of stem cell factor/c-kit signaling in the activation of human melanocytes in ultraviolet-B-induced pigmentation. *J. Invest. Dermatol.* **116**, 578–586 (2001).

83. Baba, H., Uchiwa, H. & Watanabe, S. UVB irradiation increases the release of SCF from human epidermal cells. *J. Invest. Dermatol.* **124**, 1075–1077 (2005).

84. Schmitt, M. *et al.* Paneth Cells Respond to Inflammation and Contribute to Tissue Regeneration by Acquiring Stem-like Features through SCF/c-Kit Signaling. *Cell Rep.* **24**, 2312-2328.e7 (2018).

85. Taylor, W. E. *et al.* Human stem cell factor promoter deoxyribonucleic acid sequence and regulation by cyclic 3',5'-adenosine monophosphate in a Sertoli cell line. *Endocrinology* **137**, 5407–5414 (1996).

86. Costa, J. J. *et al.* Recombinant human stem cell factor (kit ligand) promotes human mast cell and melanocyte hyperplasia and functional activation in vivo. *J. Exp. Med.* **183**, 2681–2686 (1996).

87. Walker, B. E. & Leblond, C. P. Sites of nucleic acid synthesis in the mouse visualized by radioautography after administration of C14-labelled adenine and thymidine. *Exp. Cell Res.* **14**, 510–531 (1958).

88. Cheng, H. & Leblond, C. P. Origin, differentiation and renewal of the four main epithelial cell types in the mouse small intestine V. Unitarian theory of the origin of the four epithelial cell types. *Am. J. Anat.* **141**, 537–561 (1974).

89. Beumer, J. *et al.* BMP gradient along the intestinal villus axis controls zonated enterocyte and goblet cell states. *Cell Rep.* **38**, 110438 (2022).

90. Rowland, K. J., Choi, P. M. & Warner, B. W. The role of growth factors in intestinal regeneration and repair in necrotizing enterocolitis. *Semin. Pediatr. Surg.* **22**, 101–111 (2013).

91. Herbert, D. R. *et al.* Intestinal epithelial cell secretion of RELM-β protects against gastrointestinal worm infection. *J. Exp. Med.* **206**, 2947–2957 (2009).

92. Matsumoto, I., Ohmoto, M., Narukawa, M., Yoshihara, Y. & Abe, K. Skn-1a (Pou2f3) specifies taste receptor cell lineage. *Nat. Neurosci.* **14**, 685–687 (2011).

93. Howitt, M. R. *et al.* Tuft cells, taste-chemosensory cells, orchestrate parasite type 2 immunity in the gut. *Science* **351**, 1329–1333 (2016).

94. Lei, W. *et al.* Activation of intestinal tuft cell-expressed Sucnr1 triggers type 2 immunity in the mouse small intestine. *Proc. Natl. Acad. Sci.* **115**, 5552–5557 (2018).

95. Nadjsombati, M. S. *et al.* Detection of Succinate by Intestinal Tuft Cells Triggers a Type 2 Innate Immune Circuit. *Immunity* **49**, 33-41.e7 (2018).

96. Schneider, C. *et al.* A Metabolite-Triggered Tuft Cell-ILC2 Circuit Drives Small Intestinal Remodeling. *Cell* **174**, 271-284.e14 (2018).

97. Bao, K. & Reinhardt, R. L. The differential expression of IL-4 and IL-13 and its impact on type-2 immunity. *Cytokine* **75**, 25–37 (2015).

98. Eshleman, E. M. *et al.* Microbiota-derived butyrate restricts tuft cell differentiation via histone deacetylase 3 to modulate intestinal type 2 immunity. *Immunity* **57**, 319-332.e6 (2024).

99. Lindholm, H. T. *et al.* BMP signaling in the intestinal epithelium drives a critical feedback loop to restrain IL-13-driven tuft cell hyperplasia. *Sci. Immunol.* **7**, eabl6543 (2022).

100. Xu, H. *et al.* ILC3s promote intestinal tuft cell hyperplasia and anthelmintic immunity through RANK signaling. *Sci. Immunol.* **10**, eadn1491 (2025).

101. Mol, C. D. *et al.* Structure of a c-Kit Product Complex Reveals the Basis for Kinase Transactivation*. *J. Biol. Chem.* **278**, 31461–31464 (2003).

102. Lennartsson, J. *et al.* Phosphorylation of Shc by Src family kinases is necessary for stem cell factor receptor/c-kit mediated activation of the Ras/MAP kinase pathway and c-fos induction. *Oncogene* **18**, 5546–5553 (1999).

103. Hulzinga, J. D. *et al.* W/kit gene required for interstitial cells of Cajal and for intestinal pacemaker activity. *Nature* **373**, 347–349 (1995).

104. Rothenberg, M. E. *et al.* Identification of a cKit+ Colonic Crypt Base Secretory Cell That Supports Lgr5+ Stem Cells in Mice. *Gastroenterology* **142**, 1195-1205.e6 (2012).

105. Xu, Q. *et al.* c-Kit+ cells that intercalate with crypt Lgr5+ cells are distinctively multipotent in colonic epithelium renewal and repair. *Cell Death Differ.* 1–15 (2025) doi:10.1038/s41418-025-01471-1.

106. Grimbaldeston, M. A. *et al.* Mast Cell-Deficient *W-sash* c-*kit* Mutant *Kit*W-sh/W-sh Mice as a Model for Investigating Mast Cell Biology *in Vivo*. *Am. J. Pathol.* **167**, 835–848 (2005).

107. Donaldson, L. E., Schmitt, E., Huntley, J. F., Newlands, G. F. J. & Grencis, R. K. A critical role for stem cell factor and c- *kit* in host protective immunity to an intestinal helminth. *Int. Immunol.* **8**, 559–567 (1996).

108. Feyerabend, T. B. *et al.* Cre-Mediated Cell Ablation Contests Mast Cell Contribution in Models of Antibody- and T Cell-Mediated Autoimmunity. *Immunity* **35**, 832–844 (2011).

109. Hepworth, M. R. *et al.* Mast cells orchestrate type 2 immunity to helminths through regulation of tissue-derived cytokines. *Proc. Natl. Acad. Sci.* **109**, 6644–6649 (2012).

110. Newlands, G. F. J., Miller, H. R. P., MacKellar, A. & Galli, S. J. Stem Cell Factor Contributes to Intestinal Mucosal Mast Cell Hyperplasia in Rats Infected With *Nippostrongylus brasiliensis* or *Trichinella spiralis*, but Anti-Stem Cell Factor Treatment Decreases Parasite Egg Production During *N brasiliensis* Infection. *Blood* **86**, 1968–1976 (1995).

111. Vlajic, K. *et al.* Appearance of tuft cells during prostate cancer progression. *Oncogene* **42**, 2374–2385 (2023).

112. Huang, L. *et al.* Tuft cells act as regenerative stem cells in the human intestine. *Nature* **634**, 929–935 (2024).

113. Haber, A. L. *et al.* A single-cell survey of the small intestinal epithelium. *Nature* **551**, 333–339 (2017).

114. Yamada, Y. *et al.* A Tuft Cell–Like Signature Is Highly Prevalent in Thymic Squamous Cell Carcinoma and Delineates New Molecular Subsets Among the Major Lung Cancer Histotypes. *J. Thorac. Oncol.* **16**, 1003–1016 (2021).

115. Yamada, Y. *et al.* Tuft cell-like carcinomas: novel cancer subsets present in multiple organs sharing a unique gene expression signature. *Br. J. Cancer* **127**, 1876–1885 (2022).

116. Allaire, J. M. *et al.* The Intestinal Epithelium: Central Coordinator of Mucosal Immunity. *Trends Immunol.* **39**, 677–696 (2018).

117. Sato, T. *et al.* Single Lgr5 stem cells build crypt-villus structures in vitro without a mesenchymal niche. *Nature* **459**, 262–265 (2009).

118. Pérez-González, C., Ceada, G., Matejčić, M. & Trepat, X. Digesting the mechanobiology of the intestinal epithelium. *Curr. Opin. Genet. Dev.* **72**, 82–90 (2022).

119. Westphalen, C. B. *et al.* Long-lived intestinal tuft cells serve as colon cancer–initiating cells. *J. Clin. Invest.* **124**, 1283–1295 (2014).

120. Reboll, M. R. *et al.* Meteorin-like promotes heart repair through endothelial KIT receptor tyrosine kinase. *Science* **376**, 1343–1347 (2022).

121. Ezen, C. & Dando, R. The c-kit Receptor Tyrosine Kinase Marks Sweet or Umami Sensing T1R3 Positive Adult Taste Cells in Mice. *Chemosens. Percept.* **14**, 41–46 (2021).

122. Aladegbami, B. *et al.* Epithelial cell specific Raptor is required for initiation of type 2 mucosal immunity in small intestine. *Sci. Rep.* **7**, (2017).

123. McKinley, E. T. *et al.* Optimized multiplex immunofluorescence single-cell analysis reveals tuft cell heterogeneity. *JCI Insight* **2**, (2017).

124. Tantin, D. Oct transcription factors in development and stem cells: insights and mechanisms. *Dev. Camb. Engl.* **140**, 2857–2866 (2013).

125. Li, J. *et al.* Structural basis for DNA recognition by STAT6. *Proc. Natl. Acad. Sci. U. S. A.* **113**, 13015–13020 (2016).

126. Sethumadhavan, A. & Mani, M. Kit activates interleukin-4 receptor and effector signal transducer and activator of transcription 6 independent of its cognate ligand in mouse mast cells. *Immunology* **159**, 441–449 (2020).

127. Sui, X. *et al.* gp130 and c-Kit signalings synergize for ex vivo expansion of human primitive hemopoietic progenitor cells. *Proc. Natl. Acad. Sci. U. S. A.* **92**, 2859–2863 (1995).

128. Lee, S. J. & Wang, J. Y. Exploiting the promiscuity of imatinib. *J. Biol.* **8**, 30 (2009).

129. Piarowski, C. M. *et al.* Tyrosine kinase inhibitors affect sweet taste and dysregulate fate selection of specific taste bud cell subtypes via KIT inhibition. 2025.08.15.670608 Preprint at https://doi.org/10.1101/2025.08.15.670608 (2025).

130. Voehringer, D., Reese, T. A., Huang, X., Shinkai, K. & Locksley, R. M. Type 2 immunity is controlled by IL-4/IL-13 expression in hematopoietic non-eosinophil cells of the innate immune system. *J. Exp. Med.* **203**, 1435–1446 (2006).

131. Johnston, C. J. C. *et al.* Cultivation of Heligmosomoides Polygyrus: An Immunomodulatory Nematode Parasite and its Secreted Products. *J. Vis. Exp. JoVE* e52412 (2015) doi:10.3791/52412.

132. Buchdunger, E., Matter, A. & Druker, B. J. Bcr-Abl inhibition as a modality of CML therapeutics. *Biochim. Biophys. Acta BBA - Rev. Cancer* **1551**, M11–M18 (2001).

133. le Coutre, P. *et al.* In Vivo Eradication of Human BCR/ABL-Positive Leukemia Cells With an ABL Kinase Inhibitor. *JNCI J. Natl. Cancer Inst.* **91**, 163–168 (1999).

134. Uber, C. L., Roth, R. L. & Levy, D. A. Expulsion of Nippostrongylus brasiliensis by mice deficient in mast cells. *Nature* **287**, 226–228 (1980).

135. Buissant des Amorie, J. R. *et al.* Intestinal tuft cell subtypes represent successive stages of maturation driven by crypt-villus signaling gradients. *Nat. Commun.* **16**, 6765 (2025).

136. Geissler, E. N., Ryan, M. A. & Housman, D. E. The dominant-white spotting (W) locus of the mouse encodes the c-kit proto-oncogene. *Cell* **55**, 185–192 (1988).

137. Kimura, Y. *et al.* c-Kit-Mediated Functional Positioning of Stem Cells to Their Niches Is Essential for Maintenance and Regeneration of Adult Hematopoiesis. *PLoS ONE* **6**, e26918 (2011).

138. Branda, C. S. & Dymecki, S. M. Talking about a Revolution: The Impact of Site-Specific Recombinases on Genetic Analyses in Mice. *Dev. Cell* **6**, 7–28 (2004).

139. Hachiya, A., Kobayashi, A., Ohuchi, A., Takema, Y. & Imokawa, G. The Paracrine Role of Stem Cell Factor/c-kit Signaling in the Activation of Human Melanocytes in Ultraviolet-B-Induced Pigmentation. *J. Invest. Dermatol.* **116**, 578–586 (2001).

140. Pathania, S., Pentikäinen, O. T. & Singh, P. K. A holistic view on c-Kit in cancer: Structure, signaling, pathophysiology and its inhibitors. *Biochim. Biophys. Acta BBA - Rev. Cancer* **1876**, 188631 (2021).

141. Klug, L. R., Corless, C. L. & Heinrich, M. C. Inhibition of KIT Tyrosine Kinase Activity: Two Decades After the First Approval. *J. Clin. Oncol.* **39**, 1674–1686 (2021).

142. Bednarz-Misa, I. *et al.* Interleukins 4 and 13 and Their Receptors Are Differently Expressed in Gastrointestinal Tract Cancers, Depending on the Anatomical Site and Disease Advancement, and Improve Colon Cancer Cell Viability and Motility. *Cancers* **12**, 1463 (2020).

143. Bartolomé, R. A., Jaén, M. & Casal, J. I. An IL13Rα2 peptide exhibits therapeutic activity against metastatic colorectal cancer. *Br. J. Cancer* **119**, 940–949 (2018).

144. Shi, J., Song, X., Traub, B., Luxenhofer, M. & Kornmann, M. Involvement of IL-4, IL-13 and Their Receptors in Pancreatic Cancer. *Int. J. Mol. Sci.* **22**, 2998 (2021).